DESIGN AND CHARACTERIZATION OF FLEXIBLE AND IMPLANTABLE ELECTRODES

by

Aseel Dirar Alatoom

A Thesis presented to the Faculty of the
American University of Sharjah
College of Engineering
In Partial Fulfillment
of the Requirements
for the Degree of

Master of Science in
Biomedical Engineering

Sharjah, United Arab Emirates

April 2019.

Approval Signatures

We, the undersigned, approve the Master's Thesis of Aseel Dirar Alatoom

Thesis Title: Design and Characterization of Flexible and Implantable Electrodes.

Signature	**Date of Signature** (dd/mm/yyyy)
_____	_____
Dr. Amani Al-Othman Assistant Professor, Department of Chemical Engineering Thesis Advisor	
_____	_____
Dr. Hasan Awad Moh'd Al-Nashash Professor, Department of Electrical Engineering Thesis Co-Advisor	
_____	_____
Dr. Mohammad Hussein Al-Sayah Professor, Department of Biology, Chemistry, and Environmental Sciences Thesis Co-Advisor	
_____	_____
Dr. Dana Abouelnasr Professor, Department of Chemical Engineering Thesis Committee Member	
_____	_____
Dr. Yassir Makkawi Associate Professor, Department of Chemical Engineering Thesis Committee Member	
_____	_____
Dr. Hasan Awad Moh'd Al-Nashash Director, Biomedical Engineering Graduate Program	
_____	_____
Dr. Lotfi Romdhane Associate Dean for Graduate Affairs and Research College of Engineering	
_____	_____
Dr. Naif Darwish Acting Dean, College of Engineering	
_____	_____
Dr. Mohamed El-Tarhuni Vice Provost for Graduate Studies	

Acknowledgement

I would like to thank my advisors Dr. Al-Othman, Dr. Al-Nashash and Dr. Al-Sayah for providing knowledge, guidance, support, and motivation throughout my research stages. I'm deeply beholden for their great assistance, worthy discussion and suggestions.

I would like to thank the professors of the Biomedical Engineering graduate program who taught me the master level courses with mighty teaching methods and skills. I am appreciative of their perceptive advices and motivation.

I would like to thank the Biosciences and Bioengineering Research Institute for sponsoring this project through the graduate assistantship program.

As a final word, I would like to thank each individual who have been a source of support and encouragement and helped me achieve my work successfully.

Dedication

To my brothers,

my sincere gratitude for your endless love, support and help during the hardest of times.

To my father,

I am forever indebted to you for your love and patience with me.

To my mother,

for always believing in me, even when I did not believe in myself, this would not have been possible if not for your support; I dedicate this to you

Abstract

Implantable bioelectrodes have the potential to advance neural sensing and muscle stimulation, especially in cases of peripheral nerve injuries. In such cases, the application of electrical stimulation to the muscles prevents muscular atrophy and helps to bridge the gap between the injured nerve and the corresponding muscle. Conventional materials for these implantable electrodes are usually metals, but they suffer from several limitations ranging from mechanical mismatch to immunological responses. Another problem is damage to tissues due to mechanical forces exerted on soft tissues by the stiff mechanical electrodes. Therefore, there is a need for the development of flexible, durable implantable electrodes with low interfacial impedance characteristics. This thesis discusses the fabrication and characterization of novel, low-cost, flexible bioelectrodes based on silicone polymer (polysiloxane) and other electrode materials, including titanium dioxide and stainless steel powder as well as their combinations. For this purpose, this work synthesized and characterized three types of implantable electrodes based on their electrochemical and mechanical properties; where titanium dioxide, stainless steel, and a mixture of the two were used as the main conducting components for fabrication. The titanium dioxide-based samples exhibited a bulk impedance of 353±13.5 Ω with an impedance of 198±183 kΩ at frequency of 1 kHz; in addition, they had a modulus of elasticity of 4.52±1.15 MPa. The stainless steel-based electrodes had a bulk impedance of 1.69±1.16 kΩ and an impedance of 1.21±1.13 MΩ at frequency of 1 kHz, and they had a modulus of elasticity of 0.722±0.393 MPa. The third type, which was a mixture of both titanium dioxide and stainless steel-based samples, had a bulk impedance of 1.71±0.849 kΩ and an impedance of 191 ± 160 kΩ at frequency of 1 kHz; along with a modulus of elasticity of 0.453±0.32 MPa. The results for the silicone with metal powders showed promising electrochemical and mechanical characteristics with flexible and ductile properties, with the titanium dioxide-based material performing the best. Compared with the values reported in the literature, the results show superior performance. Thus, supporting the composite material's potential for being used in implantable electrode applications.

Keywords: ***implantable electrodes; conductive polymers; electrochemical impedance spectroscopy; silicone-titanium dioxide, silicone-stainless steel.***

Table of Contents

Abstract 6
List of Figure 9
List of Tables 13
List of Abbreviation 15
Chapter 1. Introduction 16
1.1. Overview and Problem Formulation 16
1.2. Thesis Objectives 17
1.3. Research Contribution 17
1.4. Thesis Organization 18
Chapter 2. Literature Review 19
2.1. Nervous System 19
2.1.1. Structural classification 19
2.1.2. Function classification 19
2.1.3. Nervous tissue 19
2.2. Bioelectrodes 22
2.2.1. Types of bioelectrodes 23
2.2.2. Implantable electrode material 24
2.3. Electrical Stimulation 27
2.3.1. Neuromodulation (NM) 27
2.3.2. Functional electrical stimulation (FES) 27
Chapter 3. Methodology 31
3.1. Sample Electrode Preparation 31
3.1.1. Material selection 31
3.1.2. Preparation protocol 31
3.1.3. Ratio testing 32
3.2. Sample Electrode Characterization 32
3.2.1. Electrochemical impedance spectroscopy (EIS) 32
3.2.2. Cyclic voltammetry (CV) 34
3.2.3. Mechanical testing 35
3.2.4. Impedance with Time Test 36
Chapter 4. Titanium Dioxide-Based Material Results 38
4.1. EIS Results 38
4.2. CV Results 40

4.3. Mechanical Testing Results 42
4.4. SEM 42
4.5. Impedance with Time Results 44
4.5.1. Glycerol leaching results 46
4.6. Price Comparison 48
Chapter 5. Stainless Steel-Based Material Results 49
5.1. EIS Results 49
5.2. CV Results 51
5.3. Mechanical Testing Results 52
5.4. Impedance with Time Results 54
5.5. Price Comparison 56
Chapter 6. Mixture of Titanium Dioxide and Stainless Steel-Based Material Results 57
6.1. EIS Results 57
6.2. CV Results 58
6.3. Mechanical Testing Results 60
6.4. Price Comparison 61
Chapter 7. Discussion 62
Chapter 8. Conclusion and Future Work 65
References 66
Appendix A: Detailed Experimental Results 74
A.1. Titanium Dioxide-Based Samples EIS Results 74
A.2. Titanium Dioxide-Based Samples Mechanical Testing Results 78
A.3. Titanium Dioxide-Based Samples Impedance with Time Test Results 79
A.4. Stainless Steel-Based Samples EIS Results 83
A.5. Stainless Steel-Based Samples Mechanical Testing Results 84
A.6. Stainless Steel-Based Samples Impedance with Time Test Results 85
A.7. Titanium Dioxide and Stainless Steel-Based Samples EIS Results 90
A.8. Titanium Dioxide and Stainless Steel-Based Samples Mechanical Testing Results 91
A.9. Code Used for Calculation of Charge Storage Capacity 92
Vita 93

List of Figures

Figure 1.1: Commercial neural electrodes mechanical mismatch with nervous tissue. Figure reproduced from ref. [9] with permission from Springer Nature publication 16
Figure 2.1: Neuron basic structure. Figure reproduced from ref. [16] with permission from Wolters Kluwer Health publication 20
Figure 2.2: Peripheral nerve axons' regeneration process. Figure reproduced from ref. [18] (CC BY-NC 4.0) 21
Figure 2.3: Axon regeneration process. Adopted from ref. [15] 22
Figure 2.4: Types of bioelectrodes interfacing with PNS. Figure reproduced from ref. [19] with permission from John Wiley and Sons publication 22
Figure 2.5: Log scale plot for young's modulus of common material for implantable bioelectrodes. Figure adapted from [20] 24
Figure 2.6: SEM image of gold flexible multi-channel microelectrode. Figure reproduced from ref. [21] with permission from Elsevier publication 25
Figure 2.7: SEM image of PEDOT flexible multi-channel microelectrode. Figure reproduced from ref. [21] with permission from Elsevier publication 27
Figure 2.8: Basic model for closed-loop electronic control in FES. Figure adapted from ref. [20] 28
Figure 2.9: Sketch of implanted upper-extremity neuroprosthesis using myoelectric control. Figure reproduced from ref. [76] with permission from Elsevier publication 29
Figure 2.10: Daily activities of patients two years post-implantation. Figure reproduced from ref. [78] with permission from Elsevier publication 29
Figure 3.1: (a) Teflon mold (b) Bioelectrode batch prepared with a ratio (50% of silicone, 30% titanium dioxide and 20% glycerol) 32
Figure 3.2: Equivalent Randle's circuit and its corresponding Nyquist and impedance bode plots [95] 33
Figure 3.3: Potentiostat (SP-200, Biologic) with customized cell 33
Figure 3.4: General voltammograms for (A) reversible, (B) quasi-reversible, and (C) irreversible electron transfers. Figures reproduced from ref. [98] with permission from Springer Nature publication 34
Figure 3.5: Typical stress-strain curve for tensile testing of polymer film. Figure reproduced from ref. [100] with permission from Springer Nature publication 35
Figure 3.6: Mechanical test performed for TiO_2-based batches 36
Figure 4.1: Nyquist plots for three samples from prepared electrode batch of 30% TiO_2 38
Figure 4.2: Bode plots for three samples from prepared electrode batch of 30% TiO_2 39
Figure 4.3: Voltammogram plot for three samples from prepared electrode batch of 30% TiO_2 40

Figure 4.4: Voltammogram plots for three samples from prepared electrode batch of 30% TiO_2 at different scanning rates 41
Figure 4.5: Stress-strain curve for a TiO_2-based sample 42
Figure 4.6: Top-view of SEM images for one sample of (50% silicone, 30% TiO_2 and 20% glycerol) at different magnifications (a) 2x (b) 10x (c) 35x 43
Figure 4.7: Voltammogram for immersed samples of (50% silicone, 30% TiO_2 and 20% glycerol) in PBS solution (scanning rate of 20 mV/s) 45
Figure 4.8: Current density vs. time plots for immersed samples of (50% silicone, 30% TiO_2 and glycerol) in PBS solution (scanning rate of 20 mV/s).....45
Figure 4.9: Calibration curve samples with increasing quantities of glycerol 15 mg, 30 mg, 45 mg, 55 mg and 70 mg (left to right) 46
Figure 4.10: UV-Visible spectrophotometric absorbance readings of prepared samples for calibration curve 46
Figure 4.11: Calibration curve for glycerol analysis at 650 nm via UV-Visible spectrophotometric analysis 46
Figure 4.12: UV-Visible spectrophotometric absorbance readings of PBS samples ..47
Figure 4.13: UV-Visible spectrophotometric absorbance readings of PBS samples ..48
Figure 5.1: Nyquist plots for three samples from prepared electrode batch of 30% stainless steel 49
Figure 5.2: Bode plots for three samples from prepared electrode batch of 30% stainless steel 50
Figure 5.3: Voltammogram plots for three samples from prepared electrode batch of 30% stainless steel 51
Figure 5.4: Voltammogram for one sample from prepared electrode batch of 30% stainless steel at different scanning rates 52
Figure 5.5: Mechanical test performed for a stainless steel-based sample 53
Figure 5.6: Stress-strain curve for a stainless steel-based sample 53
Figure 5.7: Voltammogram for immersed samples of 30% stainless steel in PBS solution (scanning rate of 20 mV/s) 55
Figure 5.8: Current density vs. time plots for immersed samples of 30% stainless steel in PBS solution (scanning rate of 20 mV/s) 55
Figure 6.1: Nyquist plots for three samples from prepared electrode batch of 20% TiO_2 and 10% stainless steel 57
Figure 6.2: Bode plots for three samples from prepared electrode batch of 20% TiO_2 and 10% stainless steel 58
Figure 6.3: Voltammogram plots for three samples from prepared electrode batch of 20% TiO_2 and 10% stainless steel 59
Figure 6.4: Voltammogram plots for three samples from prepared electrode batch of 20% TiO_2 and 10% stainless steel at different scanning rates 59
Figure 6.5: Stress-strain curve for a TiO_2 and stainless steel-based sample.....60
Figure A.1: Nyquist plots for three samples from first batch of 30% TiO_2 74
Figure A.2: Nyquist plots for three samples from second batch of 30% TiO_2.....74
Figure A.3: Nyquist plots for three samples from third batch of 30% TiO_2 74
Figure A.4: Nyquist plots for three samples from fourth batch of 30% TiO_2 75
Figure A.5: Nyquist plots for three samples from fifth batch of 30% TiO_2 75

Figure A.6: Nyquist plots for three samples from sixth batch of 30% TiO_2 75
Figure A.7: Nyquist plots for three samples from seventh batch of 30% TiO_2 76
Figure A.8: Nyquist plots for three samples from eighth batch of 30% TiO_2 76
Figure A.9: Nyquist plots for three samples from ninth batch of 30% TiO_2 76
Figure A.10: Nyquist plots for three samples from tenth batch of 30% TiO_2 77
Figure A.11: Stress-strain curve for first 30% TiO_2 sample 78
Figure A.12: Stress-strain curve for second 30% TiO_2 sample 78
Figure A.13: Stress-strain curve for third 30% TiO_2 sample 78
Figure A.14: Nyquist plots for three samples of 30% TiO_2 pre-immersion 79
Figure A.15: Nyquist plots for three samples of 30% TiO_2 one week post-immersion 79
Figure A.16: Nyquist plots for three samples of 30% TiO_2 two weeks post-immersion 79
Figure A.17: Nyquist plots for three samples of 30% TiO_2 three weeks post-immersion 80
Figure A.18: Nyquist plots for three samples of 30% TiO_2 four weeks post-immersion 80
Figure A.19: Nyquist plots for three samples of 30% TiO_2 five weeks post-immersion 80
Figure A.20: Nyquist plots for three samples of 30% TiO_2 six weeks post-immersion 81
Figure A.21: Nyquist plots for three samples of 30% TiO_2 seven weeks post-immersion 81
Figure A.22: Nyquist plots for three samples of 30% TiO_2 eight weeks post-immersion 81
Figure A.23: Nyquist plots for three samples from first batch of 30% stainless steel 83
Figure A.24: Nyquist plots for three samples from second batch of 30% stainless steel 83
Figure A.25: Nyquist plots for three samples from third batch of 30% stainless steel 83
Figure A.26: Nyquist plots for three samples from fourth batch of 30% stainless steel 84
Figure A.27: Stress-strain curve for first 30% stainless steel sample 84
Figure A.28: Stress-strain curve for second 30% stainless steel sample 85
Figure A.29: Stress-strain curve for third 30% stainless steel sample 85
Figure A.30: Nyquist plots for three samples of 30% stainless steel pre-immersion 85
Figure A.31: Nyquist plots for three samples of 30% stainless steel one week post-immersion 86
Figure A.32: Nyquist plots for three samples of 30% stainless steel two weeks post-immersion 86
Figure A.33: Nyquist plots for three samples of 30% stainless steel three weeks post-immersion 86
Figure A.34: Nyquist plots for three samples of 30% stainless steel four weeks post-immersion 87
Figure A.35: Nyquist plots for three samples of 30% stainless steel five weeks post-immersion 87

Figure A.36: Nyquist plots for three samples of 30% stainless steel six weeks post-immersion 87
Figure A.37: Nyquist plots for three samples of 30% stainless steel seven weeks post-immersion 88
Figure A.38: Nyquist plots for three samples of 30% stainless steel eight weeks post-immersion 88
Figure A.39: Stainless steel samples post-immersion in PBS 89
Figure A.40: Nyquist plots for three samples from first batch of 20% TiO_2 and 10% stainless steel 90
Figure A.41: Nyquist plots for three samples from second batch of 20% TiO_2 and 10% stainless steel 90
Figure A.42: Nyquist plots for three samples from third batch of 20% TiO_2 and 10% stainless steel 90
Figure A.43: Stress-strain curve for first 20% TiO_2 and 10% stainless steel sample 91
Figure A.44: Stress-strain curve for second 20% TiO_2 and 10% stainless steel sample 91

List of Tables

Table 2.1: Factors influencing material selection for bioelectrodes [1] 24
Table 3.1: Quantities for preparation of calibration curve samples 37
Table 4.1: Comparison of prepared samples impedance for different ratios 38
Table 4.2: ANOVA test for bulk impedance variance between 10 electrode batches .. 39
Table 4.3: ANOVA test for impedance at 1 kHz variance between 10 electrode batches 39
Table 4.4: Comparison table for electrochemical properties from literature 40
Table 4.5: Comparison table for charge storage capacity from literature 41
Table 4.6: Comparison table for mechanical properties from literature 42
Table 4.7: Change of weight of TiO_2-based samples over testing period 44
Table 4.8: Change of bulk impedance in long-term samples before/after CV 44
Table 4.9: Change of impedance at 1 kHz in long-term samples before/after CV 44
Table 4.10: Change of charge storage capacity in long-term TiO_2-based samples 45
Table 4.11: Calculations for estimation of glycerol content and leached percentage of PBS samples 47
Table 4.12: Calculations for estimation of glycerol content and leached percentage of PBS samples 48
Table 4.13: Comparison table for material prices 48
Table 5.1: Comparison of prepared samples impedance for different ratios 49
Table 5.2: ANOVA test for bulk impedance variance between five electrode batches 50
Table 5.3: ANOVA test for impedance at 1 kHz variance between five electrode batches 50
Table 5.4: Comparison table for electrochemical properties from literature 51
Table 5.5: Comparison table for charge storage capacity from literature 52
Table 5.6: Comparison table for mechanical properties from literature 53
Table 5.7: Change of weight of stainless steel-based samples over testing period 54
Table 5.8: Change of bulk impedance in long-term samples before/after CV 54
Table 5.9: Change of impedance at 1 kHz in long-term samples before/after CV 54
Table 5.10: Change of charge storage capacity in long-term stainless steel-based samples 55
Table 5.11: Comparison table for material prices 56
Table 6.1: Comparison of prepared samples impedance for different ratios 57
Table 6.2: Comparison table for electrochemical properties from literature 58
Table 6.3: Comparison table for charge storage capacity from literature 60
Table 6.4: Comparison table for mechanical properties from literature 60
Table 6.5: Comparison table for material prices 61
Table 7.1: Comparison of electrochemical properties between the three investigates materials 62
Table A.1: Bulk impedance results for 10 batches of 30% TiO_2-based samples 77
Table A.2: Impedance at 1 kHz results for 10 batches of 30% TiO_2-based samples ... 77
Table A.3: Change of bulk impedance in 30% TiO_2 based samples during immersion period 82

Table A.4: Change of impedance at 1 kHz in 30% TiO_2 based samples during immersion period....82
Table A.5: Change of charge storage capacity in 30% TiO_2 based samples during immersion period....82
Table A.6: Bulk impedance results for four batches of 30% stainless steel-based samples....84
Table A.7: Impedance at 1 kHz results for four batches of 30% stainless steel-based samples....84
Table A.8: Change of bulk impedance in 30% stainless steel-based samples during immersion period....88
Table A.9: Change of impedance at 1 kHz in 30% stainless steel-based samples during immersion period....89
Table A.10: Change of charge storage capacity in 30% stainless steel-based samples during immersion period....89
Table A.11: Bulk impedance results for three batches of mixture samples of 20% TiO_2 and 10% stainless steel....91
Table A.12: Impedance at 1 kHz results for three batches of mixture samples of 20% TiO_2 and 10% stainless steel....91

List of Abbreviations

CNS	Central Nervous System
Pt	Platinum
Pt-Ir	Platinum-Iridium
PNS	Peripheral Nervous System
FINE	Flat Interface Neural Electrodes
PI	Polyimide
PANI	Polyaniline
PTh	Polythiophene
PPy	Polypyrrole
PEDOT:PSS	Poly (3, 4-ethylenedioxythiophene) Polystyrene Sulfonate
FBR	Foreign Body Response
NM	Neuromodulation
FES	Functional Electrical Stimulation
TENS	Transcutaneous Electrical Stimulation
DBS	Deep Brain Stimulation
TiO_2	Titanium (IV) Dioxide
EIS	Electrochemical Impedance Spectroscopy
CV	Cyclic Voltammetry
CSC	Charge Storage Capacity
PBS	Phosphate Buffer Solution
PPy-PTs	Polypyrrole *Para*-Toluene Sulfonate
PPy-SO_4	Polypyrrole Sulfonate

Chapter 1. Introduction

In this Chapter, an introduction of implantable bioelectrode material is presented, followed by an overview of the topics examined throughout this study, as well as the thesis's contribution. Finally, general organization of the thesis proposal is provided.

1.1. Overview and Problem Formulation

Bioelectrodes serve as the interface between the body and instrumentation system, carrying out functions like recording electrical activity from the body and/or stimulating units within the body [1]. Flexible bioelectrodes are one of the most prominent ventures in the bioelectrodes field. While neuroprosthetic programs have shown remarkable results for neurological injuries, the need for implantable electrodes has intensified. Primarily, market bioelectrodes are metal-based, ranging from noble metals such as platinum-iridium alloys to non-noble metals as stainless steel. Such bioelectrodes face complications originating from mechanical mismatch, shown in Figure 1.1, between the body soft tissues with the rigid electrode; this issue arises in implantable applications as it causes chronic inflammatory response, due to the repetitive abrasion between the two surfaces with tissue and/or electrode micro-motion [2-4]. Additionally, the smooth exterior of metal-based electrodes suppress cell attachment to the surface, creating an inconsistency that triggers the immune system to attempt encapsulating the electrode and repeatedly try to decompose it. Consequently, the electrodes' electrical impedance and mechanical integrity is affected in addition to a risk of creating cytotoxic elements [2, 5]. Several clinical trials have been supported with in-vivo testing, an example is a study conducted on mice: an implanted silicon microelectrode array caused neuronal cell loss in the surrounding tissue [5]; other studies have arrived at the same conclusion [6-8]

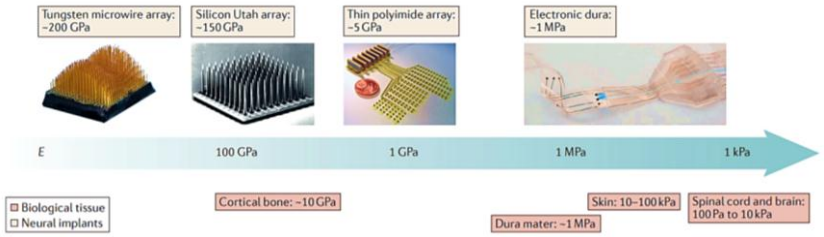

Figure 1.1: Commercial neural electrodes mechanical mismatch with nervous tissue. Figure reproduced from ref. [9] with permission from Springer Nature publication

Although research has offered various solutions to these limitations, including organic coating of metal electrodes [10] and synthesis of metal-polymer hybrids, none have been able to provide materials that excel in all needed qualities. This thesis presents the fabrication and properties of novel bioelectrode material with comparable properties to those of conventional electrodes. The material is composed of silicone polymer (polysiloxanes), metal powder of titanium (IV) dioxide (TiO_2) or stainless steel (316 grade) powder or both, and glycerol. The prepared material is biocompatible, flexible and conductive at comparable levels to those of conventional electrodes.

1.2. Thesis Objectives

Within this work, we aim to produce a low-cost, bioelectrode material that is biocompatible and stable over time, to prevent foreign body response during long-term implantation. Additionally, it should possess mechanical properties that are comparable to the muscular and neural body tissue, and electrical conductivity, to transmit the electrical impulses to the target tissue. Thus, we designed our electrodes to be composed of a composite mixture of silicone polymers and metal-based material. The polymers provide the desired mechanical properties while the metals provide conductivity. In order to achieve our goal we performed the following:

- Prepare electrodes with different combinations of polymer and metal/metal oxide:
  - Silicone + titanium dioxide
  - Silicone + stainless steel
  - Silicone + stainless steel + titanium dioxide
- Conduct testing protocols to assess the electrical, electrochemical, mechanical, durability and biocompatibility properties of the prepared material.
- Based on the testing results, optimize the electrodes performance and electrochemical and mechanical properties by varying the composition (mass %) of the different components (polymers, metals…etc) and monitoring the effect on the electrode properties.

1.3. Research Contribution

Research work has been going in the field of implantable electrodes [4, 10-12], and different electrodes materials were investigated including noble metals such as gold, or conductive polymers such as PEDOT:PSS. Although functional, these

materials still suffer from different limitations. In this project, titanium dioxide and stainless steel are proposed to fabricate implantable electrodes. The combination of titanium dioxide/stainless steel within silicone polymer and glycerol (to improve mixing and conductive properties) is investigated for the first time in the literature. Generally, silicone has been used as an insulating material due to its biocompatibility and stability [13]. The result of this work would be the fabrication of functional implantable flexible electrodes at a lower cost and obtain improved properties such as flexibility and lower interfacial impedance.

1.4. Thesis Organization

The rest of this thesis is arranged as follows: Chapter 2 reviews background of anatomy and physiology of the body's nervous system, followed by a discussion of bioelectrodes types and materials, then applications of the implanted bioelectrodes are examined. Chapter 3 discusses the experimental plan, the preparation process, in addition to the assessment methods of bioelectrode material and the preliminary results obtained so far are presented. Chapters 4, 5 and 6 discuss the results of assessing titanium dioxide, stainless steel and the mixture of both, respectively. In Chapter 7 the results are discussed. Finally, Chapter 8 consists of the conclusion and suggested future work.

Chapter 2. Literature Review

In this chapter, the nervous system and its anatomical and physiological components are reviewed. Then, an examination of bioelectrodes, their types, compositions and medical application is presented. Finally, clinical trials based on implantable electrode systems are discussed.

2.1. Nervous System

The nervous system is responsible for regulating the body's main functions, it is a rapid control system that conducts its signals via electrical nerve impulses that stimulate muscles and gland [14]. It is an inherently complex system with many classifications to explain its functionality.

2.1.1. Structural classification. The nervous system is structurally divided into the central nervous system (CNS) and the peripheral nervous system (PNS). The CNS consists of the brain and the spinal cord, whereas the PNS comprises of everything else. These two systems are coordinated in such way that the PNS is responsible for sensory input and carrying out signals generated by the CNS in response [14].

2.1.2. Functional classification. The PNS is further classified into the sensory branch (Afferent) that transmits sensory inputs to the CNS, and the motor branch (Efferent) that carries ensuing output from the CNS to stimulate muscles/glands [14]. Even though the PNS controlling effects are mostly involuntary (autonomic control) with sympathetic and parasympathetic systems, there is also the segment that controls the skeletal muscles, which falls under voluntary control that is the somatic subdivision [14].

2.1.3. Nervous tissue. Comprising of only two main types: Nerve cells (neurons) and glial (supporting) cells, in which neurons represent the structural/ functional unit of the nervous system [15]. While the neurons are responsible for conducting the impulses to and from the CNS, they are fragile and in need of support in the form of nourishment, insulation and protection that is provided by the glial cells. There are many types of glial cells, such as schwann cells that form the myelin sheath to insulate PNS axons, allowing faster nerve impulse conduction through the

axons [15]. Furthermore, research has shown that they are crucial for the peripheral nerves regeneration (discussed in 2.3.4) [17].

2.1.3.1. ***Neuron structure.*** As shown in Figure (2.1), there are basic structures that are prevalent in all the neurons in the nervous system; the cell body and its processes: dendrites, which are relatively shorter and responsible for receiving signals, and axons (nerve fibers) that are longer and transmit the signal to other neurons at the synaptic cleft [14]. Within the cell body there are many internal structures, including neurofilaments that give rise to neurofibrils, structural component that provide form and strength to dendrites and axons [15]. Moreover, there are layers that envelope the axons in most neurons, called the mayelin sheath, formed by the glial cells (oligodendrocytes in CNS, schwann cells in PNS). The myelin sheath is responsible for supporting and insulating the axons, in addition to boosting up the nerve impulse along the axon with the help of the nodes of ranvier, which are gaps within the myelin sheath at evenly matched distances [14]. The myelin sheath formed by the schwann cells has an outer layer referred to as the neurilemma, composed of the cytoplams of the schwann cells; it plays an important role in the regeneration process of the PNS neural axons [15].

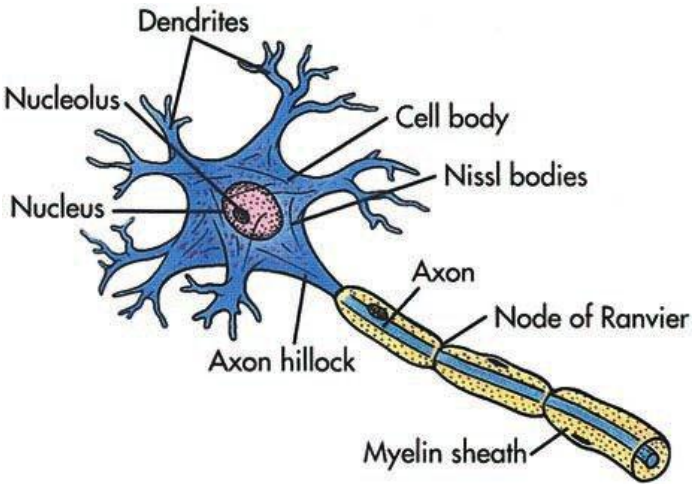

Figure 2.1: Neuron basic structure. Figure reproduced from ref. [16] with permission from Wolters Kluwer Health publication

2.1.3.2. ***Neuron functional classification.*** Based on the direction of the electrical impulse, to or away from the CNS, neurons can be classified into sensory (afferent) neurons and motor (efferent) neurons. Sensory neurons' cell bodies exist in ganglions outside the CNS, and they are characterized by specialized receptors within their dendritic endings. Whereas, motor neurons carry impulses to the effector

structure and to the interneurons that attach to both types and are important for reflex reactions [14].

2.1.3.3. ***Nerve impulses.*** At resting state, the plasma membrane of a neuron axon is polarized. When a part of the neuron is stimulated, it starts to depolarize and an action potential is formed at the site of depolarization, after some period, the membrane starts to go back to its resting state while the next part goes through depolarization [14]. Figure 2.2 shows nerve impulse propagation process through unmyelinated axons, in which the axon membrane has to undergo depolarization/repolarization in a process referred to as continuous conduction, a relatively slow process [15]. However, in motor neurons in which the nerve impulse has to travel in a more rapid manner, the process is different due to the presence of myelin sheath, an insulator that causes the action potential to form only at the gaps (nodes of ranvier), and travel along the axon in a process called saltatory conduction [15, 17].

2.1.3.4. ***Axon regeneration.*** As a delicate tissue, PNS axons are susceptible to injuries and damage; nonetheless, if small parts of neurilemma remain, the axon can be regenerated. This regeneration process depends on the extent of the injury, production of nerve growth factors by neurilemma, and the gap length between the damaged axon and the effector organ, as shown in Figure (2.2) [15]. The regeneration process is referred to as Wallerian Degeneration, explained in Figure (2.3), and it is guided by the schwann cells [15].

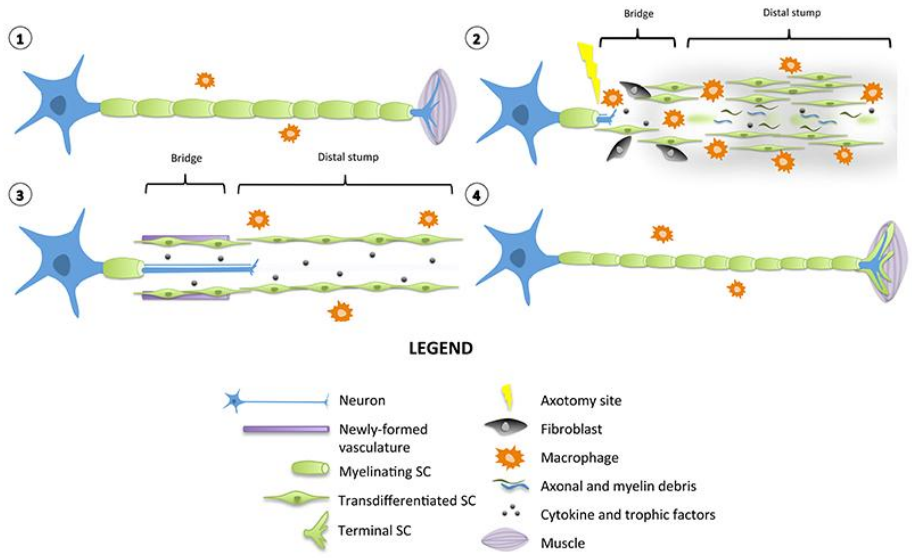

Figure 2.2: Peripheral nerve axons' regeneration process. Figure reproduced from ref. [18] (CC BY-NC 4.0)

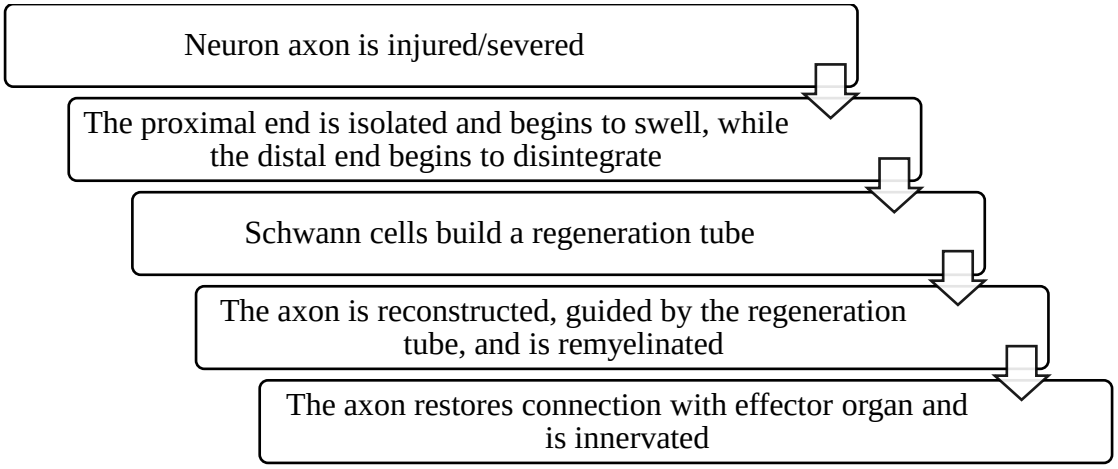

Figure 2.3: Axon regeneration process. Adopted from ref. [15]

2.2. Bioelectrodes

As the interface between the electronic system and biological tissue, the neural electrode must have the ability to register the bioelectrical signals within the body and deliver any stimulation signal from the instrumentation system to the target tissue (nerve/muscle), thereby functioning in a bidirectional manner. In this work, the focus will be on PNS electrodes, and their types and compositions will be discussed as such.

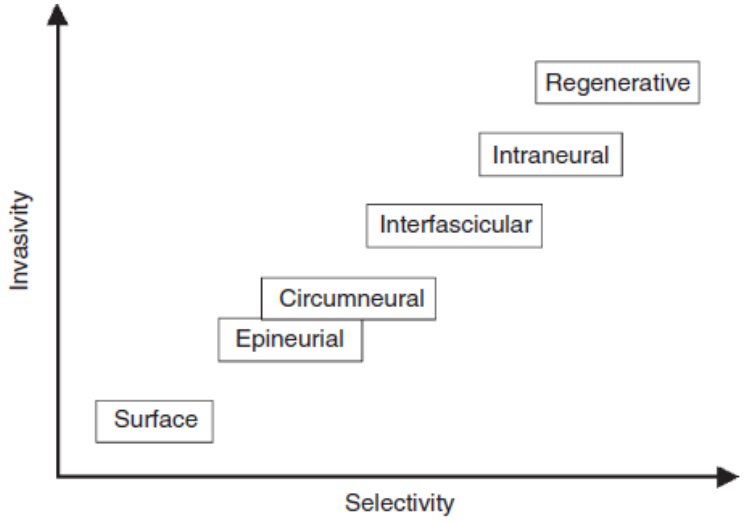

Figure 2.4: Types of bioelectrodes interfacing with PNS. Figure reproduced from ref. [19] with permission from John Wiley and Sons publication

2.2.1. Types of bioelectrodes. PNS electrodes are inserted next to, surrounding or within the peripheral nerve trunks or spinal roots [15]. With respect to the invasiveness and selectivity of the bioelectrodes, they can be classified into different groups, arranged in Figure 2.4.

2.2.1.1. ***Surface electrodes***. Also referred to as transcutaneous electrodes, such electrodes are minimally invasive; they are employed in physiological signals recording such as electrocardiogram (ECG) and electroencephalogram (EEG) in addition to the stimulation of nerves/muscles close to skin surface. However, such electrodes have little selectivity, and therefore cannot be used in precise nerve stimulation [19]. An example of such electrode is the silver/silver chloride electrodes.

2.2.1.2. ***Muscle electrodes.*** That include epimysial electrodes, which are flat strips secured on the epimysium of the muscle, and intramuscular percutaneous electrodes that generally consist of exposed tip of a conductive wire; for instance, Teflon-insulated stainless steel wire, inserted into the intended muscle. These electrodes deliver electrical signals to nerve fibers interconnected within the muscle, they can also record good quality electromyogram (EMG) signals. However, maintaining muscle stimulation is a complex procedure that requires multiple electrodes and proper calibration; additionally, the needed stimulation charge is much higher due to the lack of direct connection with the nerve fibers [19].

2.2.1.3. ***Neural electrodes.*** Such electrodes are classified into extraneural and intraneural electrodes depending on the insertion site. These electrodes are customarily manufactured from flexible material such as silicon, for protection and insulation, with specific conductive points that are placed in contact with the nerve.

2.2.1.3.1. *Extraneural electrodes.* These neural electrodes are usually attached to the epineurium of the PNS and they vary according to their attachment method. The subtypes of these electrodes include epineurial and helicoidal which are implanted alongside the nerve. Additionally, there are circumneural (cuff) electrodes that envelope the nerve fibers with little flexibility, and flat interface nerve electrodes (FINE) that directly press and enclose the nerve. There is also interfascicular electrode that slightly differs from its counterparts; these are implanted via puncturing the epineurium to establish contact with the nerve fascicles [1, 19].

2.2.1.3.2. *Intraneural electrodes.* These neural electrodes have improved accuracy and signal-to-noise ratio in comparison with extraneural electrodes. They consist of intrafascicular electrodes that are implanted directly onto the designated nerve fascicle, in addition to penetrating microelectrodes that are miniaturized arrays of intrafascicular electrodes. Furthermore, there are regenerative electrodes that incorporate arrangements of spaces designated for severed PNS axons, which guide

the regenerating axons and transfer electrical signals to facilitate in the reconstruction process [17, 19].

2.2.2. Implantable electrode material. The material used in manufacturing implantable electrodes, consisting of muscular and neural electrodes, is of paramount importance with multiple factors, shown in Table 2.1. Commonly used material in implantable electrodes include: inert metals and conductive polymers.

Table 2.1: Factors influencing material selection for bioelectrodes [1]

Electrode	Surface area, geometry, and surface condition
Electrical	Potential, current, and quantity of charge
Environmental	Mass-transfer variables and solution variables
Engineering	Availability, cost, strength, and fabricability

2.2.2.1. *Inert Metals.* Traditional bioelectrode interfaces were metal based, including inert metals such as platinum (Pt), gold (Au) and silver (Ag), in addition to metal alloys such as platinum-iridium (Pt-Ir) [1, 2]. Platinum is the leading material in neural prosthesis [2] and deep brain stimulation (DBS) [11]. However, such platinum electrodes are inherently rigid and have mechanical mismatch with the soft tissue; this is demonstrated in the log-scale plot of Figure 2.5.

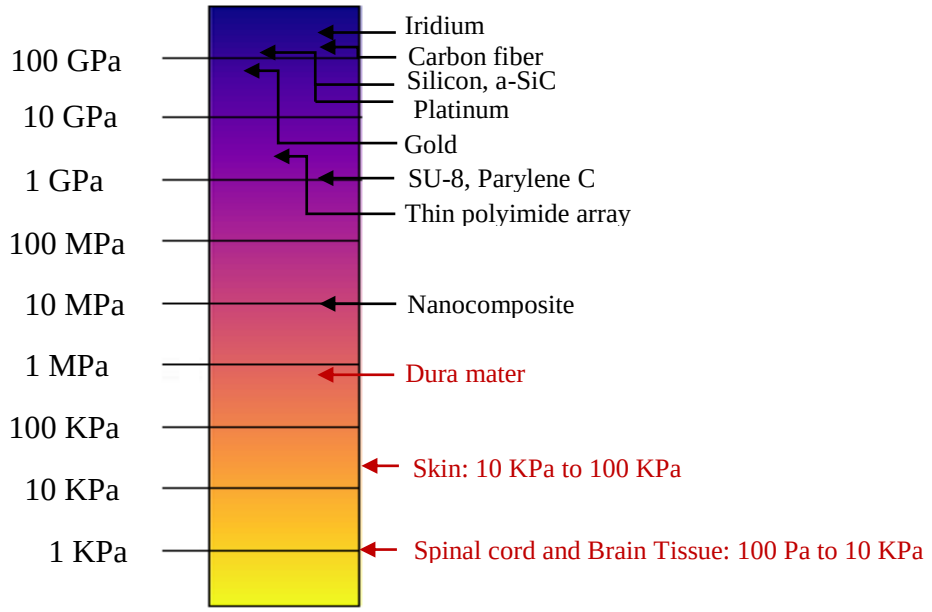

Figure 2.5: Log scale plot for young's modulus of common material for implantable bioelectrodes. Figure adapted from [20]

This issue arises in implantable applications as it causes chronic inflammatory response, due to the repetitive abrasion between the two surfaces with tissue and/or electrode micro-motion [2-4].

Additionally, the smooth exterior of metal-based electrodes, as shown in Figure 2.6, suppress cell attachment to the surface, creating an inconsistency that triggers the immune system to attempt encapsulating the electrode; thereby increasing the electrode's impedance, and repeatedly try to decompose it; thus risking a possibility of creating a cytotoxic elements [2].

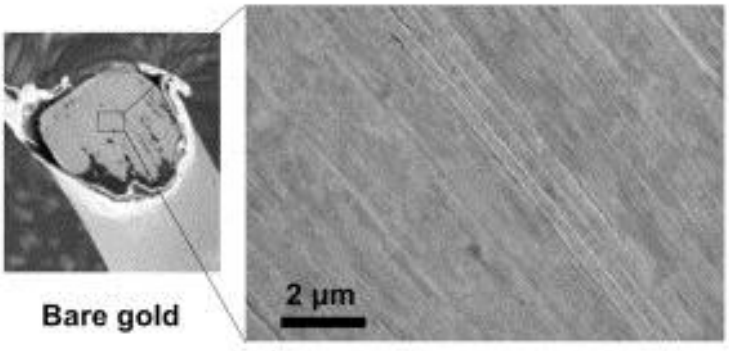

Figure 2.6: SEM image of gold flexible multi-channel microelectrode. Figure reproduced from ref. [21] with permission from Elsevier publication

There has been research work to overcome foreign body response (FBR) by coating metal electrodes with organic coating [22], particularly in the work of Harris et al [10], in which iridium-based electrodes were coated with polypyrrole (Ppy) and 3,4-ethylenedioxythiophene (PEDOT). On the other hand, market implantable electrodes are generally metal-based with polymer coating layer, such as NeuroNexus that fabricate neural electrodes that are coated with silicon or polyimide (PI) [23]. Besides with the rigidity of the metals, the issue of mechanical mismatch remains unresolved.

2.2.2.2. ***Conductive polymers.*** Of the many proposed substitutes of metal bioelectrodes, the use of conductive polymers presented a breakthrough in the bioelectrode materials research. They possess high conductivity [24-30], and improved mechanical properties [29, 30]. In addition, the physical and chemical properties can be adjusted according to the function, via the incorporation of organic components [27, 31, 32].

2.2.2.2.1. *Polyimide (PI).* Composed of a chain of imide monomers, this polymer has the properties of high conductivity with doping [33], and insulation as a pure polymer [4, 33], as well as the biocompatibility in long-term implantation [4]. In addition, it possesses the required chemical and mechanical stability under physiological conditions [34]. Consequently, PI has been used in multiple biomedical application i.e. neural probes exemplified by NeuroNexus neural probes [23]. However, PI is a rigid material with a modulus of 6 GPA approximately [35]. Moreover, it is a brittle material that can only reach an elongation of <10% before rupturing [34]. Such limitations affect the PI's implantable applications.

2.2.2.2.2. *Polyaniline (PANi).* Also referred to as aniline black, this polymer is made up of aniline monomers [36]. It has been researched extensively in the past 20 years, due to its relatively low cost, ease of synthesis, stability and easy modifications [37-41]. However, similar to PI, PANi is rigid, and it is not a biodegradable material that can cause chronic inflammation for long-term implants [38, 42, 43]. Even so, there are researches into incorporating PANi into biosensors and drug delivery applications [44, 45].

2.2.2.2.3. *Polythiophene (PTh).* Polymerized thiophene monomers that become conductive when oxidized [46]. It has many derivatives, including poly(3,4-ethylenedioxythiophene) (PEDOT), which along with its modification poly(3,4-ethylenedioxythiophene) polystyrene sulfonate (PEDOT:PSS) has been proposed as one of the best conductive polymer, due to its high conductivity, in addition to chemical, electrical, environmental and thermal stability under physiological conditions [29, 30]. Therefore, PEDOT:PSS has been used in medical applications i.e. biosensors [36], neural electrodes and nerve grafts [30, 47]. Unlike other conductive polymers, PEDOT:PSS is relatively ductile material, however, it is still rigid with its thin films having a modulus 1.8 GPa approximately, indicating issues arising from long-term implantation [48].

2.2.2.2.4. *Polypyrrole (PPy).* The precedent of conductive polymers, as it is the most studied polymer for bioelectrodes, especially with its simple fabrication and modification [24-27, 32, 49, 50], biocompatibility [24, 25, 32, 51], in addition to its high electrical conductivity and stability [24-28]. Despite such promising properties, polymer it is a rigid and brittle material [32, 36, 52], and when fabricated, it is difficult to process [53], therefore, limiting its long-term implantation

applications. However, it has been widely used in neural tissue engineering [36, 54-57] and drug delivery systems [27, 36].

2.2.2.2.5. *Poly (3, 4-Ethylenedioxythiophene) (PEDOT).* Considered to be the most promising conductive polymer for its properties of high conductivity and easy processing [58]. Figure 2.7 shows an SEM image for a PEDOT-based microelectrode. It is commercially available as aqueous dispersion that can be used to form thin films via solvent casting or spin coating [59]. Recent research projects have included PEDOT Polystyrene Sulfonate (PEDOT:PSS) in bioelectrodes, biosensors, organic electrochemical transistors and for coating of metals [60-62].

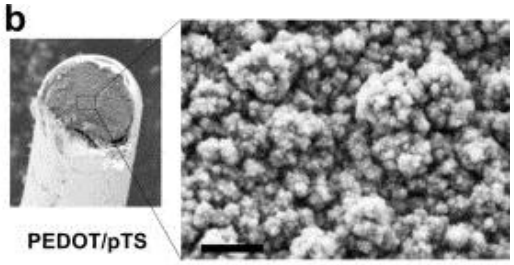

Figure 2.7: SEM image of PEDOT flexible multi-channel microelectrode. Figure reproduced from ref. [21] with permission from Elsevier publication

To summarize, conductive polymers have superior electrochemical and biocompatibility properties. However, their mechanical properties are still restricting their implantable applications due to their rigidity and brittleness material.

2.3. Electrical Stimulation

As the interface with the biological tissue, implantable bioelectrodes dualistic function of recording and delivering electrical signals has been capitalized in many medical and therapeutic applications, including neuromodulation (NM) and functional electrical stimulation (FES).

2.3.1. Neuromodulation (NM). Largely used in pain subjugation, this type of practice depends on the application of electrical stimulation to the afferent nerves advancing to the brain and spinal cord, which induce a variation in the excitatory or inhibitory signals of the neural network [20, 63]. Pain management by means of NM is based on Melzack and Wall's ''gate control theory of pain'', that explains the inhibitory effect of stimulating specific fibers on the pain nerve pathways within the spine; the concept is also applied on spasticity disorders such as Parkinson's disease

[64]. Additionally, NM is an established practice in managing conditions of respiratory problems such as hypoventilation [65], bladder [66] and bowel disorders [67], in addition to augmentation of sexual function [68]. Such stimulation is accomplished by means of transcutaneous electrical stimulation (TENS), peripheral nerve, spinal cord, cortical or deep brain simulations [64].

2.3.2. Functional electrical stimulation (FES). Similar to NM, an electrical signal is applied to nerves; however, in FES, the motor neurons and their corresponding muscles are targeted; additionally, muscular contractions are synchronized to perform their functions. This treatment is focused on attenuating muscle atrophy [69] whilst simultaneously facilitating the neural connection reparation [20]. Although stimulation electrodes are commonly attached to the muscles (muscles electrodes), the applied stimulation is more likely to activate the nerves rather than the muscle fibers due to their lower threshold. Accordingly, FES's purpose is the recovery of the neuromuscular activity in cases of partial or complete spinal/brain lesions that lead to loss of voluntary motor control. In such cases, the connection between the lower (spinal) motor neurons innervating the muscles, and the upper (cortical) ones is severed; consequently the voluntary activation fails and the patient loses movement ability [70].

There have been multiple FES systems produced for rehabilitation of upper and lower extremities, in addition rectification of disorders in bladder, bowel and respiratory system [70]. Furthermore, FES has been utilized in exercise regimen for healthy adults and athletes [71]. Such systems utilize a closed-loop model as shown in Figure 2.8.

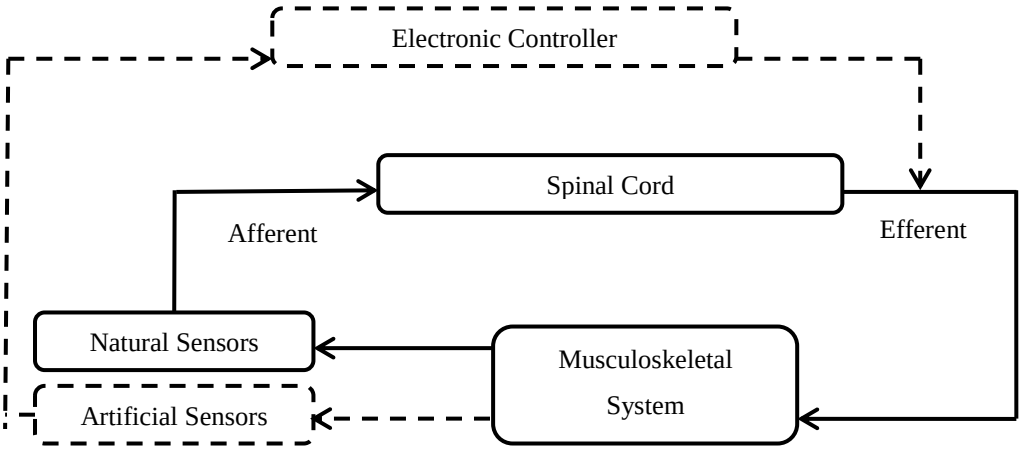

Figure 2.8: Basic model for closed-loop electronic control in FES. Figure adapted from ref. [20]

In addition to preventing muscle atrophy, electrical stimulation has shown significant results in peripheral axonal regeneration, this is stipulated by the presence of schwann cells in the injury site. In the paper "Electrical Stimulation of Schwann Cells Promotes Sustained Increases in Neurite Outgrowth", it was demonstrated that the electrical co-stimulation *in vitro* of neurons and schwann cell advanced neurite outgrowth, this has been supported by numerous studies that show larger neurite outgrowth with electrical stimulation [12, 17, 44, 72-75].

There have been multiple clinical trials of FES in upper and lower extremities. An example is the implanted stimulator-telemeter (IST-12) system shown in Figure 2.9, consisting of an 8-channel system with 8 epimysial electrodes for stimulation and 2 EMG electrodes for control [76]. The system was implanted in patients suffering from upper spinal injuries leading to the loss of arm movement, and was evaluated over a period of 2 years. The merit of the system was the use of closed-loop model with no external controls needed. The trial results showed a considerable improvement of daily activities, as shown in Figure 2.10, and no device failure [76]. This is backed up by additional clinical trials for upper extremity FES systems, including the freehand system [77].

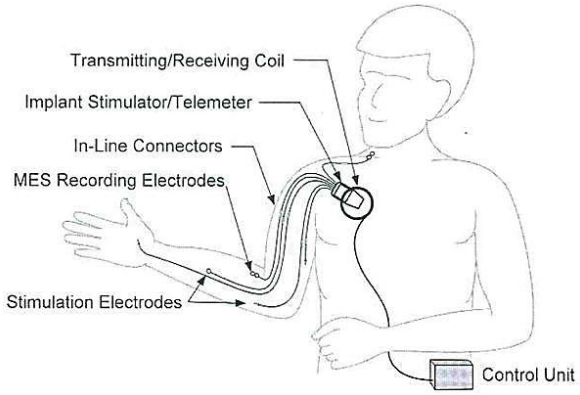

Figure 2.9: Sketch of implanted upper-extremity neuroprosthesis using myoelectric control. Figure reproduced from ref. [76] with permission from Elsevier publication

Figure 2.10: Daily activities of patients two years post-implantation. Figure reproduced from ref. [78] with permission from Elsevier publication

In regards to complex lower limb movements, over 48 muscles have to be stimulated and managed [79]. Multiple studies have attempted to simplify this process; i.e. stimulating simpler motion of foot inversion/eversion using implanted two-channel systems [80]. Whereas other trials have incorporated more complex systems to generate simple motions such as standing or transferring, such as the trials carried out at the Case Western Reserve University, with an 8-channel system, consisting of epimysial electrodes, that was tested over the period of 4 years and had successful results [81]. In addition to FES systems progress in peripheral nerve rehabilitation; there have been successful trials in improvement of gait patterns for stroke patients, similar to the rehabilitation departments of Sun Yat-sen Memorial Hospital after 3 weeks of training [82].

Chapter 3. Methodology

In this chapter, the preparation protocol of the samples is discussed, in addition to the testing methods used to assess the material's electrochemical and mechanical properties.

3.1. Sample Electrode Preparation

3.1.1. Material selection. In this thesis, novel bioelectrode batches were synthesized from silicone polymer, with titanium dioxide or stainless steel powders or both, in addition to glycerol. Silicone has been used in neuroprosthetic interfaces [83] and plastic surgery implants for many years and showed good biocompatibility with little to no immunological response [84]. In addition to the recent research into employing it for biosensor applications [85]. On the other hand, titanium dioxide (TiO_2) is a metal oxide that possesses valuable conductive and biocompatible properties [86-88]. Similarly, stainless steel has been widely used in medical implants due to its excellent biocompatibility properties [89, 90]. Additionally its' electrodes have been reported to produce very little immunological reaction with resistance to corrosion when implanted long term in clinical trials [91] and in animal trials [92]. Glycerol has unique properties of biocompatibility and stability [93] in addition to its conductivity [94], and it assists in mixing and dispersion.

The material to be used are the commercially available silicone sealant from Red Devil (100% silicone), titanium (IV) oxide powder (Anatase ≥ 99%, −325 mesh) from Sigma-Aldrich, stainless steel powder (AISI 316 alloy, Fe/Cr18/Ni10/Mo3, 45 μm) from GoodFellow, in addition to glycerol ($C_3H_8O_3$) (Certified ACS from Fisher, assay ≥ 99.5%).

3.1.2. Preparation protocol. After obtaining the needed ratio needed for the batches, the mixture is mixed well manually for a two minutes at most until a uniform blend is achieved. Then, the material was set in custom-made Teflon mold, shown in Figure 3.1a, prepared in the machine shop on campus, with a length of 5.0 cm, width of 0.6 cm and thickness of 0.2 cm. These are left to dry for 24 hours in the fume hood at room temperature, (Figure 3.1b shows a finalized batch).

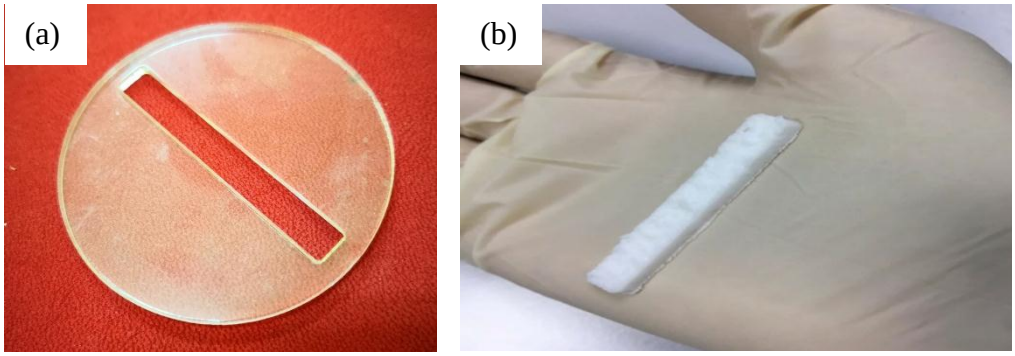

Figure 3.1: (a) Teflon mold (b) Bioelectrode batch prepared with a ratio (50% of silicone, 30% titanium dioxide and 20% glycerol)

3.1.3. Ratio testing. Initially, multiple batches with different ratios of the material are tested to determine the optimal ratio of the materials. The tested ratios were 70% silicone, 15% metal powder and 15% glycerol, and 50% silicone, 30% metal powder and 20% glycerol, this can be justified by glycerol proportion as it cannot exceed 20% or the prepared batches will not dry properly. Additionally, if the metal powder proportion exceeded 35%, then it will hinder mixing and a uniform mixture becomes difficult to achieve. After the initial testing, multiple batches were prepared from 50% silicone, 30% metal powder and 20% glycerol; this ratio showed the best performance as will be discussed in the following section. Statistical analysis was performed on the prepared batches based on either titanium dioxide or stainless steel to verify the reproducibility.

3.2 Sample Electrode Characterization

3.2.1. Electrochemical impedance spectroscopy (EIS). A non-destructive assessment technique that involves evaluating the corresponding impedance to a sinusoidal input of varying frequency, with a mathematical approach analogous to Ohm's law; interdependency of sinusoidal voltage potential *E(t)* with a frequency of *(w)* and corresponding current *I(t)* with the same frequency and a phase shift of *(Φ)*, accordingly the electrochemical impedance is calculated as shown in equation 3.1.

$$Z(w) = \frac{E(t)}{I(t)} = \frac{|E_o|\sin(wt)}{|I_o|\sin(wt-\Phi)} = Z_o \frac{\sin(wt)}{\sin(wt-\Phi)} \tag{3.1}$$

where

$$E(t) = E_o e^{jwt} \tag{3.2}$$

$$I(t) = I_o e^{jwt-j\Phi} \tag{3.3}$$

$$Z(w) = |Z_o|e^{j\Phi} = |Z_o|\cos\Phi + j|Z_o|\sin\Phi = Z_{Re} + jZ_{Im} \quad (3.4)$$

Thus, the impedance can be expressed as a sum of the real (Z_{Re}) and imaginary impedance (Z_{Im}), this is utilized in the Nyquist Plot, in which the real impedance is plotted against the imaginary impedance at each frequency. The importance of such representation is that it allows the determination of the analogous electrical circuit and its components [95].

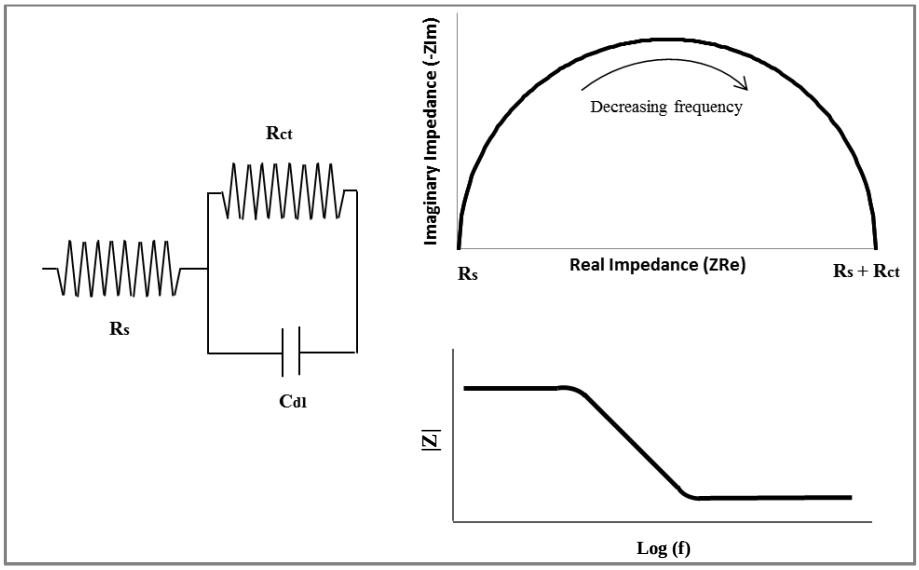

Figure 3.2: Equivalent Randle's circuit and its corresponding Nyquist and impedance bode plots [95]

The model, shown in Figure 3.2, is composed of a resistor in series with a parallel combination of a second resistor and a capacitor. Its corresponding nyquist plot is a semi-circle with an x-axis intersection, at high frequencies, representing the ohmic/bulk resistance; also, the diameter is equal to the charge transfer resistance, originated from the electrochemical reactions. While the capacitance of the double electric layer that is loaded along the electrochemical reaction is found via the calculation of the highest impedance magnitude [95].

Figure 3.3: Potentiostat (SP-200, Biologic) with customized cell

EIS was conducted on the batches prepared, it was performed using Potentiostat (SP-200, Biologic), shown in Figure 3.3, in which a customized cell with stainless steel electrodes was used, the electrode samples' cross sectional area was 0.785 cm^2. The applied voltage was set to 10 mV with a frequency range of f_i = 7 MHz to f_f = 100 Hz, while the software (EC lab software v11.02) recorded the response of the sample. The data was fitted into the model shown in Figure 3.2, and analysed as such. Additionally, the impedance at 1 kHz was extracted, as it represents the neural activity frequency [96]. Moreover, the test samples' thickness and cross-sectional area were measured using vernier caliper. This will be used to calculate the material's conductivity based on equation 3.5 [95].

$$\sigma = \frac{T}{R_S \times A} \tag{3.5}$$

where T is the thickness, A is the cross sectional area and Rs is the electrical resistance.

3.2.2. Cyclic voltammetry (CV). A non-destructive qualitative test that enables the investigation of reduction/oxidation reactions on the molecular level [97], it is carried out by applying a cyclic potential at the electrode and measuring the generated current within, then plotting the data in a voltammogram, as shown in Figure 3.4. The peaks height and location are recorded and used in the characterization process [98].

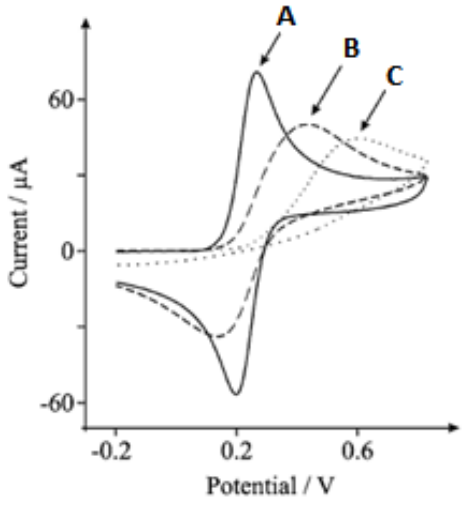

Figure 3.4: General voltammograms for (A) reversible, (B) quasi-reversible, and (C) irreversible electron transfers. Figure reproduced from ref. [98] with permission from Springer Nature publication

Cyclic voltammetry is an important tool to understand the reduction/oxidation reactions and possible adsorption process that takes place when alternating voltage is applied, in addition to ascertaining the stability of reaction products or the possibility of intermediates. Additionally, it helps to interpret the kinetics of electron transfer [97, 98]. The test was carried out in the same equipment used for EIS, Potentiostat Potentiostat (SP-200, Biologic), with similar frequency range, f_i = 7 MHz to f_f = 100 Hz, while the voltage range will be from -2V, 2V. In addition, software (EC lab software v11.02) was used to record and analyse the data.

Furthermore, the data was used to calculate the Charge Storage Capacity (CSC), which represents the upper limit of charge density allowed during a single pulse of electrical stimulation [97, 99]. Based on D. Park et al, CSC can be calculated by integrating the cathodal current density, which is the recorded current divided by the samples area of 0.785 cm^2, followed by dividing by the square root of scanning rate [99].

3.2.3. Mechanical testing. The testing method chosen was a quasi-stastic uniaxial tension test using Instron (5582 Universal Testing Method, Instron), in which a batch undergoes controlled tensile force until failure. The data were plotted in a stress-strain format, similar to Figure 3.5, and the parameters chosen to be studied were the modulus of elasticity and elongation% as they are indicators of flexibility and ductility respectively.

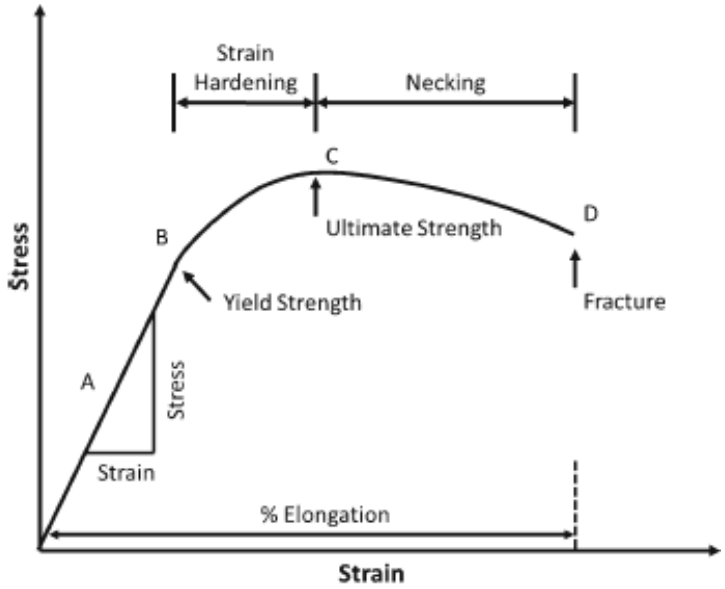

Figure 3.5: Typical stress-strain curve for tensile testing of polymer film. Figure reproduced from ref. [100] with permission from Springer Nature publication

The batch, as shown in Figure 3.6, was subjected to a displacement rate of 5 mm/min, and the test was carried out until rupture, then the results were displayed and extracted by Instron Bluehill.

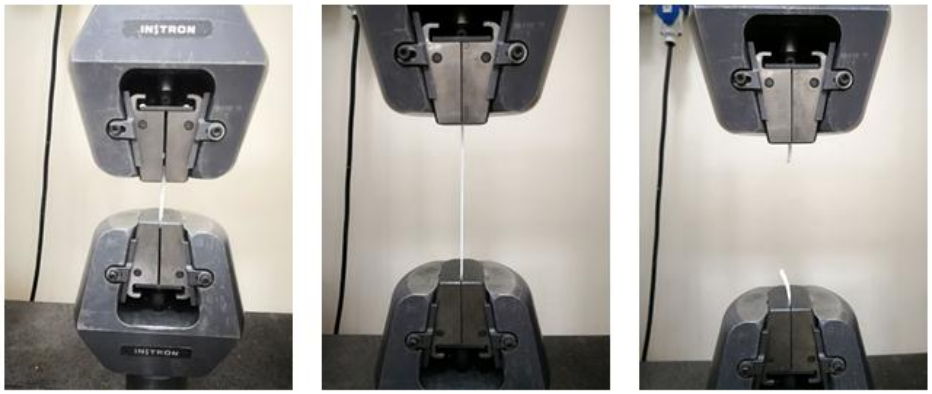

Figure 3.6: Mechanical test performed for TiO_2-based batches

3.2.4. Impedance with time test. For better understanding of the effects of long-term implantation on the material's properties, multiple samples were immersed in a neural tissue model comprising of phosphate buffer solution (PBS) and agrose gel [101] for eight weeks with a one-week testing interval. At the end of each week, an EIS test was performed to measure the change of impedance with time. The benefit of this test is to evaluate the durability/impedance of these implantable electrodes as a function of time when exposed to body fluids.

3.2.4.1. Glycerol Leaching. Afterwards, the long-term immersion test was carried out, in which 24 electrode samples with 30% titanium dioxide were prepared and immersed in eight tubes containing 10.5 mL of 10% PBS solution with a one-week testing interval. At each week (with the exception of week five) three samples were extracted from their tubes, and the PBS solution was tested for leached glycerol from the material.

The protocol for testing leached glycerol was based on Spagnolo [102], which describes a procedure for testing solution containing a range from 15 mg to 90 mg of glycerol. The glycerol reacts with the cupic chloride reagent to form a sodium-cupri-glycerol complex that can be detected using spectrophotometer at a wavelength of 650 nm.

First, calibration curve samples were prepared using stock solution of glycerol composed of 600 mg of glycerol in 39.4 mL of PBS, which is equivalent to one mg of glycerol per one mL of solution. Then specified amounts of stock solution and PBS were pipetted into 100-mL volumetric flask according to Table 3.1.

Table 3.1: Quantities for preparation of calibration curve samples

Calibration Curve Sample	Glycerol Mass (mg)	Stock Solution (mL)	PBS (mL)
Sample 1	1.5	1.5	8.5
Sample 2	3.0	3.0	7.0
Sample 3	4.5	4.5	5.5
Sample 4	5.5	5.5	4.5
Sample 5	7.0	7.0	3.0

Then 10 mL of NaOH solution were added, followed by 60 mL of ethanol. Later, using a burret six mL of cupic chloride reagent was slowly added to the mixture, which was then shaken vigorously for two minutes. The mixture was diluted to 100 mL by adding 14 mL and shaken again. 10 mL of the solution was transferred into a tube and centrifuged using (HERMLE Labortechnik) centrifuge for 10 min at r.c.f of 4180. Finally, two mL of the clear solution was transferred to a spectrophotometric cell, and then absorbency readings are taken using Cary 50 Conc UV-Visible Spectrophotometer (Varian, Australia) from 400 nm to 800 nm, to determine the absorbency at 635 nm that is the wavelength in which the complex absorbs light. The baseline and references samples prepared consisted of 1.06 mL of NaOH, 7.88 mL of ethanol and 1.06 mL of PBS. After preparing calibration curve; the procedure was repeated for the PBS samples in which the specimens were immersed in.

Chapter 4. Titanium Dioxide-Based Material Results

In this chapter, the experimental results for the electrochemical and mechanical testing of titanium dioxide-based batches are presented, followed by a comparison with market bioelectrode material discussed in previous chapters.

4.1 EIS Results

The tested ratios were of silicone, titanium dioxide and glycerol were 70:15:15 and 50:30:20 respectively, this can be justified by glycerol proportion as it cannot exceed 20% or the prepared batch will not dry properly. Additionally, if the titanium dioxide proportion exceeded 35%, then it will hinder mixing and a uniform mixture becomes difficult to achieve. The bioelectrode batches were settled into their mold shape and were able to be extricated in an intact form. EIS testing showed an improved electrochemical property with lower bulk impedance for the 30% titanium dioxide, as shown in Table 4.1. Therefore, further testing was carried out for 30% titanium dioxide ratio.

Following the ratio testing, statistical analysis was conducted on 10 electrode batches with 30% titanium dioxide with three samples cut from each batch and tested. Figure 4.1 shows an example of an EIS Nyquist plot, whereas Figure 4.2 shows the frequency vs. impedance plot for the same samples.

Table 4.1: Comparison of prepared samples impedance for different ratios

Si:TiO_2:Gl / Batch	70:15:15		50:30:20	
	Bulk Impedance (kΩ)	**Impedance at 1 kHz (kΩ)**	**Bulk Impedance (kΩ)**	**Impedance at 1 kHz (kΩ)**
Batch 1	17.2	1480	4.25	78.2
Batch 2	7.62	1140	3.55	24.2
Batch 3	17.5	1510	4.38	105
Average	**8.96 ± 0.799**	**1370 ± 206**	**4.06 ± 0.448**	**69.0 ± 41.0**

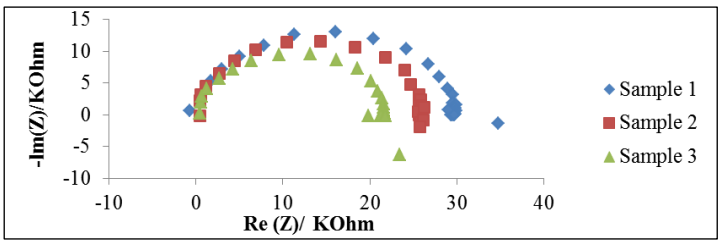

Figure 4.1: Nyquist plots for three samples from prepared electrode batch of 30% TiO_2

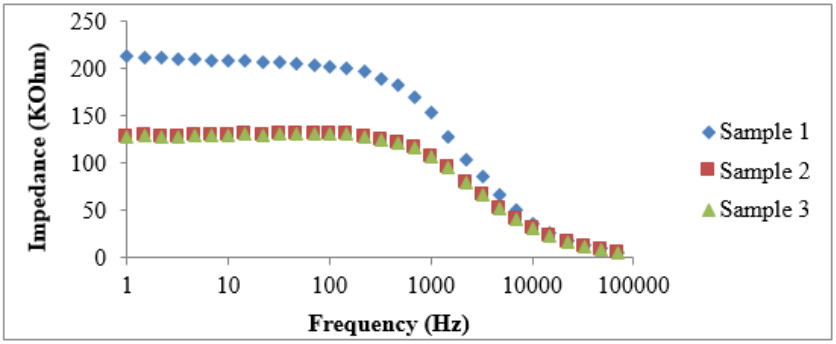

Figure 4.2: Bode plots for three samples from prepared electrode batch of 30% TiO_2

Similarly, the software was used to measure EIS, and the data was again fitted to the same model to find the bulk impedance and the impedance at 1 kHz, they were used for comparison. The bulk impedance was found to be 0.353 ± 0.0135 kΩ, whereas the impedance at 1 kHz was found to be 198 ± 183 kΩ.

Additionally, an ANOVA single factor test (alpha value of 0.05) was done for the samples with the null hypothesis that all the samples' bulk impedances and impedance at 1 kHz are equivalent, while the alternative hypothesis contradicts that. The results of the analysis are presented in Tables 4.2 and 4.3. Therefore, the null hypothesis cannot be rejected. This test supports the reproducibility of the impedances.

Table 4.2: ANOVA test for bulk impedance variance between 10 electrode batches

Source of Variance	SS	dF	MS	F	P-Value	F-Critical
Between Groups	$1.07x10^5$	9	$1.18x10^3$	0.539	0.824	2.59
Within Groups	$3.29x10^5$	15	$2.19\ x10^4$			
Total	$4.26x10^5$	24				

Table 4.3: ANOVA test for impedance at 1 kHz variance between 10 electrode batches

Source of Variance	SS	dF	MS	F	P-Value	F-Critical
Between Groups	$4.33x10^{13}$	9	4.81×10^{10}	1.78	0.135	2.39
Within Groups	$5.40x10^3$	20	2.70×10^{10}			
Total	$9.72x10^{13}$	29				

The results of ANOVA analysis for bulk impedance generated an F-value of 0.539 and F-critical value of 2.59 with a p-value of 0.824. Therefore, the null hypothesis cannot be rejected. This test supports the reproducibility of the bulk impedance.

The results of ANOVA analysis for impedance at 1 kHz generated an F-value of 1.78 and F-critical value of 2.39 with a p-value of 0.135. Therefore, the null hypothesis cannot be rejected. This test supports the reproducibility of the impedance at 1 kHz.

Furthermore, for better appraisal of the prepared electrode batches, a comparison was carried with the recorded impedances of literature material. The comparison is shown in Table 4.3, further discussion is provided in Chapter 7.

Table 4.4: Comparison table for electrochemical properties from literature

Material	Specimen	Bulk Impedance (kΩ)	Conductivity (S/cm)	Impedance at 1 kHz (kΩ)
PEDOT:PSS	Cast film	2.23 [103]	0.2 [104]	2.54 [96]
PPy:PSS	-	-	400 [105]	256000 [2]
PPy-PTs coated iridium	Multi-electrode array probe	-	-	268.3 [10]
PPy-SO_4 coated iridium	Multi-electrode array probe	-	-	146.2 [10]
Ultrathin parylene C coated platinum	Needle-shaped	359 [11]	-	21000 [11]
Platinum	Thin film	2.96 [96]	93400 [11]	-
Iridium	Multi-electrode array probe	-	189000 [87]	193 [10]
Gold	Thin film	0.11 [106]	410000 [106]	1 [107]
This Work (TiO_2-Based)	Rectangular shape	0.353 ± 0.0135	7.22×10^{-4}	198 ± 183

4.2 CV Results

Figure 4.3 shows an example of CV voltammogram for three samples from one batch with 30% titanium dioxide.

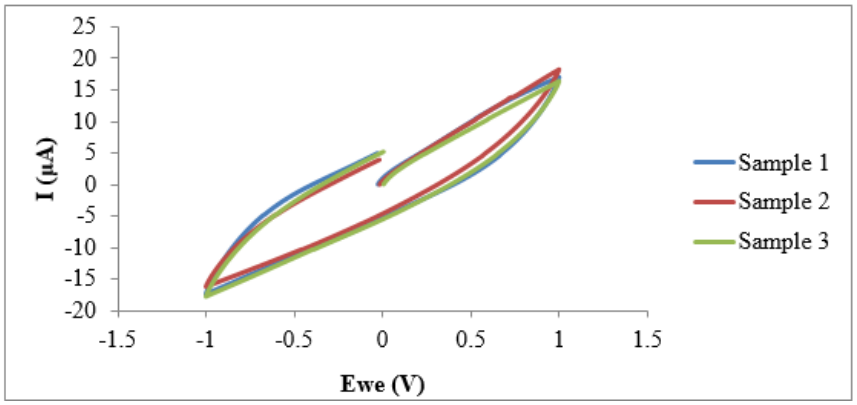

Figure 4.3: Voltammogram plot for three samples from prepared electrode batch of 30% TiO_2

Figure 4.4 displays resulting voltammograms from performing cyclic voltammetry on one of the above sample at different scanning rates. The recorded current data was used to calculate CSC based on the cathodal current. The calculated CSC for the three samples was found to be 27±1.1 mC/cm^2.

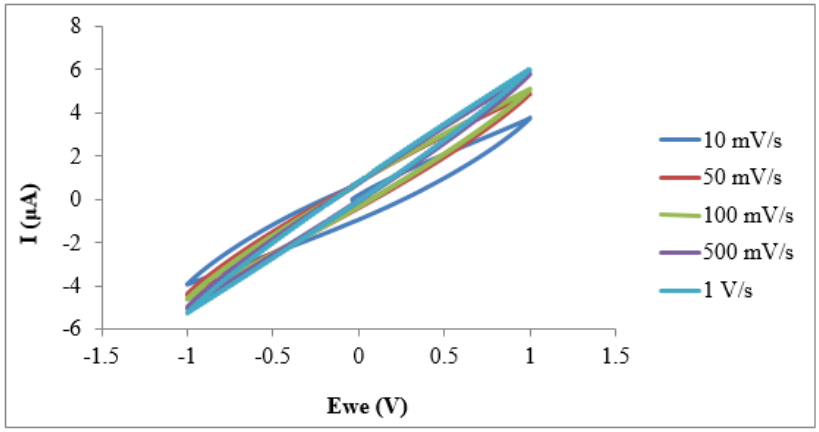

Figure 4.4: Voltammogram plots for three samples from prepared electrode batch of 30% TiO_2 at different scanning rates

An important observation of the voltammograms in Figures 4.3 and 4.4 is the lack of peaks in the plots. This indicates that no oxidation/reduction reactions taking place at the surface of the electrodes, indicating stability of electrodes during electrical stimulation.

Furthermore, for better appraisal of the prepared electrodes, a comparison was carried with the recorded charge storage capacity of literature material. The comparison is shown in Table 4.5, further discussion is provided in Chapter 7.

Table 4.5: Comparison table for charge storage capacity from literature

Material	Specimen	CSC (mC/cm^2)
Gold	-	0.32 ± 0.03 [108]
Transparent graphene electrodes	Microelectrode array	0.116−0.174 [99]
PEDOT:PSS-Coated Indium-Tin-Oxide	Microelectrode probe	0.0581 [60]
Parylene C-based cuff electrode with integrated microfluidics	Cuff electrode	1.64 ± 0.4 [109]
PVA-taurine coated platinum-iridium	Cuff electrode	160 [110]
Iridium oxide-platinum coated platinum	microelectrode	54.14 [111]
PPy	Nanotubes	16.32 ± 1.5 [108]
PEDOT	Nanotubes	4.86 ± 0.24 [108]
This Work (Titanium Dioxide-Based)	Rectangular shape	27±1.1

4.3 Mechanical Testing Results

The tensile mechanical test was performed for a bioelectrode sample; the resulting stress-strain curve is shown in Figure 4.5. The results showed an elastic modulus of 6.63 MPa and it reached an elongation of 266% before breaking.

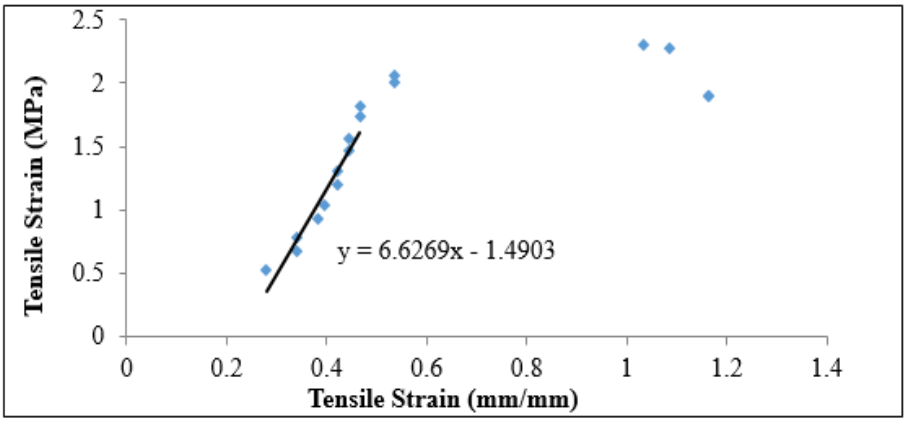

Figure 4.5: Stress-strain curve for a TiO_2-based sample

These results can be used for comparison with the previously mentioned materials, as shown in Table 4.6, further discussion is provided in Chapter 7.

Table 4.6: Comparison table for mechanical properties from literature

Material	Specimen	Modulus of Elasticity (MPa)	Elongation%
PEDOT:PSS	Cast film	1800 [48]	4.3 [112]
Polyimide	Thin film	6000 [35]	<10% [35]
Platinum	Thin film	1400 [113]	35 [113]
Gold	Thin film	69100 [113]	-
This work (TiO_2-based)	Rectangular shape	4.519 ± 1.154	293 ± 27.1

The measured mechanical properties were compared to both of PEDOT:PSS and polyimide polymers, in addition to metals of gold and platinum The materials had a much larger modulus in comparison to the samples tested, indicating a might higher rigidity than the titanium dioxide-based samples. Consequently, the material in this work would have lesser mechanical mismatch with biological tissue. Moreover, with an elongation of 293% ± 27.1% before breaking, it demonstrates that the material is highly ductile as it can stretch to almost three-fold of its length before breaking.

4.4 SEM

Top-view SEM images for the titanium dioxide-based electrodes fabricated in this work at different magnifications are shown in Figure 4.6.

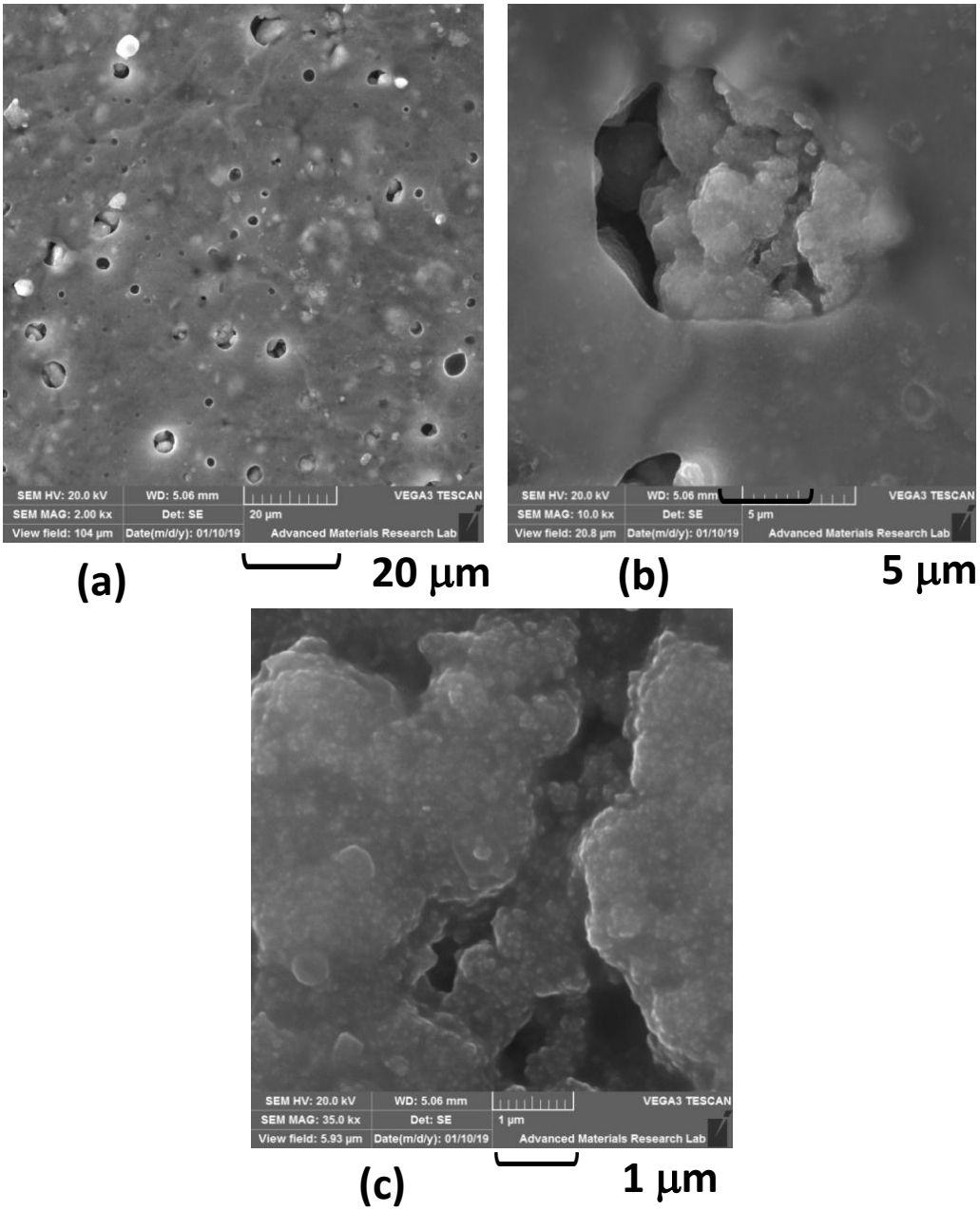

Figure 4.6: Top-view of SEM images for one sample of (50% silicone, 30% TiO_2 and 20% glycerol) at different magnifications (a) 2x (b) 10x (c) 35x

Figure 4.6 shows top-view SEM images for the titanium dioxide-based electrodes fabricated in this work at different magnifications. Examination of the surface morphology shows the small titanium dioxide particles embedded within the silicone polymer matrix. Higher magnifications (image c) show the distribution of very small spherical particles (in the size of 100 nm). In general, a smooth surface is observed with a few pores present. The surface of the synthesized electrodes appears fairly smooth when compared with the morphology of PEDOT based electrodes from Figure 2.7.

4.5 Impedance with Time Results

The long-term immersion test was carried out, in which three electrode samples with 30% TiO_2 were prepared and immersed in eight tubes containing 10.5 mL of 10% PBS solution with a one-week testing interval. At each week, the samples were extracted from their tubes, left to dry for 10 min, and then weighed to track the change of weight over time as shown in Table 4.7. EIS-CV-EIS was performed (this test is recommended by device supplier). The results of EIS analysis pre-CV and post-CV are shown in Tables 4.8 and 4.9. Further discussion is provided in Chapter 7.

Table 4.7: Change of weight of TiO_2-based samples over testing period

Week	Weight (g)	Weight Change %
0 (Before Immersion)	0.558	-
1	1.00	79.7
2	1.06	89.3
3	0.888	59.0
4	0.732	31.2
5	0.693	24.1
6	0.651	16.6
7	0.801	43.4
8	0.638	14.3

Table 4.8: Change of bulk impedance in long-term samples before/after CV

Week	Bulk Impedance before CV (kΩ)	Bulk Impedance after CV (kΩ)
0 (Before Immersion)	0.739 ± 0.0849	1.80 ± 0.197
1	1.26 ± 0.448	1.10 ± 0.173
2	1.23 ± 0.205	1.42 ± 0.201
3	1.80 ± 0.940	1.38 ± 0.353
4	1.15 ± 0.180	1.48 ± 0.438
5	1.22 ± 0.490	0.815 ± 0.00983
6	1.94 ± 0.362	2.03 ± 0.323
7	1.18 ± 0.622	1.62 ± 0.155
8	0.755 ± 0.181	0.743 ± 0.163

Table 4.9: Change of impedance at 1 kHz in long-term samples before/after CV

Week	Impedance at 1 kHz before CV (kΩ)	Impedance at 1 kHz after CV (kΩ)
0 (Before Immersion)	160 ± 7.38	209 ± 83.7
1	96.6 ± 0.663	92.5 ± 3.34
2	47.2 ± 3.49	45.6 ± 6.28
3	84.6 ± 34.4	82.1 ± 36.9
4	95.2 ± 27.8	83.5 ± 20.8
5	69.5 ± 16.4	62.7 ± 12.6
6	49.2 ± 12.2	42.8 ± 10.6
7	61.7 ± 27.6	57.4 ± 25.9
8	16.3 ± 4.21	13.5 ± 4.57

Figure 4.7 displays resulting voltammograms from performing cyclic voltammetry on prepared samples after immersion in PBS.

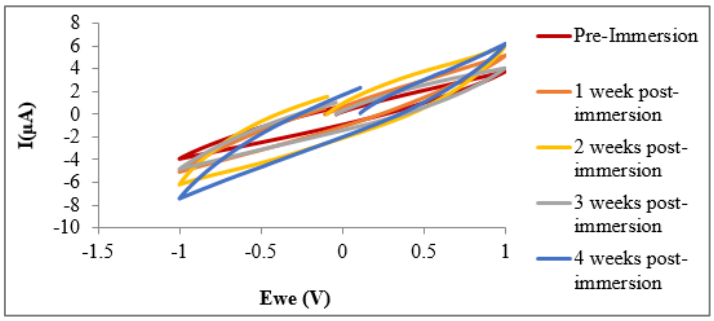

Figure 4.7: Voltammogram for immersed samples of (50% silicone, 30% TiO_2 and 20% glycerol) in PBS solution (scanning rate of 20 mV/s)

Figure 4.8 displays the change of current density during the cyclic voltammetry test over 4 weeks of immersion.

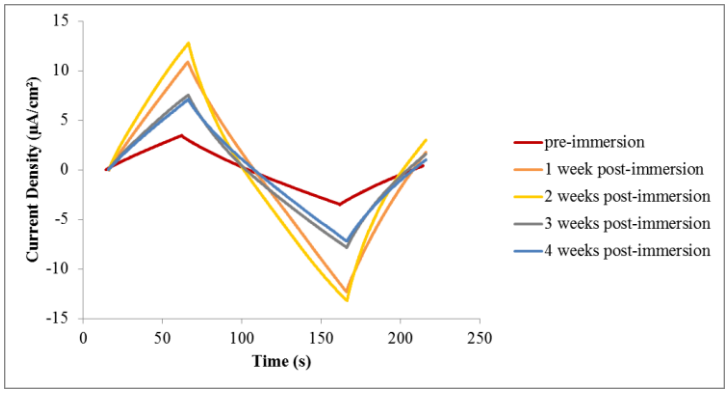

Figure 4.8: Current density vs. time plots for immersed samples of (50% silicone, 30% TiO_2 and glycerol) in PBS solution (scanning rate of 20 mV/s)

The readings from Figure 4.8 are used to calculate the change of charge storage capacity over the immersion period, as shown in Table 4.10, further discussion is provided in Chapter 7.

Table 4.10: Change of charge storage capacity in long-term TiO_2-based samples

Week	**Charge storage capacity (mC/cm²)**
0 (Before Immersion)	43.8 ± 17.9
1	82.6 ± 1.34
2	108 ± 5.98
3	89.5 ± 18.4
4	80.5 ± 14.1
5	61.5 ± 3.64
6	117 ± 16.8
7	77.0 ± 19.5
8	132 ± 41.2

4.5.1. Glycerol leaching. Figures 4.9 and 4.10 show the calibration curve sample containing specified amounts of glycerol, and their spectrophotometry readings each with their distinctive peaks a 635 nm. The absorbance readings at 635 nm were used to set up the calibration curve of Figure 4.11 that helps to estimate the amount of glycerol content in unknown samples.

Figure 4.9: Calibration curve samples with increasing quantities of glycerol 15 mg, 30 mg, 45 mg, 55 mg and 70 mg (left to right)

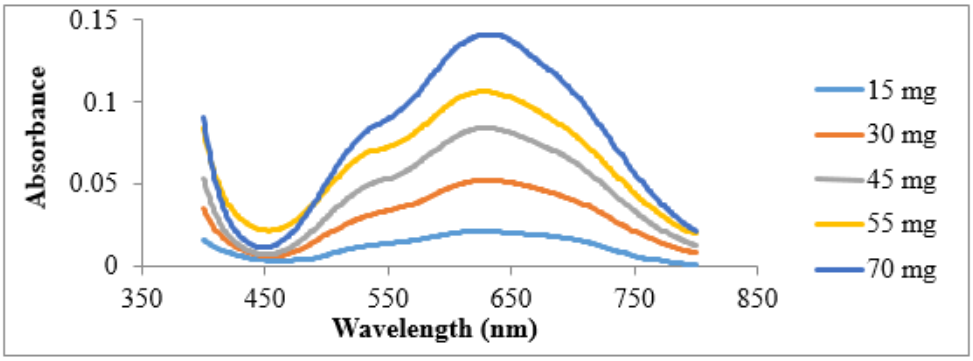

Figure 4.10: UV-Visible spectrophotometric absorbance readings of prepared samples for calibration curve

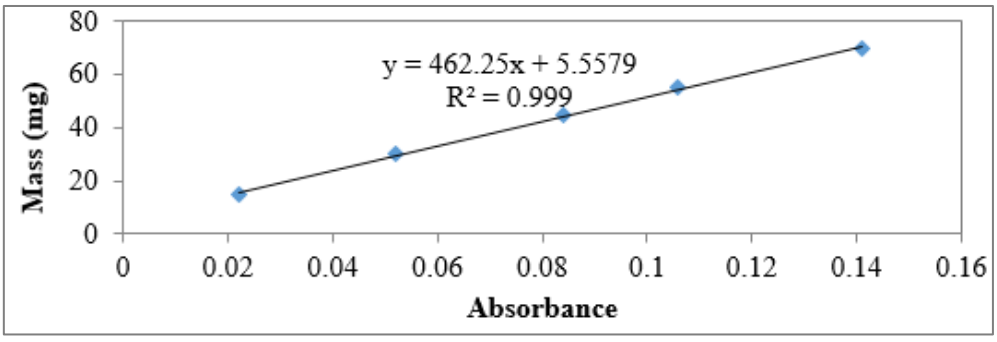

Figure 4.11: Calibration curve for glycerol analysis at 650 nm via UV-Visible spectrophotometric analysis

Figure 4.12 displays the spectrophotometry readings for the PBS samples, each with their distinctive peaks a 635 nm.

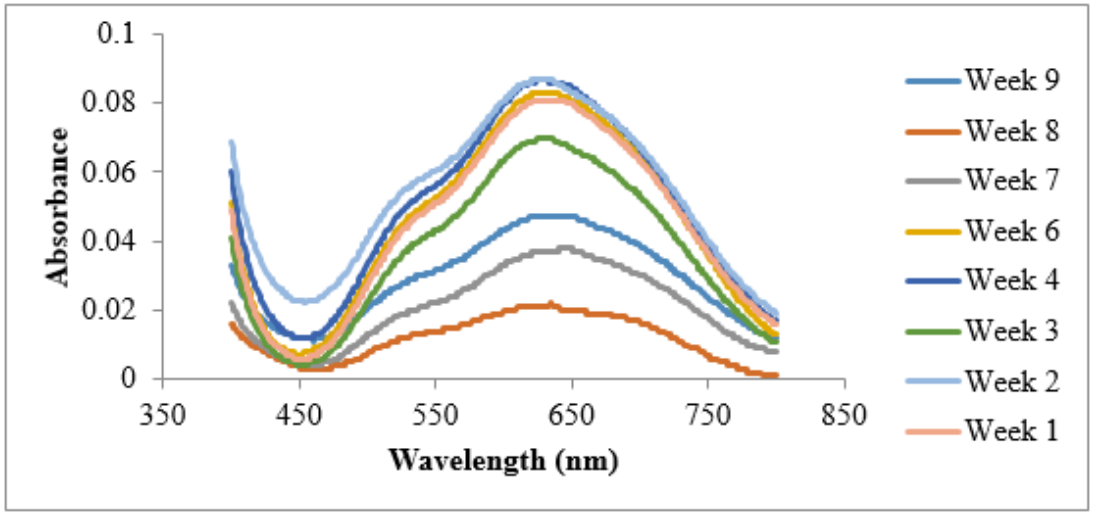

Figure 4.12: UV-Visible spectrophotometric absorbance readings of PBS samples

Table 4.11 displays the absorbance readings for the PBS samples at 635 nm, and the estimated glycerol content followed by the percentage of glycerol leached from titanium dioxide-based samples.

Table 4.11: Calculations for estimation of glycerol content and leached percentage of PBS samples

Week	Sample (mL)	Absorbance Reading	Estimated Glycerol Content (mg)	Leached Glycerol%
Week 1	1.0	0.081	43.0	25.1
Week 2	1.0	0.087	45.8	26.7
Week 3	1.0	0.07	37.9	22.1
Week 4	1.0	0.086	45.3	26.4
Week 6	1.0	0.083	43.9	25.6
Week 7	0.5	0.037	22.7	26.4
Week 8	0.5	0.022	15.7	18.3
Week 9	0.5	0.047	27.3	31.8

Glycerol leaching is relatively consistent throughout the testing period (~25%). So, further testing is needed to check if there is more leaching takes place after one-week long immersion.

The three samples that were immersed for one week were re-immersed in seven tubes containing 10.5 mL of 10% PBS each with an immersion period of one day. The PBS samples were run with UV-Visible spectrophotometry and the results of the analysis are shown in Figure 4.13.

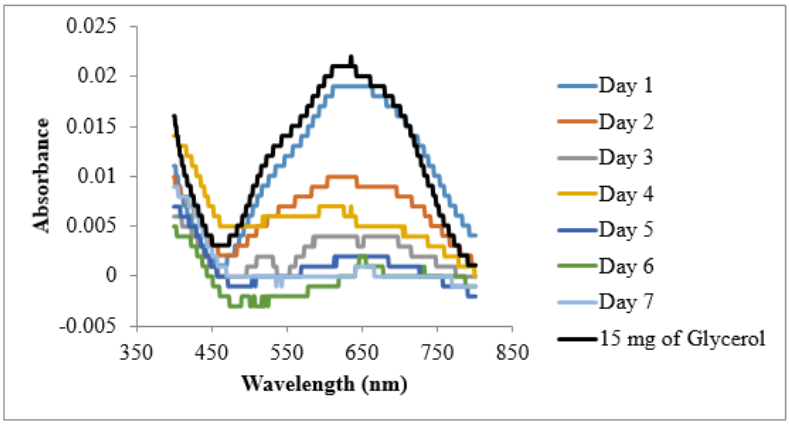

Figure 4.13: UV-Visible spectrophotometric absorbance readings of PBS samples

The readings at wavelength of 635 nm are shown in Table 4.12, the absorbance readings shown in Figure 4.13 and Table 4.12 are below the readings from the range of calibration curve. Accordingly, they are below the threshold of detection, and it can be inferred that after one week of immersion, all of the excess of glycerol has leached out and no further leaching occurs.

Table 4.12: Calculations for estimation of glycerol content and leached percentage of PBS samples

Day	Sample (mL)	Absorbance Reading	Estimated Glycerol Content	
Day 1	6.0	0.019	<0.022	Undetected
Day 2	7.0	0.01	<0.022	Undetected
Day 3	10	0.004	<0.022	Undetected
Day 4	10	0.007	<0.022	Undetected
Day 5	10	0.002	<0.022	Undetected
Day 6	10	0	<0.022	Undetected
Day 7	10	0	<0.022	Undetected

4.6 Price Comparison

In the original objectives of the prepared material was the low cost of fabrication. Therefore, an investigation of costs of bioelectrode material in literature was carried out based on Sigma Aldrich prices and a comparison was done with the material used in this work, as shown in Table 4.13.

Table 4.13: Comparison table for material prices

Material	Cost (AED/g)
PEDOT:PSS (ref: 655201) [114]	41.8
PPy (ref: 577030) [115]	124
Platinum (ref: 685453) [116]	10,400
Gold (ref: 636347) [117]	2,110
This Work (TiO_2-based) [118-120]	1.81

Chapter 5. Stainless Steel-Based Material Results

In this chapter, the experimental results for the electrochemical and mechanical testing are presented, followed by a comparison with market bioelectrode material discussed in previous chapters.

5.1 EIS Results

The tested ratios were of silicone, stainless steel and glycerol were 70:15:15 and 50:30:20 respectively, this can be justified by glycerol proportion as it cannot exceed 20% or the prepared batch will not dry properly. Additionally, if the stainless steel proportion exceeded 35%, then it will hinder mixing and a uniform mixture becomes difficult to achieve. The bioelectrode batches were settled into their mold shape and were able to be extricated in an intact form. EIS testing showed an improved electrochemical property with lower bulk impedance for the 30% stainless steel, as shown in Table 5.1. Therefore, further testing was carried out for 30% stainless steel ratio.

Following the ratio testing, statistical analysis was conducted on four electrode batches with 30% stainless steel with three samples cut from each batch and tested. Figure 5.1 shows an example of an EIS Nyquist plot, whereas Figure 5.2 shows the frequency vs. impedance plot for the same samples.

Table 5.1: Comparison of prepared samples impedance for different ratios

Si:SS:Gl / Batch	70:15:15		50:30:20	
	Bulk Impedance (kΩ)	**Impedance at 1 kHz (kΩ)**	**Bulk Impedance (kΩ)**	**Impedance at 1 kHz (kΩ)**
Batch 1	3.36	10800	1.346	2750
Batch 2	4.82	8830	0.206	2070
Batch 3	2.42	4600	1.70	1930
Average	**2.68 ± 1.67**	**7830 ± 2530**	**2.02 ± 1.08**	**2450 ± 412**

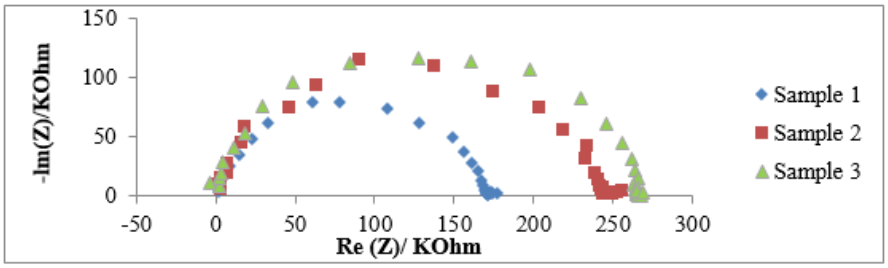

Figure 5.1: Nyquist plots for three samples from prepared electrode batch of 30% stainless steel

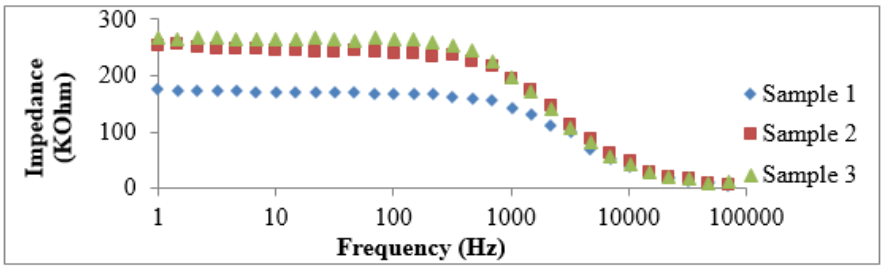

Figure 5.2: Bode plots for three samples from prepared electrode batch of 30% stainless steel

Similarly, the software was used to measure EIS and the data was again fitted to the same model to find the bulk impedance and the impedance at 1 kHz, they were used for comparison. The bulk impedance was found to be 1.69 ± 1.16 kΩ, whereas the impedance at 1 kHz was found to be 1.21 ± 1.13 MΩ.

Additionally, an ANOVA single factor test (alpha value of 0.05) was done for the samples with the null hypothesis that all the samples' bulk impedances and impedance at 1 kHz are equivalent, while the alternative hypothesis contradicts that. The results of the analysis are presented in Tables 5.2 and 5.3. This test is to check the reproducibility of the impedances.

Table 5.2: ANOVA test for bulk impedance variance between five electrode batches

Source of Variance	SS	dF	MS	F	P-Value	F-Critical
Between Groups	5.93×10^{6}	4	1.48×10^{6}	1.91	0.395	4.12
Within Groups	8.76×10^{6}	7	1.25×10^{6}			
Total	1.47×10^{7}	11				

Table 5.3: ANOVA test for impedance at 1 kHz variance between five electrode batches

Source of Variance	SS	dF	MS	F	P-Value	F-Critical
Between Groups	1.37×10^{13}	4	3.42×10^{12}	54.4	2.35×10^{-5}	4.12
Within Groups	4.4×10^{11}	7	6.28×10^{10}			
Total	1.41×10^{13}	11				

The results of ANOVA analysis for bulk impedance generated an F-value of 1.91 and F-critical value of 4.12 with a p-value of 0.395. Therefore, the null hypothesis cannot be rejected. This test supports the reproducibility of the bulk impedance .

The results of ANOVA analysis for impedance at 1 kHz generated an F-value of 54.4 and F-critical value of 4.12 with a p-value of 2.35×10^{-5}. Therefore, the null hypothesis is rejected; further discussion is provided in Chapter 7.

Furthermore, for better appraisal of the prepared electrode batches, a comparison was carried with the recorded impedances of literature material. The comparison is shown in Table 5.4.

Table 5.4: Comparison table for electrochemical properties from literature

Material	Specimen	Bulk Impedance (kΩ)	Conductivity (S/cm)	Impedance at 1 kHz (kΩ)
PEDOT:PSS	Cast film	2.23 [103]	0.2 [104]	2.54 [96]
PPy:PSS	-	-	400 [105]	256000 [2]
PPy-PTs coated iridium	Multi-electrode array probe	-	-	268.3 [10]
PPy-SO_4 coated iridium	Multi-electrode array probe	-	-	146.2 [10]
Ultrathin parylene C coated platinum	Needle-shaped	359 [11]	-	21000 [11]
Platinum	Thin film	2.96 [96]	93400 [11]	-
Iridium	Multi-electrode array probe	-	189000 [87]	193 [10]
Gold	Thin film	0.11 [106]	410000 [106]	1 [107]
This Work (TiO_2-Based)	Rectangular shape	0.353 ± 0.0135	7.22×10^{-4}	198 ± 183
This Work (Stainless steel-based)	Rectangular shape	1.69 ± 1.16	1.51×10^{-4}	1210 ± 1130

5.2 CV Results

Figure 5.3 shows an example of CV voltammogram for three samples from one batch with 30% stainless steel.

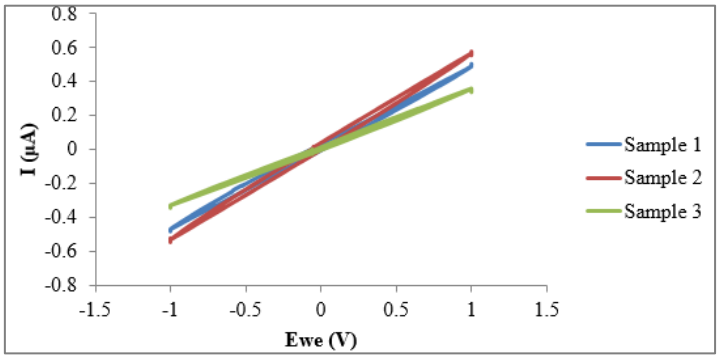

Figure 5.3: Voltammogram plots for three samples from prepared electrode batch of 30% stainless steel

Figure 5.4 displays resulting voltammograms from performing cyclic voltammetry on one of the above sample at different scanning rates. The recorded current data was used to calculate CSC based on the cathodal current. The calculated CSC for the three samples was found to be 31.8 ± 11.8 mC/cm^2.

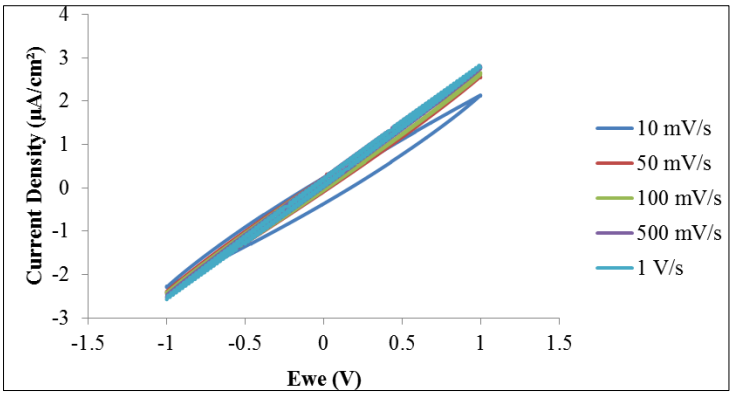

Figure 5.4: Voltammogram for one sample from prepared electrode batch of 30% stainless steel at different scanning rates

An important observation of the voltammograms in Figures 5.3 and 5.4 is the lack of peaks in the plots. This indicates that no oxidation/reduction reactions taking place at the surface of the electrodes, indicating stability of electrodes during electrical stimulation. Additionally, the voltammogram for stainless steel-based samples are narrow, which is typical for metals [97].

Furthermore, for better appraisal of the prepared electrodes, a comparison was carried with the recorded charge storage capacity of literature material. The comparison is shown in Table 5.5, further discussion is provided in Chapter 7.

Table 5.5: Comparison table for charge storage capacity from literature

Material	Specimen	CSC (mC/cm^2)
Gold	-	0.32 ± 0.03 [108]
Transparent graphene electrodes	Microelectrode array	0.116−0.174 [99]
PEDOT:PSS-Coated Indium-Tin-Oxide	Microelectrode probe	0.0581 [60]
Parylene C-based cuff electrode with integrated microfluidics	Cuff electrode	1.64 ± 0.4 [109]
PVA-taurine coated platinum-iridium	Cuff electrode	160 [110]
Iridium oxide-platinum coated platinum	microelectrode	54.14 [111]
PPy	Nanotubes	16.32 ± 1.5 [108]
PEDOT	Nanotubes	4.86 ± 0.24 [108]
This work (TiO_2-based)	Rectangular shape	27 ± 1.1
This work (Stainless steel-based)	Rectangular shape	31.8 ± 11.8

5.3 Mechanical Testing Results

The tensile mechanical test was performed for one sample, shown in Figure 5.5; the resulting stress-strain curve is shown in Figure 5.6. The results showed an elastic modulus of 0.326 MPa and it reached an elongation of 143% before breaking.

Figure 5.5: Mechanical test performed for a stainless steel-based sample

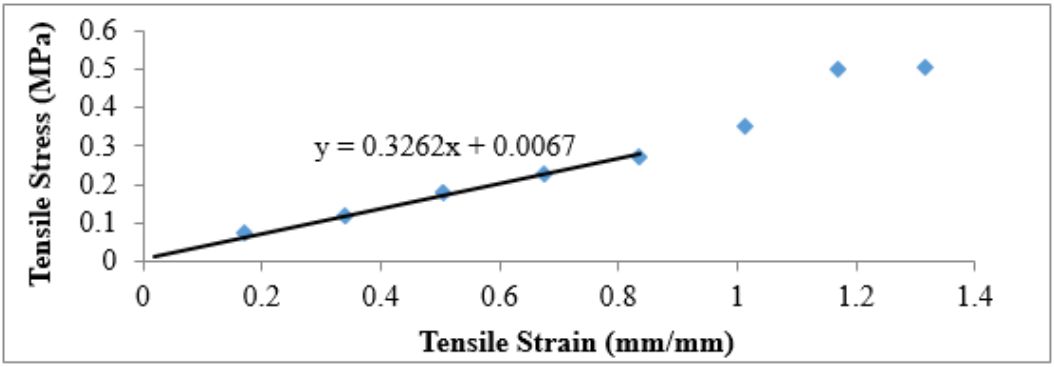

Figure 5.6: Stress-strain curve for a stainless steel-based sample

These results can be used for comparison with the previously mentioned materials, as shown in Table 5.6, further discussion is provided in Chapter 7.

Table 5.6: Comparison table for mechanical properties from literature

Material	Specimen	Modulus of Elasticity (MPa)	Elongation%
PEDOT:PSS	Cast film	1800 [48]	4.3 [112]
Polyimide	Thin film	6000 [35]	<10% [35]
Platinum	Thin film	1400 [113]	35 [113]
Gold	Thin film	69100 [113]	-
This work (TiO_2-based)	Rectangular shape	4.519 ± 1.154	293 ± 27.1
This work (Stainless steel-based)	Rectangular shape	0.722 ± 0.393	145 ± 1.74

The measured mechanical properties were compared to both of PEDOT:PSS and polyimide polymers, in addition to metals of gold and platinum The materials had a much larger modulus in comparison to the sample tested, indicating a might higher rigidity than the stainless steel-based samples. Consequently, the material in this work would have lesser mechanical mismatch with biological tissue. Moreover, with an elongation of 145% ± 1.74% before breaking, it demonstrates that the material is ductile as it can stretch to almost two-fold of its length before breaking.

5.4 Impedance with Time Results

Afterwards, the long-term immersion test was carried out, in which weight electrode batches with 30% stainless steel were prepared and immersed in eight tubes containing 10.5 mL of 10% PBS solution with a one-week testing interval. At each week, the samples were extracted from their tubes, left to dry for 10 min, then weighed to track the change of weight over time as shown in Table 5.7. EIS-CV-EIS was performed (this test is recommended by device supplier). The results of EIS analysis pre-CV and post-CV are shown in Tables 5.8 and 5.9, further discussion is provided in Chapter 7.

Table 5.7: Change of weight of stainless steel-based samples over testing period

Week	Weight (g)	Change in Weight %
0 (Before Immersion)	1.4464	-
1	3.2864	127
2	4.1972	190
3	5.1509	256
4	5.6091	288
5	5.4442	276
6	6.1823	327
7	4.9531	242
8	4.1894	189

Table 5.8: Change of bulk impedance in long-term samples before/after CV

Week	Bulk Impedance before CV (kΩ)	Bulk Impedance after CV (kΩ)
0 (Before Immersion)	1.59 ± 1.01	2.14 ± 1.63
1	1.26 ± 0.405	1.32 ± 1.66
2	0.615 ± 0.385	0.940 ± 0.420
3	0.764 ± 0.526	1.03 ± 0.376
4	1.32 ± 1.47	1.43 ± 2.12
5	0.659 ± 0.452	0.453 ± 0.395
6	0.489 ± 0.318	0.493 ± 0.249
7	0.464 ± 0.188	0.441 ± 0.164
8	0.700 ± 0.475	0.887 ± 0.465

Table 5.9: Change of impedance at 1 kHz in long-term samples before/after CV

Week	Impedance at 1 kHz before CV (kΩ)	Impedance at 1 kHz after CV (kΩ)
0 (Before Immersion)	319 ± 189	416 ± 212
1	626 ± 410	816 ± 672
2	350 ± 102	409 ± 143
3	455 ± 120	563 ± 186
4	584 ± 447	698 ± 561
5	502 ± 380	514 ± 337
6	204 ± 87.8	228 ± 103
7	57.3 ± 49.2	61.8 ± 55.7
8	29.9 ± 8.25	29.8 ± 8.93

Figure 5.7 displays resulting voltammograms from performing cyclic voltammetry on prepared samples after immersion in PBS, and Figure 5.8 displays the change of current density for these samples.

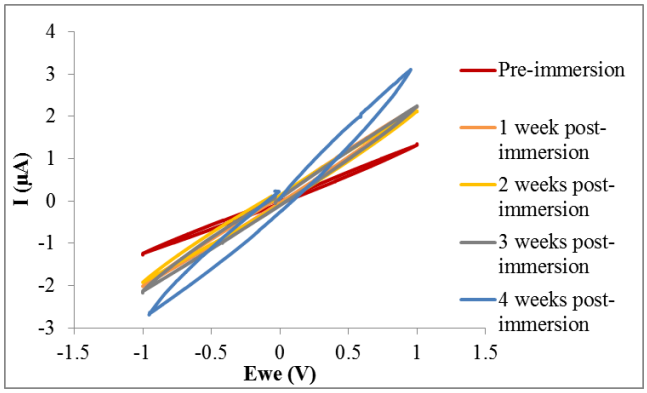

Figure 5.7: Voltammogram for immersed samples of 30% stainless steel in PBS solution (scanning rate of 20 mV/s)

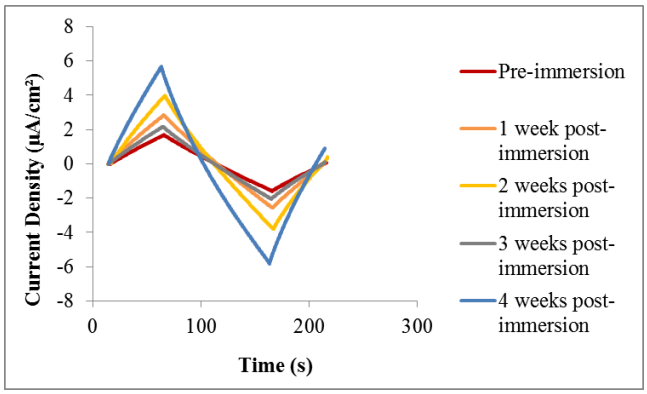

Figure 5.8: Current density vs. time plots for immersed samples of 30% stainless steel in PBS solution (scanning rate of 20 mV/s)

The readings from Figure 5.8 are used to calculate the change of charge storage capacity over the immersion period, as shown in Table 5.10, further discussion is provided in Chapter 7.

Table 5.10: Change of charge storage capacity in long-term stainless steel-based samples

Week	Charge storage capacity (mC/cm²)
0 (Before Immersion)	31.8 ± 11.8
1	17.1 ± 7.9
2	26.5 ± 6.78
3	22.2 ± 5.52
4	22.0 ± 16.5
5	24.2 ± 12.3
6	137 ± 73.5
7	108 ± 57.5
8	125 ± 61.5

5.5 Price Comparison

In the original objectives of the prepared material was the low cost of fabrication. Therefore, an investigation of costs of bioelectrode material in literature was carried out based on Sigma Aldrich prices and a comparison was done with the material used in this work, as shown in Table 5.11.

Table 5.11: Comparison table for material prices

Material	Cost (AED/g)
PEDOT:PSS (ref: 655201) [114]	41.8
PPy (ref: 577030) [115]	124
Platinum (ref: 685453) [116]	10,400
Gold (ref: 636347) [117]	2,110
This Work (TiO_2-based) [118-120]	1.81
This Work (stainless steel-based) [118, 120, 121]	3.95

Chapter 6. Mixture of Titanium-Dioxide and Stainless Steel

In this chapter, the experimental results for the electrochemical and mechanical testing of titanium dioxide-based samples are presented, followed by a comparison with market bioelectrode material discussed in previous chapters.

6.1 EIS Results

The initial ratio testing of multiple samples with 30% of TiO_2 and stainless steel, with different ratios of both, produced suitable samples for testing; the samples were settled into their mold shape and were able to be extricated in an intact form. EIS testing showed an improved electrochemical property with lowest bulk impedance for equal amount TiO_2 and stainless steel, as shown in Table 6.1. However, taking into account the effect of long-term immersion on stainless steel-based samples, the ratio of 20% TiO_2 and 10% stainless steel were chosen for further investigation.

Following the ratio testing, EIS was performed on three electrode batches with 20% TiO_2 and 10% stainless steel with three samples cut from each batch and tested. The bulk impedance of the samples was found to be 1.71±0.849 kΩ, while the impedance at 1 kHz was found to be 191±160 kΩ. Figure 6.1 shows an example of an EIS Nyquist plot, whereas Figure 6.2 shows the frequency vs. impedance plot.

Table 6.1: Comparison of prepared samples impedance for different ratios

TiO_2:Stainless steel	Bulk Impedance (kΩ)	Impedance at 1 kHz (kΩ)
5:25	3.15 ± 1.97	1400 ± 758
10:20	3.03 ± 2.07	476 ± 271
15:15	3.14 ± 2.04	187 ± 87.4
20:10	1.01 ± 0.506	1140 ± 521
25:5	2.04 ± 1.56	1150 ± 228

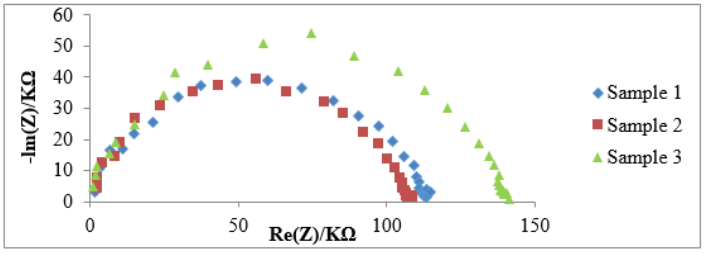

Figure 6.1: Nyquist plots for three samples from prepared electrode batch of 20% TiO_2 and 10% stainless steel

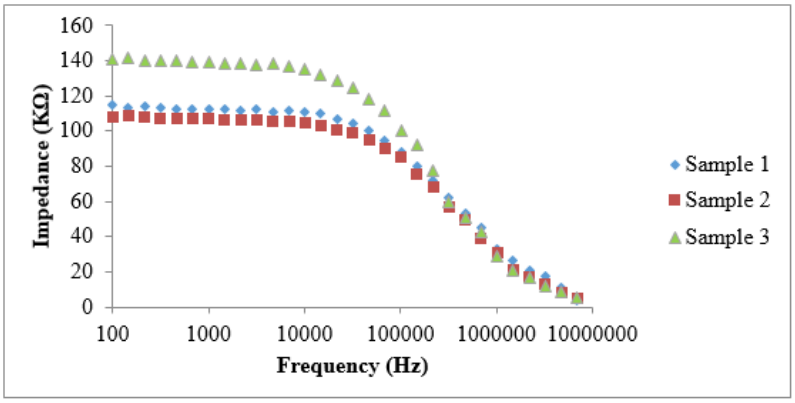

Figure 6.2: Bode plots for three samples from prepared electrode batch of 20% TiO_2 and 10% stainless steel

Furthermore, for better appraisal of the prepared electrodes, a comparison was carried with the recorded impedances of literature material. The comparison is shown in Table 6.2, further discussion is provided in Chapter 7.

Table 6.2: Comparison table for electrochemical properties from literature

Material	Specimen	Bulk Impedance (kΩ)	Conductivity (S/cm)	Impedance at 1 kHz (kΩ)
PEDOT:PSS	Cast film	2.23 [103]	0.2 [104]	2.54 [96]
PPy:PSS	-	-	400 [105]	256000 [2]
PPy-PTs coated iridium	Multi-electrode array probe	-	-	268.3 [10]
PPy-SO_4 coated iridium	Multi-electrode array probe	-	-	146.2 [10]
Ultrathin parylene C coated platinum	Needle-shaped	359 [11]	-	21000 [11]
Platinum	Thin film	2.96 [96]	93400 [11]	-
Iridium	Multi-electrode array probe	-	189000 [87]	193 [10]
Gold	Thin film	0.11 [106]	410000 [106]	1 [107]
This Work (TiO_2-Based)	Rectangular shape	0.353 ± 0.0135	7.22×10^{-4}	198 ± 183
This Work (Stainless steel-based)	Rectangular shape	1.69 ± 1.16	1.51×10^{-4}	1210 ± 1130
This work (TiO_2 and stainless steel-based)	Rectangular shape	1.71 ± 0.849	1.49×10^{-4}	191 ± 160

6.2 CV Results

Figure 6.3 shows an example of CV voltammogram for three samples from one batch with 30% stainless steel.

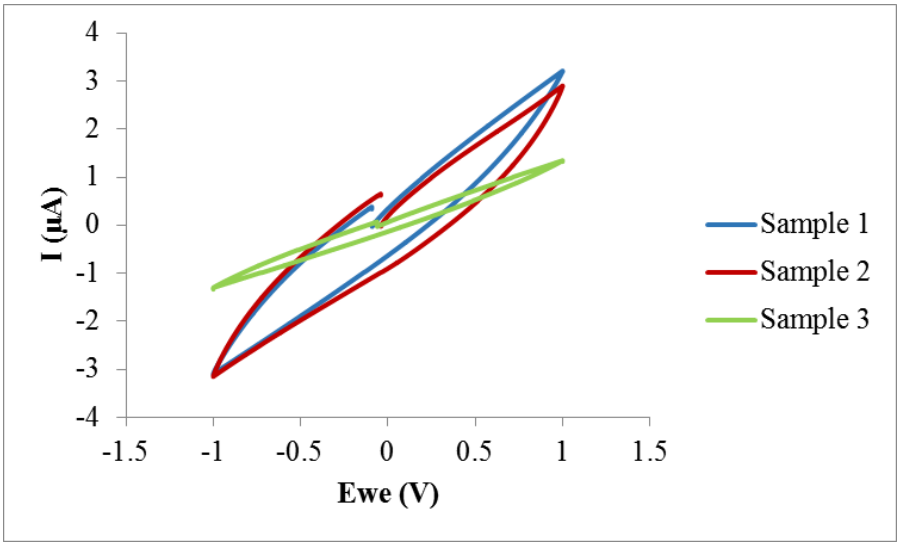

Figure 6.3: Voltammogram plots for three samples from prepared electrode batch of 20% TiO_2 and 10% stainless steel

Figure 6.4 displays resulting voltammograms from performing cyclic voltammetry on one of the above sample at different scanning rates. The recorded current data was used to calculate CSC based on the cathodal current. The calculated CSC for the three samples was found to be 31 ± 13 mC/cm^2.

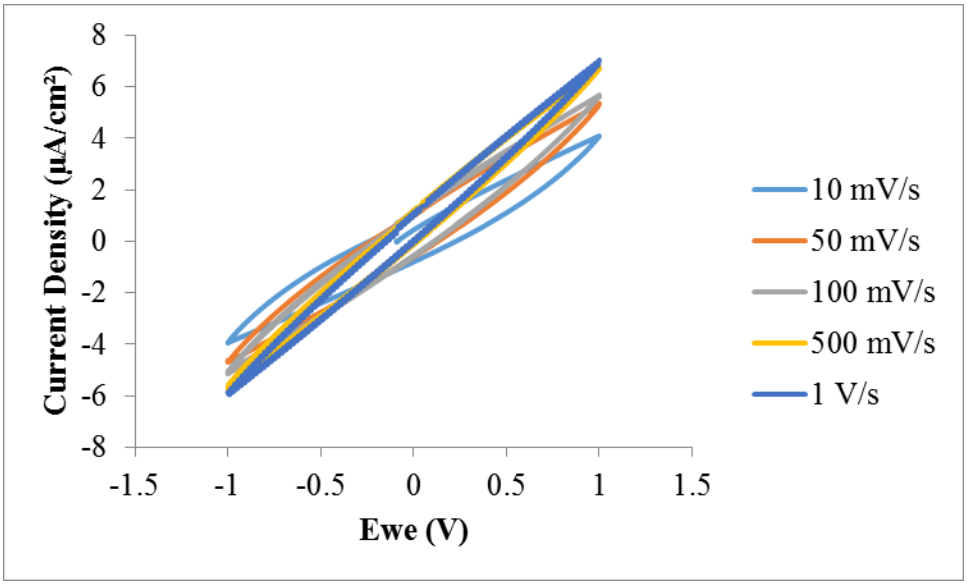

Figure 6.4: Voltammogram plots for three samples from prepared electrode batch of 20% TiO_2 and 10% stainless steel at different scanning rates

Furthermore, for better appraisal of the prepared electrode samples, a comparison was carried with the recorded charge storage capacity of literature material. The comparison is shown in Table 5.5.

Table 6.3: Comparison table for charge storage capacity from literature

Material	Specimen	CSC (mC/cm^2)
Gold	-	0.32 ± 0.03 [108]
Transparent graphene electrodes	Microelectrode array	0.116−0.174 [99]
PEDOT:PSS-Coated Indium-Tin-Oxide	Microelectrode probe	0.0581 [60]
Parylene C-based cuff electrode with integrated microfluidics	Cuff electrode	1.64 ± 0.4 [109]
PVA-taurine coated platinum-iridium	Cuff electrode	160 [110]
Iridium oxide-platinum coated platinum	microelectrode	54.14 [111]
PPy	Nanotubes	16.32 ± 1.5 [108]
PEDOT	Nanotubes	4.86 ± 0.24 [108]
This work (TiO_2-based)	Rectangular shape	27±1.1
This work (Stainless steel-based)	Rectangular shape	31.8 ± 11.8
This work (TiO_2 and stainless steel-based)	Rectangular shape	31 ± 13

6.3 Mechanical Testing Results

The tensile mechanical test was performed for a sample; the resulting stress-strain curve is shown in Figure 6.5. The results showed an elastic modulus of 0.679 MPa and it reached an elongation of 119% before breaking.

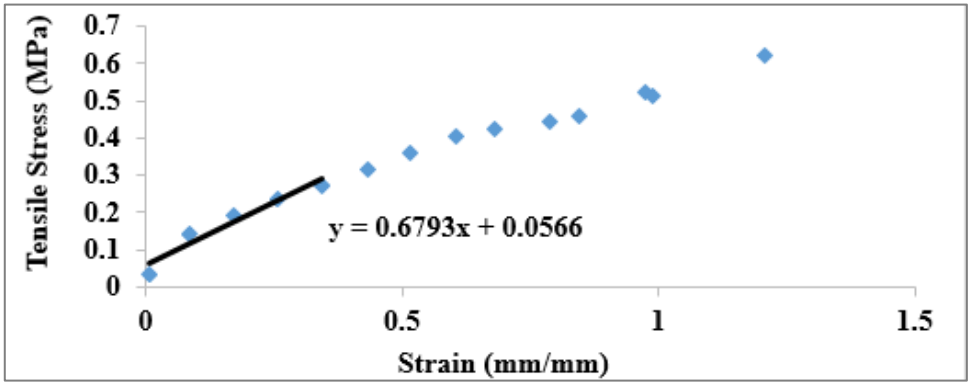

Figure 6.5: Stress-strain curve for a TiO_2 and stainless steel-based sample

These results can be used for comparison with the previously mentioned materials, as shown in Table 6.4.

Table 6.4: Comparison table for mechanical properties from literature

Material	Specimen	Modulus of Elasticity (MPa)	Elongation%
PEDOT:PSS	Cast film	1800 [48]	4.3 [112]
Polyimide	Thin film	6000 [35]	<10% [35]
Platinum	Thin film	1400 [113]	35 [113]
Gold	Thin film	69100 [113]	-
This work (TiO_2-based)	Rectangular shape	4.519 ± 1.154	293 ± 27.1
This work (Stainless steel-based)	Rectangular shape	0.722 ± 0.393	145 ± 1.74
This work (TiO_2 and stainless steel-based)	Rectangular shape	0.453 ± 0.32	96.8± 15.8

6.4 Price Comparison

An investigation of costs of bioelectrode material in literature was carried out based on Sigma Aldrich prices and a comparison was done with the material used in this work, as shown in Table 6.5.

Table 6.5: Comparison table for material prices

Material	Cost (AED/g)
PEDOT:PSS (ref: 655201) [114]	41.8
PPy (ref: 577030) [115]	124
Platinum (ref: 685453) [116]	10,400
Gold (ref: 636347) [117]	2,110
This Work (TiO_2-based) [118-120]	1.81
This Work (stainless steel-based) [118, 120, 121]	3.95
This Work (stainless TiO_2 and stainless steel-based)[118- 121]	2.37

Chapter 7. Discussion

The experimental results resulted from the synthesized titanium based powder samples, stainless steel or the mixture of stainless steel and titanium on silicone showed enhanced electrochemical properties when compared with the values in the literature. The three prepared materials' bulk impedance was comparable to that of gold, platinum and PEDOT:PSS, and surpassed the coated metals such as platinum coated with ultrathin parlyne C. In terms of the impedance at 1 kHz (neural activity frequency), the experimental values of the composite materials was comparable to conductive polymers such as polypyrrole; however, it is higher than that of gold and PEDOT:PSS, which are considered the golden standard for conductivity.

The comparison of the electrochemical properties of the three prepared electrodes in this thesis to each other is shown in Table 7.1. In terms of impedance, the titanium dioxide-based material preformed best for bulk impedance and conductivity; while, the mixture of both titanium dioxide and stainless steel had the lowest impedance at 1 kHz. However, during experimental testing there was variance and many outliers between different batches of the same ratios; this can be attributed to the mixing process during sample preparation, in addition to the observed higher density of stainless steel in comparison to titanium dioxide that affected the mixing. Stainless steel-based sample had the highest bulk impedance and impedance at 1 kHz, with variance in impedance at 1 kHz.

Table 7.1: Comparison of electrochemical properties between the three investigates materials

	Bulk Impedance (kΩ)	**Impedance at 1 kHz (kΩ)**	**CSC (mC/cm²)**
Titanium dioxide-based	0.353 ± 0.0135	198 ± 183	27±1.1
Stainless steel-based	1.69 ± 1.16	$(1.21 \pm 1.13)\times10^3$	31.8 ± 11.8
Titanium dioxide and stainless steel-based	1.71 ± 0.849	191 ± 160	31 ± 13

Another important parameter for electrochemical properties comparison is the charge storage capacity, which represents the maximal value of charge density allowed during a single pulse of electrical stimulation. The calculated CSC of the prepared materials was from the top values recorded in literature, succeeding that of only coated platinum and iridium, as shown in Table 6.3

The characterized mechanical properties for the three composite materials were the most distinguished properties, with much higher elasticity and ductility. In comparison with the conductive polymers and metals, the modulus of elasticity was in the orders of giga-pascals, whereas the prepared materials' was in the order of mega-pascal. Additionally, during the tensile testing, the samples were remarkably elongated before breaking. The titanium dioxide-based samples were the most ductile of the three, whereas the mixture of both titanium dioxide and stainless steel-based material had the lowest modulus of elasticity.

The SEM images were also obtained at different magnifications for titanium dioxide-based samples. Examination of the surface morphology showed the small titanium dioxide particles embedded within the silicone polymer matrix. Higher magnifications show the distribution of very small spherical particles (in the size of 100 nm). In general, a smooth surface is observed with a few pores present.

The surface appears fairly smooth when compared with the morphology of PEDOT based electrodes reported in the literature.

In regards to the long term testing of titanium dioxide-based samples, based on observation the samples did not change shape upon inspection each week. The weight of the sample after immersion increased in the first four weeks with slight swelling; however, in the following weeks the swelling and weight started to go down, which can be explained with the assumption that titanium dioxide particles will bind better with glycerol and silicone, due to their smaller size (<44 micron). In terms of the electrochemical properties, the bulk impedance was generally decreasing throughout the immersion period, which can be explained with the assumption that after soaking the samples changed with formation of micro-spaces, which affected the conductivity properties with decreased impedance. On the other hand, the impedance at 1 kHz fluctuated slightly during the immersion period, but no trend can be inferred. There were also slight fluctuations in the CSC, but without trend or correlation to the recorded impedance values. This indicates that the material can remain resistant to change of electrochemical properties when exposed to salinity of bodily fluids.

There was glycerol leaching from the immersion samples, which remained within a certain range, 18% to 30%, regardless of the immersion period. Also, upon re-immersion of the samples that were previously immersed for one-week, the tested PBS samples had no detectable amounts of glycerol.

In regards to the long term testing of stainless steel-based samples, based on observation the samples changed drastically after immersion, with increased porosity and excessive swelling (see appendix). The samples had to be cut every week to fit into the customized cell for electrochemical characterization; this could be attributed to the weak adhesion and biding in material, due to the stainless steel larger particles' size (150 micron) in comparison to titanium dioxide. This led to formation of fissures that caused the samples to weaken and wear out. The weight of the sample after immersion increased in the first six weeks; however, in the following weeks it started to go down due to loss of part of the samples. In terms of the electrochemical properties, the bulk impedance decreased slightly during the immersion period, with the exception of weeks four and eight. On the other hand, the impedance at 1 kHz fluctuated slightly during the immersion period, but similar to the titanium dioxide-based material, no trend can be inferred. There were also slight fluctuations in the CSC, but without trend or correlation to the recorded impedance values, with an increase starting from week 6.

In the original objectives of the prepared material was the low cost of fabrication, so a comparison was carried out between the conventional electrodes materials' cost with the materials used in this research. The materials cost was of a fraction of what conventional electrodes materials were, even in comparison with PEDOT:PSS which is considered a low cost conductive polymer. This is further demonstrated by taking into account the preparation methods, which are simple and only require a weighing scale and a clean, well-ventilated area.

Nonetheless, to improve on the research presented in this thesis, biocompatibility-testing needs to be carried out to ascertain whether the material allows the conditions in which neurons and muscular cells need to seed and proliferate. In addition to developing an automated method for mixing the materials and setting them into their respective molds to reduce the variations presented in the data.

Chapter 8. Conclusion and Future Work

In this thesis, flexible bioelectrodes were synthesized and evaluated for their electrochemical and mechanical properties. Three types of electrode materials were prepared: Titanium dioxide, stainless steel in addition to a mixture of titanium dioxide and stainless steel all supported on silicone. Additionally, an investigation was conducted to fabricate samples with different samples of different ratios of silicone polymer on conjunction with titanium dioxide, stainless steel or both to find the best combination of three materials. The samples were synthesized and characterized then compared to present bioelectrodes made of conductive polymers and modified metals available in the literature. The results offered promising electrochemical impedance and enhanced mechanical properties.

The future work of this thesis will focus on assessment of the mixture that is the combination of titanium dioxide and stainless steel during long-term impedance test. In addition to further investigation of titanium dioxide-based samples, including testing for leached titanium dioxide during immersion in PBS in the long-term impedance test, and studying the effect of immersion on mechanical properties of the samples. Additional tests to incorporate in the research plan include cyclic three-point flexural test to investigate muscle movement effect on the material during implantation, energy dispersive spectroscopy to identify if there are metal particles on the surface of the samples, and in vitro testing of the cytocompatibility of the material such as live/dead and immunofluorescence assays. Furthermore, an automated preparation method/device is needed to reduce the variation between samples.

.

References

[1] B. D. Ratner, A. S. Hoffman, M. J. Yaszemski, J. E. Lemons, and F. J. Schoen, *Biomaterials Science : An Introduction to Materials in Medicine*. San Diego, United States: Elsevier Science & Technology, 2012, pp. 957-991.

[2] U. Aregueta-Robles, A. Woolley, L. Poole-Warren, N. Lovell and R. Green, "Organic electrode coatings for next-generation neural interfaces". *Frontiers in Neuroengineering*, vol. 7, no.1, pp. 1-18, 2014.

[3] V. S. Polikov, P. A. Tresco, and W. M. Reichert, "Response of brain tissue to chronically implanted neural electrodes". *J Neurosci Methods*, vol. 148, no. 1, pp. 1-18, 2005.

[4] Y. Sun, S. P. Lacour, R. A. Brooks, N. Rushton, J. Fawcett, and R. E. Cameron, "Assessment of the biocompatibility of photosensitive polyimide for implantable medical device use". *J Biomed Mater Res A*, vol. 90, no. 3, pp. 648-55, 2009.

[5] R. Biran, D. C. Martin, and P. A. Tresco, "Neuronal cell loss accompanies the brain tissue response to chronically implanted silicon microelectrode arrays". *Experimental Neurology*, vol. 195, no. 1, pp. 115-126, 2005.

[6] G. Lind, C. Linsmeier and J. Schouenborg, "The density difference between tissue and neural probes is a key factor for glial scarring". *Scientific Reports*, vol. 3, no. 1, pp. 1-7, 2013.

[7] E. Ali, E. Stella, S. F. David, and S. Mesut, "Chronic tissue response to untethered microelectrode implants in the rat brain and spinal cord". *Journal of Neural Engineering*, vol. 12, no. 1, pp. 1-19, 2015.

[8] G. C. McConnell, H. D. Rees, A. I. Levey, C.A. Gutekunst, R. E. Gross, and R. V. Bellamkonda, "Implanted neural electrodes cause chronic, local inflammation that is correlated with local neurodegeneration". *Journal of Neural Engineering*, vol. 6, no. 5, pp. 1-13, 2009.

[9] S. Lacour, G. Courtine and J. Guck, "Materials and technologies for soft implantable neuroprostheses". *Nature Reviews Materials*, vol. 1, no. 10, pp. 1-14, 2016.

[10] A. Harris, S. Morgan, J. Chen, R. Kapsa, G. Wallace and A. Paolini, "Conducting polymer coated neural recording electrodes". *Journal of Neural Engineering*, vol. 10, no. 1, pp. 3-35, 2013.

[11] L. Etemadi *et al.*, "Embedded Ultrathin Cluster Electrodes for Long-Term Recordings in Deep Brain Centers". *Nature Review Materials*, vol. 1, no. 10, pp. 1-18, 2016.

[12] Z. Zhang *et al.*, "Electrically Conductive Biodegradable Polymer Composite for Nerve Regeneration: Electricity-Stimulated Neurite Outgrowth and Axon Regeneration". *Artificial Organs*, vol. 31, no. 1, pp. 13-22, 2007.

[13] S. Khan, J. S. Ordonez, and T. Stieglitz, "Reliability of spring interconnects for high channel-count polyimide electrode arrays". *Journal of Micromechanics and Microengineering*, vol. 28, no. 5, pp. 2-9, 2018.

[14] E. N. Marieb, *Essentials of human anatomy & physiology*. Harlow : Pearson Education, 2015, pp. 251-295.

[15] M. P. McKinley and V. D. O'Loughlin, *Human anatomy*. New York: McGraw-Hill, 2012, pp. 416-436.

[16] M. Puchalski and P. Hummel, "The reality of neonatal pain". *Advances in Neonatal Care*, vol. 2, no. 5, pp. 233-247, 2002.
[17] A. N. Koppes *et al.*, "Electrical Stimulation of Schwann Cells Promotes Sustained Increases in Neurite Outgrowth". *Tissue Engineering. Part A*, vol. 20, no. 3-4, pp. 494-506, 2014.
[18] A. Boerboom, V. Dion, A. Chariot and R. Franzen, "Molecular Mechanisms Involved in Schwann Cell Plasticity". *Frontiers in Molecular Neuroscience*, vol. 10, no. 1, pp. 1-18, 2017.
[19] X. Navarro, T. B. Krueger, N. Lago, S. Micera, T. Stieglitz, and P. Dario, "A critical review of interfaces with the peripheral nervous system for the control of neuroprostheses and hybrid bionic systems". *Journal of the Peripheral Nervous System*, vol. 10, no. 3, pp. 229-258, 2005.
[20] J. Holsheimer, "Concepts and Methods in Neuromodulation and Functional Electrical Stimulation: An Introduction". *Neuromodulation: Technology at the Neural Interface*, vol. 1, no. 2, pp. 57-61, 1998.
[21] H.-C. Tian *et al.*, "Flexible multi-channel microelectrode with fluidic paths for intramuscular stimulation and recording". *Sensors and Actuators A: Physical*, vol. 228, no. 1, pp. 28-39, 2015.
[22] F. Lotti, F. Ranieri, G. Vadalà, L. Zollo, and G. Di Pino, "Invasive Intraneural Interfaces: Foreign Body Reaction Issues". *Frontiers in neuroscience*, vol. 11, no. 1, pp. 497-497, 2017.
[23] " NeuroNexus-2018 Neural Probe Catalog." Internet: http://neuronexus.com/wp-content/uploads/2018/09/2018ProbeCatalog_20180515_Web.pdf [Apr. 23, 2018]
[24] N. Gomez and C. E. Schmidt, "Nerve growth factor-immobilized polypyrrole: Bioactive electrically conducting polymer for enhanced neurite extension". *Journal of Biomedical Materials Research Part A*, vol. 81, no. 1, pp. 135-149, 2007.
[25] Y. Li, K. G. Neoh, and E.-T. Kang, "Plasma protein adsorption and thrombus formation on surface functionalized polypyrrole with and without electrical stimulation". *Journal of Colloid And Interface Science*, vol. 275, no. 2, pp. 488-495, 2004.
[26] A. Akkouch, G. Shi, Z. Zhang, and M. Rouabhia, "Bioactivating electrically conducting polypyrrole with fibronectin and bovine serum albumin". *Journal of biomedical materials research - Part A*, vol. 92, no. 1, pp. 221-31, 2010.
[27] N. Ferraz, M. Straomme, S. Pradhan, A. Mihranyan, B. Fellstrom, and L. Nyholm, "In vitro and in vivo toxicity of rinsed and aged nanocellulose-polypyrrole composites". *Journal of Biomedical Materials Research - Part A*, vol. 100 A, no. 8, pp. 2128-2138, 2012.
[28] X. Zhang and S. K. Manohar, "Bulk synthesis of polypyrrole nanofibers by a seeding approach". *Journal of the American Chemical Society*, vol. 126, no. 40, pp. 12714-12715, 2004.
[29] D. D. Zhou, X. T. Cui, A. Hines, and R. J. Greenberg, "Conducting Polymers in Neural Stimulation Applications," in *Implantable Neural Prostheses 2: Techniques and Engineering Approaches*, 2nd ed., vol. 2, Biological and Medical Physics, Biomedical Engineering, New York, NY : Spring, 2010, pp. 217-252.
[30] A. Peramo, M. Urbanchek, S. Spanninga, L. Povlich, P. Cederna and D. Martin, "In Situ Polymerization of a Conductive Polymer in Acellular Muscle

Tissue Constructs". *Tissue Engineering Part A,* vol. 14, no. 3, pp. 423-432, 2008.

[31] D. H. Kim, S. M. Richardson-Burns, J. L. Hendricks, C. Sequera, and D. C. Martin, "Effect of Immobilized Nerve Growth Factor on Conductive Polymers: Electrical Properties and Cellular Response". *Advanced Functional Materials,* vol. 17, no. 1, pp. 79-86, 2007.

[32] B. Garner, A. J. Hodgson, G. G. Wallace, and P. A. Underwood, "Human endothelial cell attachment to and growth on polypyrrole-heparin is vitronectin dependent". *Journal of materials science. Materials in medicine,* vol. 10, no. 1, pp. 19-27, 1999.

[33] E. Tolstosheeva, V. Biefeld, and W. Lang, "Accelerated soak performance of BPDA-PPD polyimide for implantable MEAs". *Procedia Engineering,* vol. 120, no. 1, pp. 36-40, 2015.

[34] C. Duan, Z. Yang, D. Zhang, L. Tao, Q. Wang, and T. Wang, "Effect of isomerism on mechanical and tribological properties of thermoplastic polyimide films". *Tribology International,* vol. 121, no. 1, pp. 373-380, 2018.

[35] C. Qu, J. Hu, X. Liu, Z. Li, and Y. Ding, "Morphology and Mechanical Properties of Polyimide Films: The Effects of UV Irradiation on Microscale Surface". *Materials,* vol. 10, no. 12, pp. 1-9, 2017.

[36] L. Ghasemi-Mobarakeh *et al.*, "Application of conductive polymers, scaffolds and electrical stimulation for nerve tissue engineering". *Journal of tissue engineering and regenerative medicine,* vol. 5, no. 4, pp. 17-35, 2011.

[37] D. K. Cullen, R. P. A, J. F. Doorish, D. H. Smith, and B. J. Pfister, "Developing a tissue-engineered neural-electrical relay using encapsulated neuronal constructs on conducting polymer fibers". *Journal of neural engineering,* vol. 5, no. 4, pp. 374-384, 2008.

[38] A. Borriello, V. Guarino, L. Schiavo, M. A. Alvarez-Perez, and L. Ambrosio, "Optimizing PANi doped electroactive substrates as patches for the regeneration of cardiac muscle". *Journal of Materials Science: Materials in Medicine,* vol. 22, no. 4, pp. 1053-1062, 2011.

[39] Y. Guo *et al.*, "Electroactive oligoaniline-containing self-assembled monolayers for tissue engineering applications". *Biomacromolecules,* vol. 8, no. 10, pp. 3025-3034, 2007.

[40] M. P. Prabhakaran, L. Ghasemi-Mobarakeh, G. Jin, and S. Ramakrishna, "Electrospun conducting polymer nanofibers and electrical stimulation of nerve stem cells". *Journal of Bioscience and Bioengineering,* vol. 112, no. 5, pp. 501-507, 2011.

[41] Q.-Z. Yu, M.-M. Shi, M. Deng, M. Wang, and H.-Z. Chen, "Morphology and conductivity of polyaniline sub-micron fibers prepared by electrospinning". *Materials Science & Engineering B,* vol. 150, no. 1, pp. 70-76, 2008.

[42] L. Huang *et al.*, "Synthesis of biodegradable and electroactive multiblock polylactide and aniline pentamer copolymer for tissue engineering applications". *Biomacromolecules,* vol. 9, no. 3, pp. 850-858, 2008.

[43] Q. S. Zhang, Y. H. Yan, S. P. Li, and T. Feng, "Synthesis of a novel biodegradable and electroactive polyphosphazene for biomedical application". *Biomedical materials (Bristol, England),* vol. 4, no. 3, pp. 52-57, 2009.

[44] X. Liu, K. J. Gilmore, S. E. Moulton, and G. G. Wallace, "Electrical stimulation promotes nerve cell differentiation on polypyrrole/poly (2-

methoxy-5 aniline sulfonic acid) composites". *Journal of Neural Engineering*, vol. 6, no. 6, pp. 1-10, 2009.

[45] P. Humpolicek, V. Kasparkova, P. Saha and J. Stejskal, "Biocompatibility of polyaniline". *Synthetic Metals*, vol. 162, no. 7-8, pp. 722-727, 2012.

[46] R. Balint, N. J. Cassidy, and S. H. Cartmell, "Conductive polymers: towards a smart biomaterial for tissue engineering". *Acta biomaterialia*, vol. 10, no. 6, pp. 2341-2353, 2014.

[47] M. Asplund *et al.*, "Toxicity evaluation of PEDOT/biomolecular composites intended for neural communication electrodes". *Biomedical Materials - Institute of Physics Publishing*, vol. 4, no. 4, pp. 1-4, 2009.

[48] U. Lang, N. Naujoks, and J. Dual, "Mechanical characterization of PEDOT:PSS thin films". *Synthetic Metals*, vol. 159, no. 5, pp. 473-479, 2009.

[49] X. Cui, J. F. Hetke, J. A. Wiler, D. J. Anderson, and D. C. Martin, "Electrochemical deposition and characterization of conducting polymer polypyrrole/PSS on multichannel neural probes". *Sensors and actuators. A, Physical.*, vol. 93, no. 1, pp. 8-18, 2002.

[50] H. K. Song, B. Toste, K. Ahmann, D. Hoffman-Kim, and G. T. R. Palmore, "Micropatterns of positive guidance cues anchored to polypyrrole doped with polyglutamic acid: A new platform for characterizing neurite extension in complex environments". *Biomaterials*, vol. 27, no. 3, pp. 473-484, 2006.

[51] P. M. George, D. A. LaVan, J. A. Burdick, C. Y. Chen, E. Liang, and R. Langer, "Electrically Controlled Drug Delivery from Biotin-Doped Conductive Polypyrrole". *Advanced Materials*, vol. 18, no. 5, pp. 577-581, 2006.

[52] G. Justin and A. Guiseppi-Elie, "Electroconductive Blends of Poly(HEMA-co-PEGMA-co-HMMAco-SPMA) and Poly(Py- co-PyBA): In Vitro Biocompatibility". *Journal of Bioactive and Compatible Polymers*, vol. 25, no. 2, pp. 121-140, 2010.

[53] J. W. Lee, F. Serna, J. Nickels, and C. E. Schmidt, "Carboxylic acid-functionalized conductive polypyrrole as a bioactive platform for cell adhesion". *Biomacromolecules*, vol. 7, no. 6, pp. 1692-1695, 2006.

[54] C. J. Bettinger, J. P. Bruggeman, A. Misra, J. T. Borenstein, and R. Langer, "Biocompatibility of biodegradable semiconducting melanin films for nerve tissue engineering". *Biomaterials*, vol. 30, no. 17, pp. 3050-3057, 2009.

[55] T. Aoki, M. Tanino, K. Sanui, N. Ogata, and K. Kumakura, "Secretory function of adrenal chromaffin cells cultured on polypyrrole films". *Biomaterials*, vol. 17, no. 20, pp. 1971-1974, 1996.

[56] N. Gomez, J. Y. Lee, J. D. Nickels, and C. E. Schmidt, "Micropatterned Polypyrrole: A Combination of Electrical and Topographical Characteristics for the Stimulation of Cells". *Advanced Functional Materials*, vol. 17, no. 10, pp. 1645-1653, 2007.

[57] P. M. George *et al.*, "Fabrication and biocompatibility of polypyrrole implants suitable for neural prosthetics". *Biomaterials*, vol. 26, no. 17, pp. 3511-3519, 2005.

[58] D. Mantione, I. Del Agua, A. Sanchez-Sanchez and D. Mecerreyes, "Poly(3,4-ethylenedioxythiophene) (PEDOT) Derivatives: Innovative Conductive Polymers for Bioelectronics". *Polymers*, vol. 9, no. 12, pp. 1-21, 2017.

[59] A. Broski, Y. Guo, W. A. Khan and W. Li, "Characteristics of PEDOT:PSS thin films spin-coated on ITO," *2017 IEEE 12th International Conference on*

Nano/Micro Engineered and Molecular Systems (NEMS), Los Angeles, CA, 2017, pp. 243-247.

[60] W. Yang, A. Broski, J. Wu, Q. H. Fan, and W. Li, "Characteristics of Transparent, PEDOT:PSS-Coated Indium-Tin-Oxide (ITO) Microelectrodes," *IEEE Transactions on Nanotechnology*, vol. 17, no. 4, pp. 701-704, 2018.

[61] S. Sarmah and R. Tamuli, "Conducting Polymers: Biomedical Engineering Applications," in *Encyclopedia of Biomedical Polymers and Polymeric Biomaterials*, 1st ed., M. Mishra, Ed. Taylor & Francis, 2016, pp. 1982-1996.

[62] D. Simon, E. Gabrielsson, K. Tybrandt and M. Berggren, "Organic Bioelectronics: Bridging the Signaling Gap between Biology and Technology". *Chemical Reviews*, vol. 116, no. 21, pp. 13009-13041, 2016.

[63] J. J. Pancrazio *et al.*, "Thinking Small: Progress on Microscale Neurostimulation Technology," *Neuromodulation*, vol. 20, no. 8, pp. 745-752, 2017.

[64] H. Fodstad and M. Hariz, "Electricity in the treatment of nervous system disease". *Acta neurochirurgica. Supplement*, vol. 97, no. 1, pp. 11-19, 2007.

[65] T. Taira and T. Hori, "Diaphragm pacing with a spinal cord stimulator: current state and future directions". *Acta Neurochir Suppl*, vol. 97, no. 1, pp. 289-292, 2007.

[66] M. T. Sanford and A. M. Suskind, "Neuromodulation in neurogenic bladder". *Translational Andrology and Urology*, vol. 5, no. 1, pp. 117-126, 2016.

[67] K. E. Matzel, "Sacral nerve stimulation for fecal disorders: evolution, current status, and future directions". *Acta Neurochir Suppl*, vol. 97, no. 1, pp. 351-357, 2007.

[68] S. Meloy, "Neurally augmented sexual function," in *Operative Neuromodulation*, Vienna: Springer, 2007, pp. 359-363.

[69] P. W. Michael, W. P. K. Stephen, J. Z. Jennifer, D. C. Cameron, G. Tessa, and H. B. Gregory, "Daily Electrical Muscle Stimulation Enhances Functional Recovery Following Nerve Transection and Repair in Rats". *Neurorehabilitation and Neural Repair*, vol. 29, no. 7, pp. 690-700, 2015.

[70] P. H. Peckham and J. S. Knutson, "Functional Electrical Stimulation for Applications". *Annual Review of Biomedical Engineering*, vol. 7, no. 1, pp. 327-360, 2005.

[71] P. Banerjee, B. Caulfield, L. Crowe, and A. Clark, "Prolonged electrical muscle stimulation exercise improves strength and aerobic capacity in healthy sedentary adults". *J Appl Physiol*, vol. 99, no. 6, pp. 2307-2311, 2005.

[72] Y. L. Jae, C. E. Schmidt, and J. W. Lee, "Neuroactive conducting scaffolds: Nerve growth factor conjugation on active ester-functionalized polypyrrole". *Journal of the Royal Society Interface*, vol. 6, no. 38, pp. 801-810, 2009.

[73] R. L. Williams and P. J. Doherty, "A preliminary assessment of poly(pyrrole) in nerve guide studies". *Journal of Materials Science: Materials in Medicine : Official Journal of the European Society for Biomaterials*, vol. 5, no. 6, pp. 429-433, 1994.

[74] B. Thompson et al., "Conducting polymers, dual neurotrophins and pulsed electrical stimulation — Dramatic effects on neurite outgrowth". *Journal of Controlled Release*, vol. 141, no. 2, pp. 161-167, 2010.

[75] X. Liu, Z. Yue, M. Higgins and G. Wallace, "Conducting polymers with immobilised fibrillar collagen for enhanced neural interfacing". *Biomaterials*, vol. 32, no. 30, pp. 7309-7317, 2011.

[76] K. L. Kilgore, H. A. Hoyen, A. M. Bryden, R. L. Hart, M. W. Keith, and P. H. Peckham, "An Implanted Upper-Extremity Neuroprosthesis Using Myoelectric Control". *The Journal of hand surgery,* vol. 33, no. 4, pp. 539-550, 2008.

[77] P. Taylor, J. Esnouf, and J. Hobby, "The functional impact of the Freehand System on tetraplegic hand function - Clinical Results". *Spinal Cord,* vol. 40, no. 11, pp. 560-566, 2002.

[78] C. H. Ho *et al.*, "Functional Electrical Stimulation and Spinal Cord Injury". *Physical medicine and rehabilitation clinics of North America,* vol. 25, no. 3, pp. 631-ix, 2014.

[79] L. R. Sheffler and J. Chae, "Neuromuscular electrical stimulation in neurorehabilitation". *Muscle & Nerve,* vol. 35, no. 5, pp. 562-590, 2007.

[80] L. Kenney *et al.*, "An implantable two channel drop foot stimulator: initial clinical results". *Artif Organs,* vol. 26, no. 3, pp. 267-270, 2002.

[81] J. A. Davis, Jr. *et al.*, "Preliminary performance of a surgically implanted neuroprosthesis for standing and transfers--where do we stand?," *J Rehabil Res Dev,* vol. 38, no. 6, pp. 609-617, 2001.

[82] Z. Tan *et al.*, "The Effectiveness of Functional Electrical Stimulation Based on a Normal Gait Pattern on Subjects with Early Stroke: A Randomized Controlled Trial". *BioMed Research International,* vol. 2014, pp. 1-9, 2014.

[83] A. Cyganowski, I. Minev, N. Vachicouras, K. Musick, and S. Lacour, "Stretchable electrodes for neuroprosthetic interfaces," i*n Proc of IEEE Sensors*, 2012, pp. 1-4.

[84] M. A. Allen, "Biocompatibility of silicone implants". *Journal of Oral and Maxillofacial Surgery,* vol. 42, no. 2, pp. 38-45, 1984.

[85] A. Brensing, R. Ruff, B. Fischer, L. Wien Sascha, and K. P. Hoffmann, "PDMS electrodes for recording and stimulation". *Current Directions in Biomedical Engineering*, vol. 3, no. 1, pp. 63-67, 2017.

[86] F. López-Huerta *et al.*, "Biocompatibility and Surface Properties of TiO2 Thin Films Deposited by DC Magnetron Sputtering". *Materials,* vol. 7, no. 6, pp. 4105-4117, 2014.

[87] A. M. Cruz and N. Casañ-Pastor, "Graded conducting titanium–iridium oxide coatings for bioelectrodes in neural systems". *Thin Solid Films,* vol. 534, pp. 316-324, 2013.

[88] M. Taiwade, A. B Bodade, and D. G. Chaudhari, "Nanostructured Rutile Titanium Dioxide Based Platform For application to Urease Biosensor". *International Journal of Pharmaceutical Science Reviews and Research*, pp. 35-42, 2016.

[89] H. Hermawan, D. Ramdan, and J. R. P. Djuansjah, "Metals for Biomedical Applications," in *Biomedical Engineering - From Theory to Applications*. 1st ed., InTech, 2011. pp. 411-430.

[90] R. K. Mishra *et al.*, "Wearable Flexible and Stretchable Glove Biosensor for On-Site Detection of Organophosphorus Chemical Threats". *ACS Sensors,* vol. 2, no. 4, pp. 553-561, 2017

[91] L. A. Geddes and R. Roeder, "Criteria for the Selection of Materials for Implanted Electrodes". *Annals of Biomedical Engineering,* vol. 31, no. 7, pp. 879-890, 2003.

[92] T. Pirttimäki *et al.*, "Implantable RF-coil with multiple electrodes for long-term EEG-fMRI monitoring in rodents". *Journal of Neuroscience Methods,* vol. 274, pp. 154-163, 2016.
[93] H. Zhang and M. W. Grinstaff, "Recent Advances in Glycerol Polymers: Chemistry and Biomedical Applications". *Macromolecular rapid communications,* vol. 35, no. 22, pp. 1906-1924, 2014.
[94] G. Ayala Valencia, A. Agudelo, and R. Zapata, "Effect of glycerol on the electrical properties and phase behavior of cassava starch biopolymers". *DYNA*, pp. 138-147, 2012.
[95] H. Cesiulis, N. Tsyntsaru, A. Ramanavicius, and G. Ragoisha, "The Study of Thin Films by Electrochemical Impedance Spectroscopy," in *Nanostructures and Thin Films for Multifunctional Applications : Technology, Properties and Devices*, 1st ed., Cham:Springer 2016, pp. 3-42.
[96] Y. Lu *et al.*, "Poly(3,4-ethylenedioxythiophene)/poly(styrenesulfonate)-poly(vinyl alcohol)/poly(acrylic acid) interpenetrating polymer networks for improving optrode-neural tissue interface in optogenetics". *Biomaterials,* vol. 33, no. 2, pp. 378-394, 2012.
[97] N. m. Elgrishi, K. J. Rountree, B. D. McCarthy, E. S. Rountree, T. T. Eisenhart, and J. L. Dempsey, "A Practical Beginner's Guide to Cyclic Voltammetry". *Journal of Chemical Education,* vol. 95, no. 2, pp. 197-206, 2017.
[98] D. A. C. Brownson and C. E. Banks, "Interpreting Electrochemistry," in *The Handbook of Graphene Electrochemistry*, London:Springer, 2014, pp. 23-77.
[99] D.-W. Park *et al.*, "Electrical Neural Stimulation and Simultaneous in Vivo Monitoring with Transparent Graphene Electrode Arrays Implanted in GCaMP6f Mice". *ACS Nano,* vol. 12, no. 1, pp. 148-157, 2018.
[100] H. Lim and S. Hoag, "Plasticizer Effects on Physical–Mechanical Properties of Solvent Cast Soluplus (R) Films". *AAPS PharmSciTech*, vol. 14, no. 3, pp. 903-910, 2013.
[101] S. Felix *et al.*, "Removable silicon insertion stiffeners for neural probes using polyethylene glycol as a biodissolvable adhesive," in *Annual International Conference of the IEEE Engineering in Medicine and Biology Society. IEEE Engineering in Medicine and Biology Society*, 2012, pp. 871-874.
[102] F. Spagnolo, "Spectrophotometric Determination of Glycerol as Sodium-Cupri-Glycerol Complex". *Analytical Chemistry,* vol. 25, no. 10, pp. 1566-1568, 1953.
[103] Y. Lu *et al.*, "Poly(3,4-ethylenedioxythiophene)/poly(styrenesulfonate)-poly(vinyl alcohol)/poly(acrylic acid) interpenetrating polymer networks for improving optrode-neural tissue interface in optogenetics". *Biomaterials*, vol. 33, no. 2, pp. 378-394, 2012.
[104] Z. Yu, Y. Xia, D. Du, and J. Ouyang, "PEDOT:PSS Films with Metallic Conductivity through a Treatment with Common Organic Solutions of Organic Salts and Their Application as a Transparent Electrode of Polymer Solar Cells". *ACS Applied Materials & Interfaces,* vol. 8, no. 18, pp. 11629-11638, 2016.
[105] T.-H. Le, Y. Kim, and H. Yoon, "Electrical and Electrochemical Properties of Conducting Polymers". *Polymers*, vol. 9, no. 4, pp. 1-32, 2017.
[106] E. T. McAdams, J. Jossinet, R. Subramanian, and R. G. McCauley, "Characterization of gold electrodes in phosphate buffered saline solution by

impedance and noise measurements for biological applications," *Conf Proc IEEE Eng Med Biol Soc*, vol. 1, 2006, pp. 4594-4597.
[107] S. Bauerdick, C. Burkhardt, D. Kern and W. Nisch, "Substrate-Integrated Microelectrodes with Improved Charge Transfer Capacity by 3-Dimensional Micro-Fabrication". *Biomedical Microdevices*, vol. 5, no. 2, pp. 93-99, 2003.
[108] M. Khorrami and M. R. Abidian, "Aligned Conducting Polymer Nanotubes for Neural Prostheses," in *40th Annual International Conference of the IEEE Engineering in Medicine and Biology Society (EMBC)*, 2018, pp. 6080-6083.
[109] A. M. Cobo *et al.*, "Parylene-Based Cuff Electrode With Integrated Microfluidics for Peripheral Nerve Recording, Stimulation, and Drug Delivery". *Journal of Microelectromechanical Systems*, vol. 28, no. 1, pp. 36-49, 2019.
[110] A. Gilmour *et al.*, "Stimulation of peripheral nerves using conductive hydrogel electrodes," in *40th Annual International Conference of the IEEE Engineering in Medicine and Biology Society (EMBC)*, 2018, pp. 5475-5478.
[111] Q. Zeng, T. Wu, B. Sun, K. Xia, M. S. Humayun, and C. O. O., "Iridium Oxide-Platinum Nanocomposite Coating for Neural Electrode," in *IEEE International Conference on Cyborg and Bionic Systems (CBS)*, 2018, pp. 1-4.
[112] C. H. Chen *et al.*, "Mechanical characterizations of cast Poly(3,4-ethylenedioxythiophene):Poly(styrenesulfonate)/Polyvinyl Alcohol thin films". *Synthetic Metals*, vol. 161, no. 21, pp. 2259-2267, 2011.
[113] M. Salvadori, I. Brown, A. Vaz, L. Melo and M. Cattani, "Measurement of the elastic modulus of nanostructured gold and platinum thin films". *Physical Review B*, vol. 67, no. 15, pp. 1-4, 2003.
[114] "Poly(3,4-ethylenedioxythiophene)-poly(styrenesulfonate), 3.0-4.0% in H2O, high-conductivity grade SIGMA-ALDRICH." Internet: https://www.sigmaaldrich.com/catalog/product/aldrich/655201?lang=en&region=AE [Apr. 23, 2018]
[115] "Polypyrrole, conductivity 10-50 S/cm (pressed pellet) SIGMA-ALDRICH." Internet: https://www.sigmaaldrich.com/catalog/product/aldrich/577030?lang=en&region=AE [Apr. 23, 2018]
[116] "Platinum, nanopowder, <50 nm particle size (TEM) SIGMA-ALDRICH." Internet: https://www.sigmaaldrich.com/catalog/product/aldrich/685453?lang=en&region=AE [Apr. 23, 2018]
[117] "Gold, nanopowder, <100 nm particle size, 99.9% trace metals basis SIGMA-ALDRICH." Internet: https://www.sigmaaldrich.com/catalog/product/aldrich/636347?lang=en&region=AE [Apr. 23, 2018]
[118] "Silicone grease, 85410 SIGMA-ALDRICH." Internet: https://www.sigmaaldrich.com/catalog/product/aldrich/85410?lang=en&region=AE [Apr. 23, 2018]
[119] "Titanium (IV) oxide, 14027 SIGMA-ALDRICH." Internet: https://www.sigmaaldrich.com/catalog/product/sigald/14027?lang=en&region=AE [Apr. 23, 2018]
[120] "Glycerol, ACS reagent, ≥99.5%, G7893 SIGMA-ALDRICH." Internet: https://www.sigmaaldrich.com/catalog/product/sigald/g7893?lang=en&region=AE [Apr. 23, 2018]
[121] "Stainless Steel - AISI 316 alloy, FeCr18Ni10Mo3 SIGMA-ALDRICH." Internet: https://www.sigmaaldrich.com/catalog/product/aldrich/gf49810721?lang=en&region=AE [Feb. 2, 2018]

Appendix A: Detailed Experimental Results

A.1. Titanium Dioxide-Based Samples EIS Results

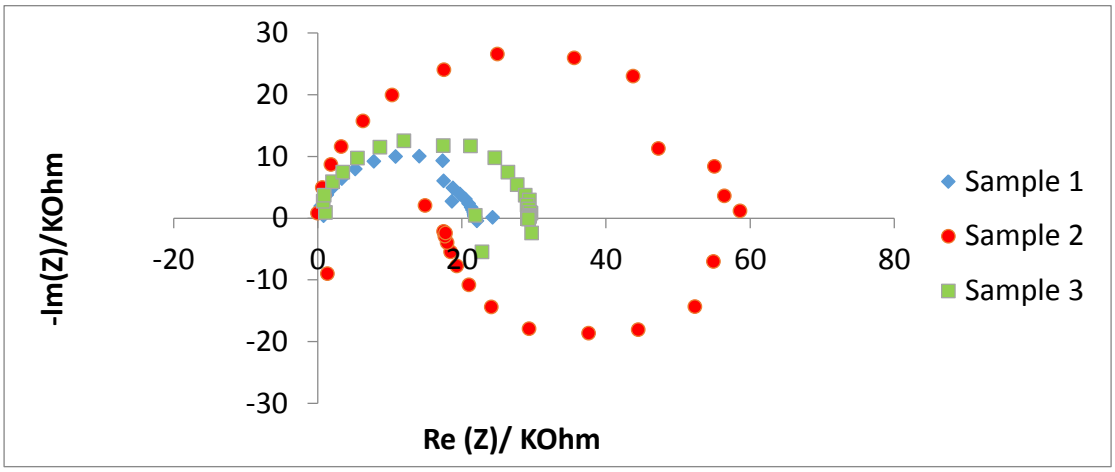

Figure A.1: Nyquist plots for three samples from first batch of 30% TiO_2

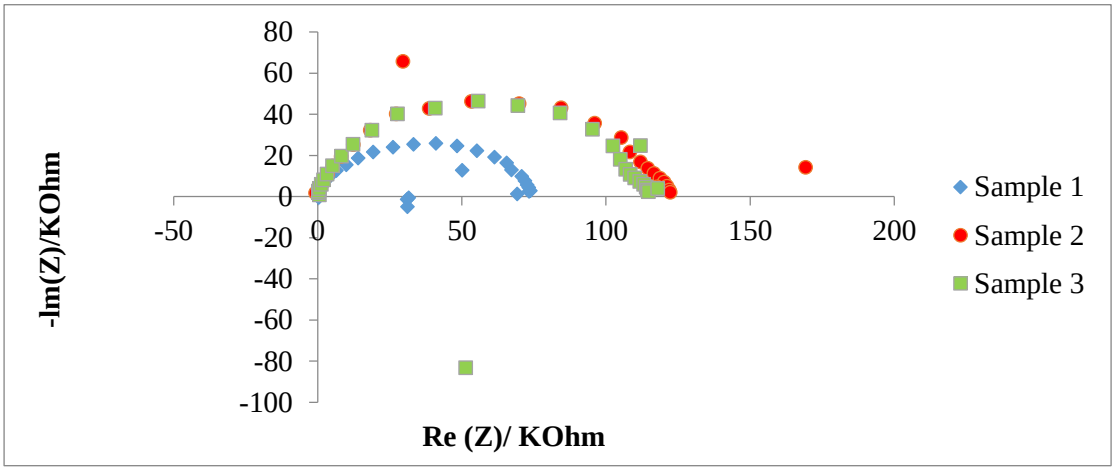

Figure A.2: Nyquist plots for three samples from second batch of 30% TiO_2

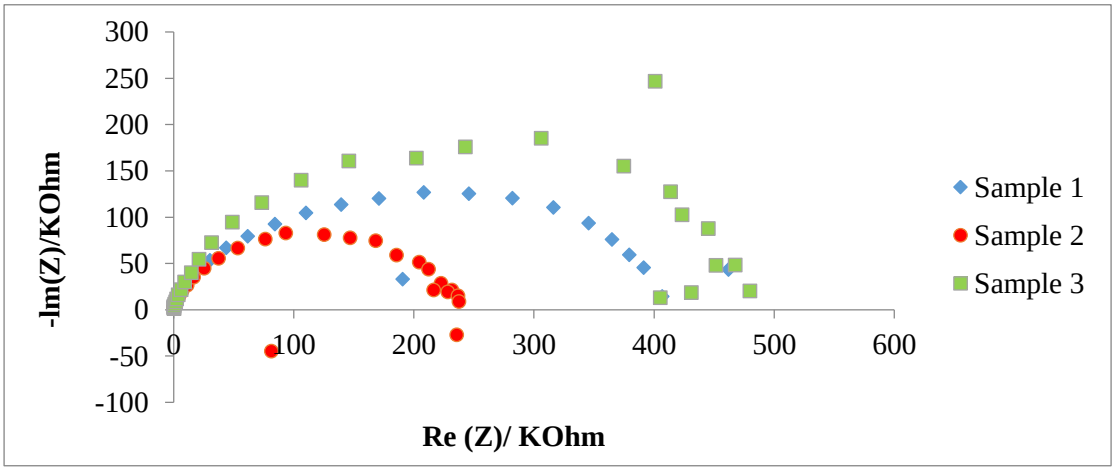

Figure A.3: Nyquist plots for three samples from third batch of 30% TiO_2

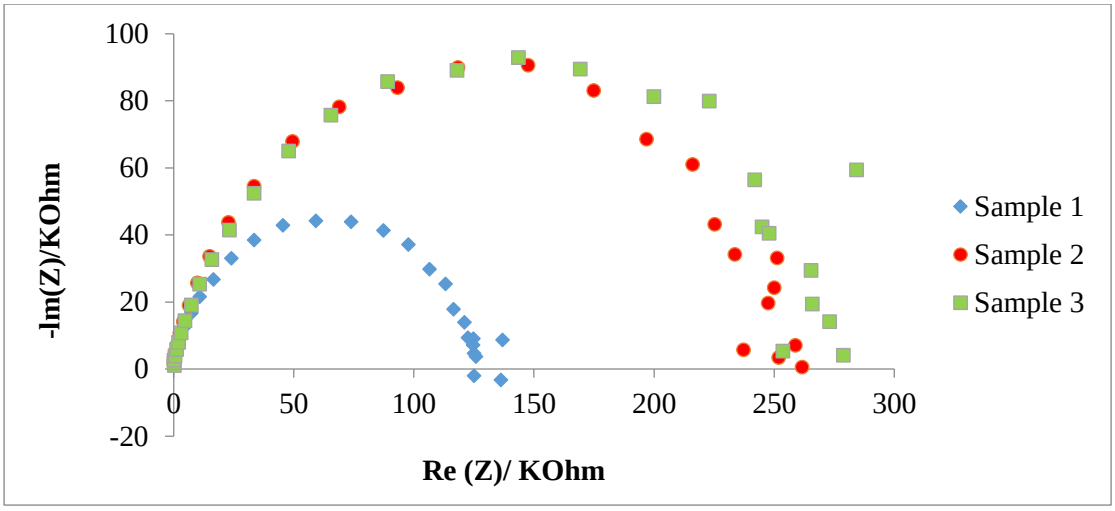

Figure A.4: Nyquist plots for three samples from fourth batch of 30% TiO_2

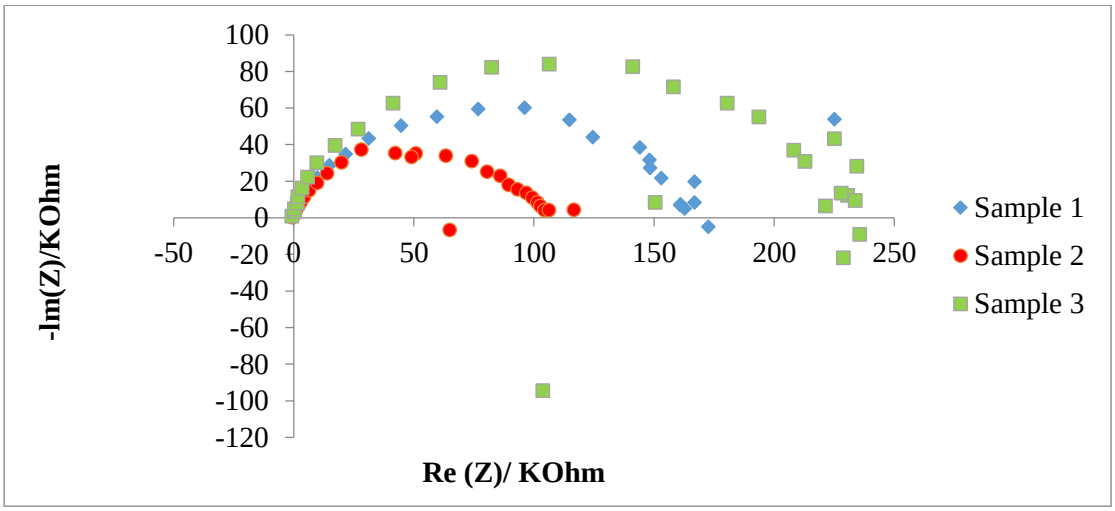

Figure A.5: Nyquist plots for three samples from fifth batch of 30% TiO_2

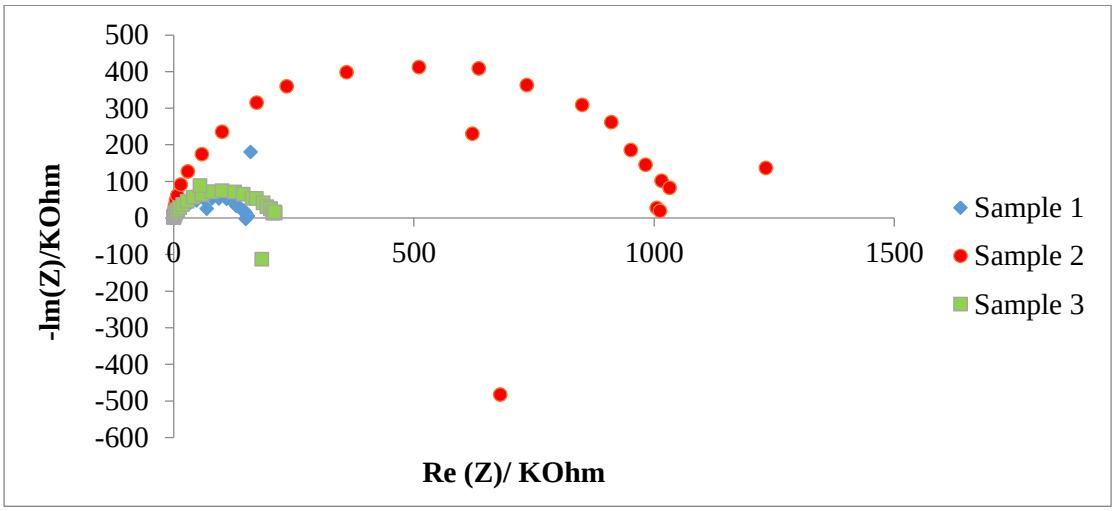

Figure A.6: Nyquist plots for three samples from sixth batch of 30% TiO_2

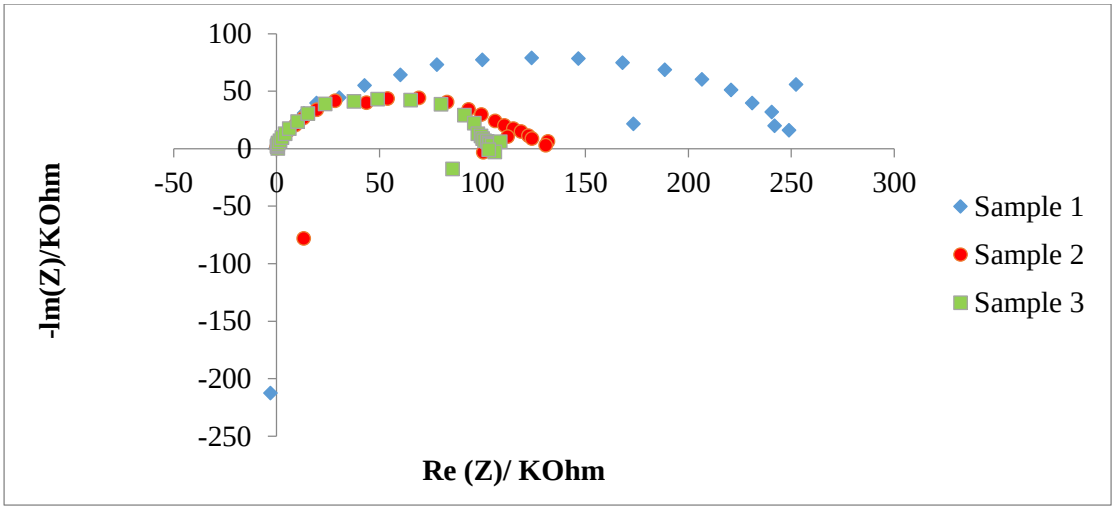

Figure A.7: Nyquist plots for three samples from seventh batch of 30% TiO_2

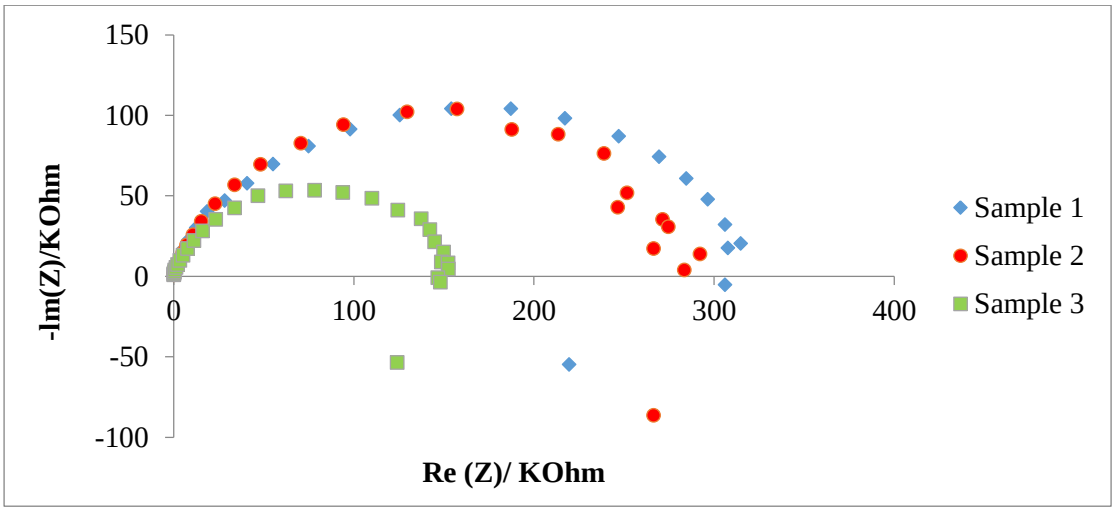

Figure A.8: Nyquist plots for three samples from eighth batch of 30% TiO_2

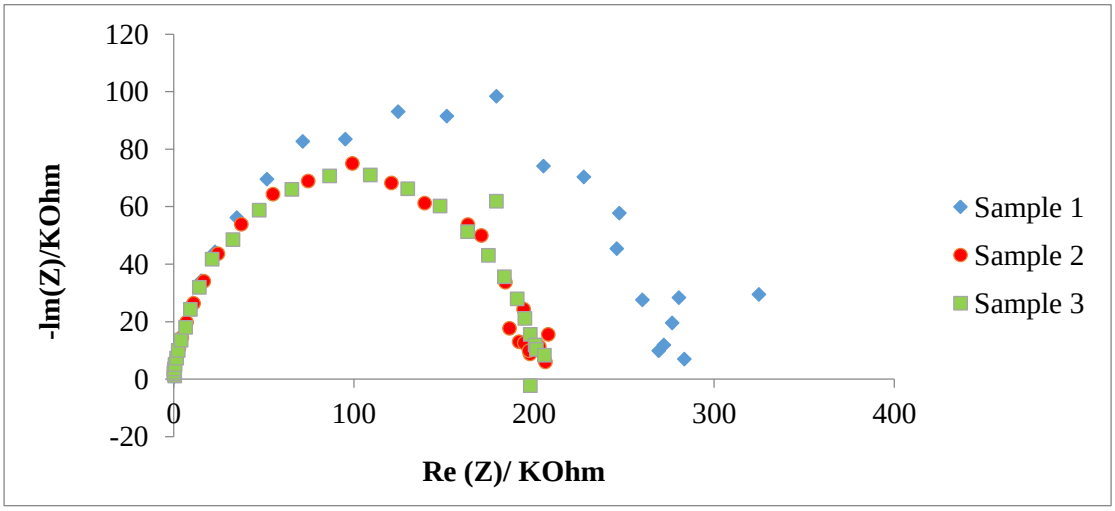

Figure A.9: Nyquist plots for three samples from ninth batch of 30% TiO_2

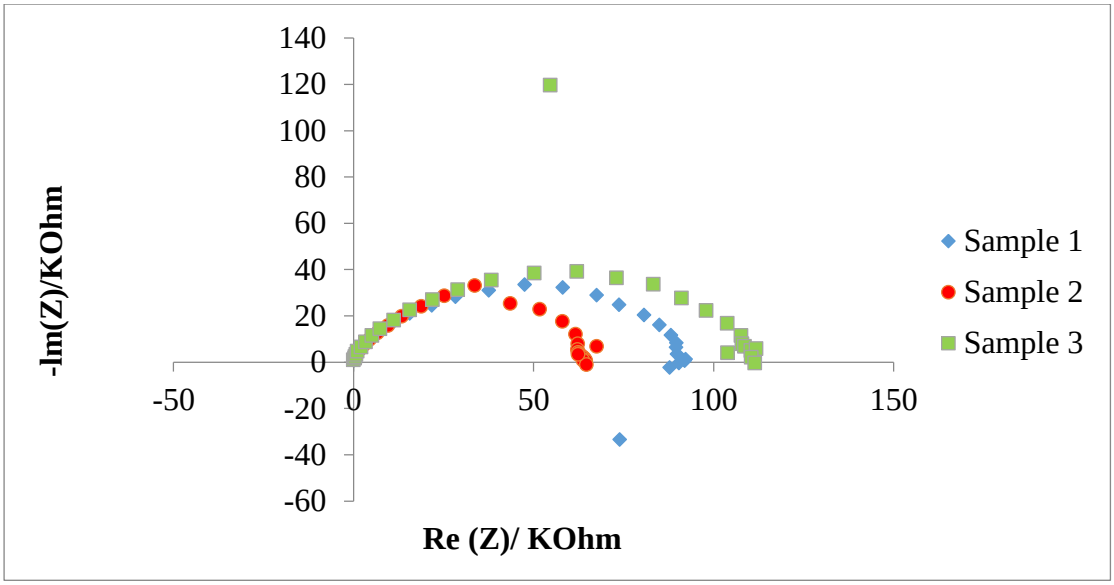

Figure A.10: Nyquist plots for three samples from tenth batch of 30% TiO_2

Table A.1: Bulk impedance results for 10 batches of 30% TiO_2-based samples

	Sample 1 Bulk Impedance (Ω)	Sample 2 Bulk Impedance (Ω)	Sample 3 Bulk Impedance (Ω)
Batch 1	532	18.8	-
Batch 2	352	456	-
Batch 3	354	385	340
Batch 4	252	247	380
Batch 5	370	-	-
Batch 6	432	447	144
Batch 7	242	622	-
Batch 8	484	379	236
Batch 9	409	427	557
Batch 10	320	250	204

Table A.2: Impedance at 1 kHz results for 10 batches of 30% TiO_2-based samples

	Sample 1 Impedance at 1 kHz (kΩ)	Sample 2 Impedance at 1 kHz (kΩ)	Sample 3 Impedance at 1 kHz (kΩ)
Batch 1	21.8	18.5	29.1
Batch 2	73.8	120	113
Batch 3	358	232	445
Batch 4	125	253	251
Batch 5	161	102	228
Batch 6	148	1020	202
Batch 7	231	122	103
Batch 8	285	247	150
Batch 9	260	192	195
Batch 10	92	63.8	109

A.2. Titanium Dioxide-Based Samples Mechanical Testing Results

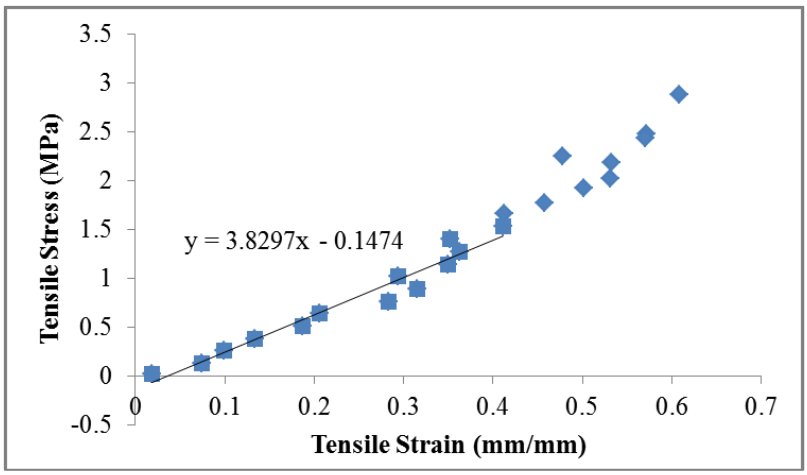

Figure A.11: Stress-strain curve for first 30% TiO_2 sample

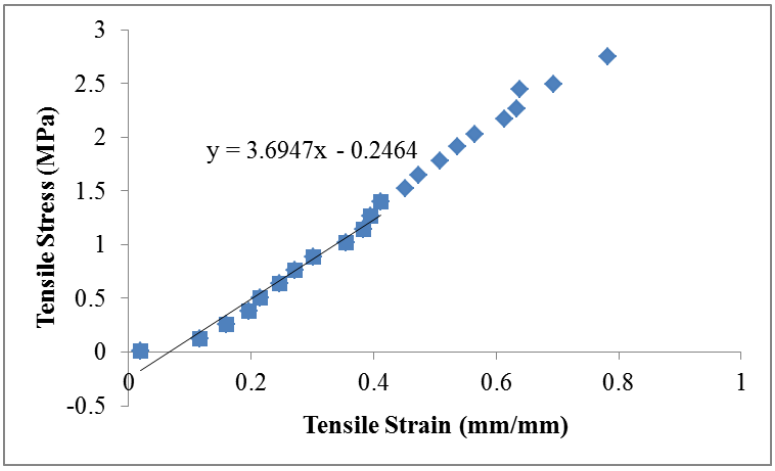

Figure A.12: Stress-strain curve for second 30% TiO_2 sample

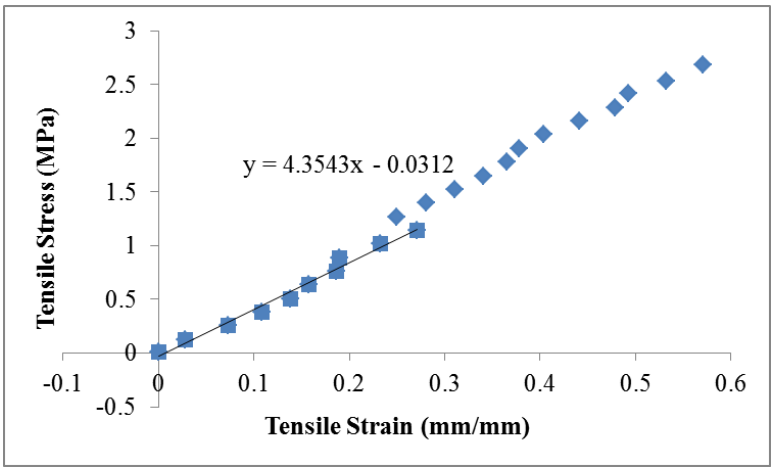

Figure A.13: Stress-strain curve for third 30% TiO_2 sample

A.3. Titanium Dioxide-Based Samples Impedance with Time Test Results

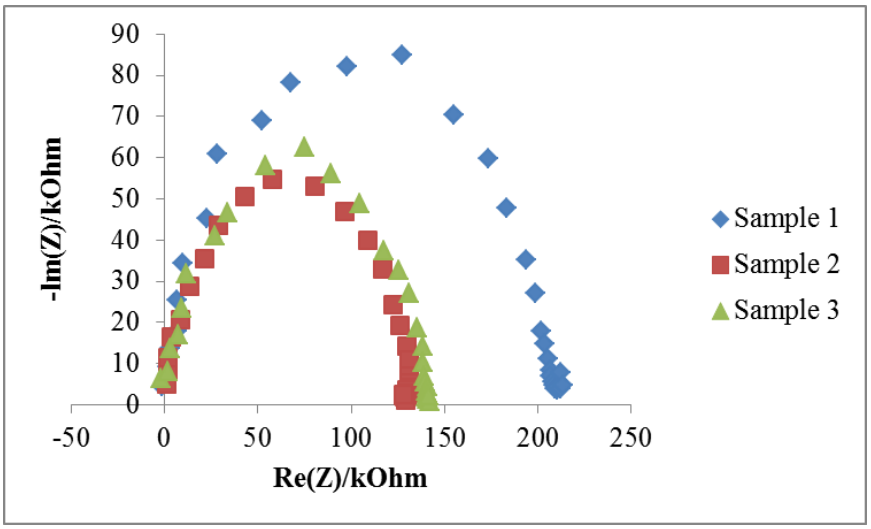

Figure A.14: Nyquist plots for three samples of 30% TiO_2 pre-immersion

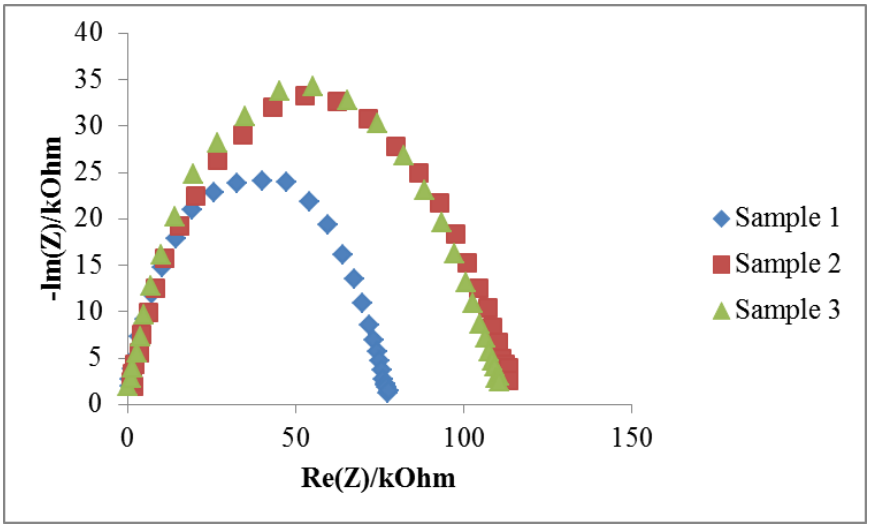

Figure A.15: Nyquist plots for three samples of 30% TiO_2 one week post-immersion

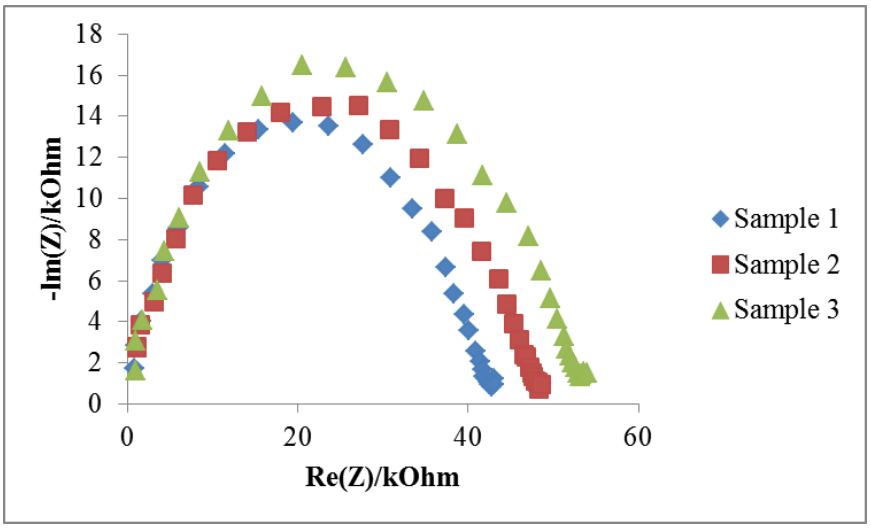

Figure A.16: Nyquist plots for three samples of 30% TiO_2 two weeks post-immersion

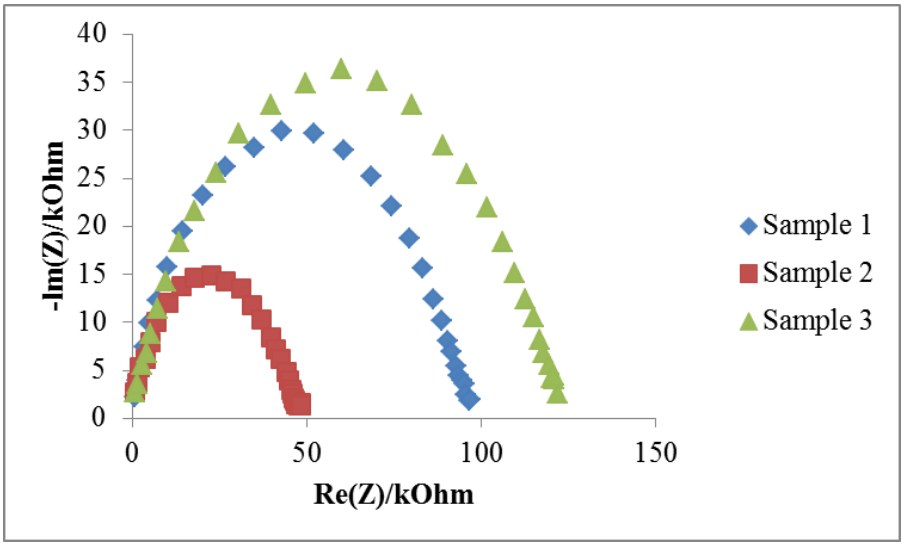

Figure A.17: Nyquist plots for three samples of 30% TiO_2 three weeks post-immersion

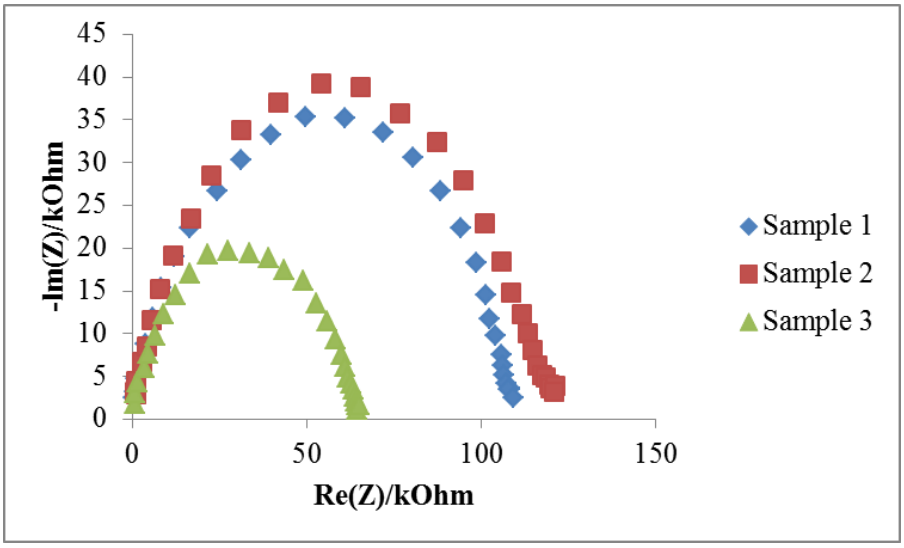

Figure A.18: Nyquist plots for three samples of 30% TiO_2 four weeks post-immersion

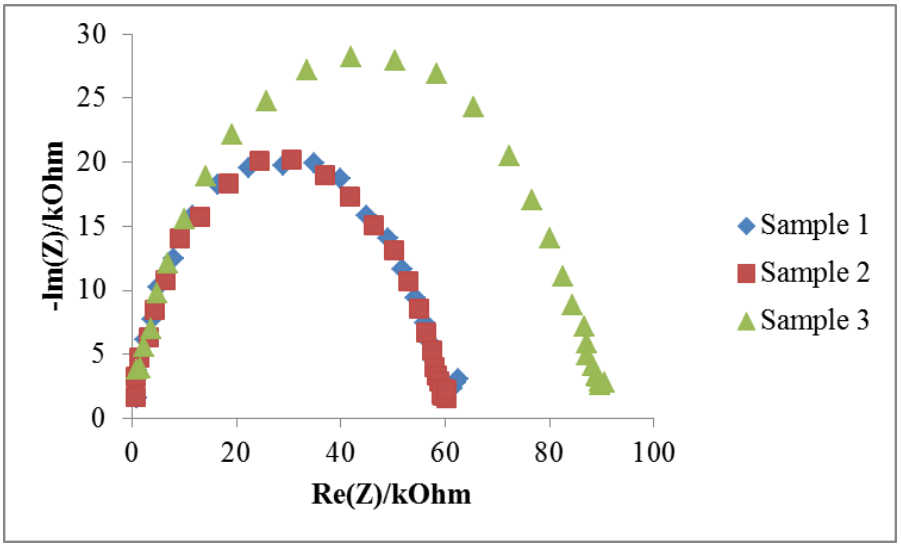

Figure A.19: Nyquist plots for three samples of 30% TiO_2 five weeks post-immersion

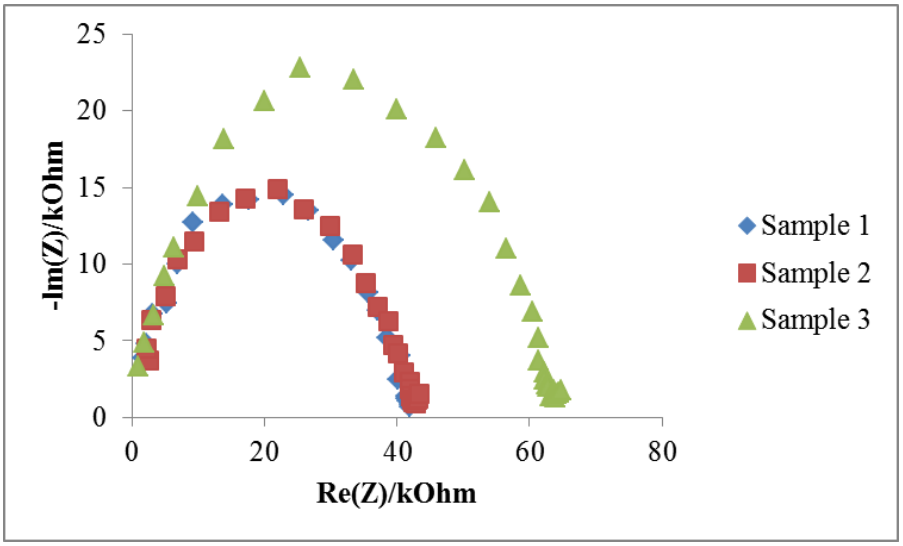

Figure A.20: Nyquist plots for three samples of 30% TiO_2 six weeks post-immersion

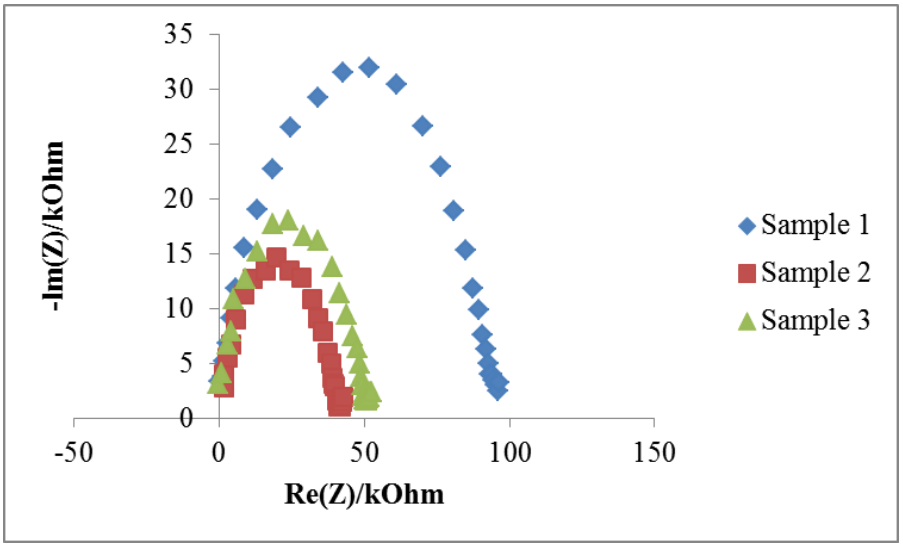

Figure A.21: Nyquist plots for three samples of 30% TiO_2 seven weeks post-immersion

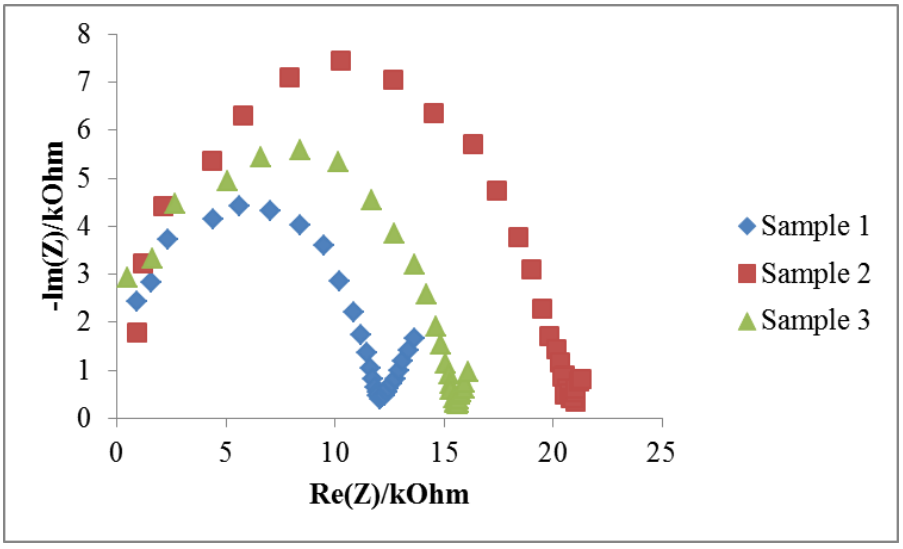

Figure A.22: Nyquist plots for three samples of 30% TiO_2 eight weeks post-immersion

Table A.3: Change of bulk impedance in 30% TiO_2 based samples during immersion period

	Sample 1 Bulk Impedance (Ω)	Sample 2 Bulk Impedance (Ω)	Sample 3 Bulk Impedance (Ω)
Pre-Immersion	-182.5	1340	138
One Week Post-Immersion	1110	1760	906
Two Weeks Post-Immersion	1010	1410	1260
Three Weeks Post-Immersion	1250	1270	2890
Four Weeks Post-Immersion	1040	1360	1060
Five Weeks Post-Immersion	1050	837	1770
Six Weeks Post-Immersion	1890	2330	1610
Seven Weeks Post-Immersion	1240	1760	522
Eight Weeks Post-Immersion	745	940	578

Table A.4: Change of impedance at 1 kHz in 30% TiO_2 based samples during immersion period

	Sample 1 Impedance at 1 kHz (kΩ)	Sample 2 Impedance at 1 kHz (kΩ)	Sample 3 Impedance at 1 kHz (kΩ)
Pre-Immersion	209	130	140
One Week Post-Immersion	75.8	107	107
Two Weeks Post-Immersion	42.1	47.3	52.2
Three Weeks Post-Immersion	92.9	46.9	114
Four Weeks Post-Immersion	106	116	63.6
Five Weeks Post-Immersion	60.2	59.8	88.4
Six Weeks Post-Immersion	41.9	42.4	63.2
Seven Weeks Post-Immersion	93.2	41.4	50.5
Eight Weeks Post-Immersion	12.5	20.8	15.6

Table A.5: Change of charge storage capacity in 30% TiO_2 based samples during immersion period

	Sample 1 CSC (mC/cm^2)	Sample 2 CSC (mC/cm^2)	Sample 3 CSC (mC/cm^2)
Pre-Immersion	33.2	33.7	64.5
One Week Post-Immersion	84.1	82.4	81.4
Two Weeks Post-Immersion	111	10.1	111
Three Weeks Post-Immersion	77.4	111	80.3
Four Weeks Post-Immersion	67.5	78.5	95.5
Five Weeks Post-Immersion	57.3	63.6	63.5
Six Weeks Post-Immersion	131	121	98.0
Seven Weeks Post-Immersion	55.1	92.3	83.6
Eight Weeks Post-Immersion	177	77.6	141

A.4. Stainless Steel-Based Samples EIS Results

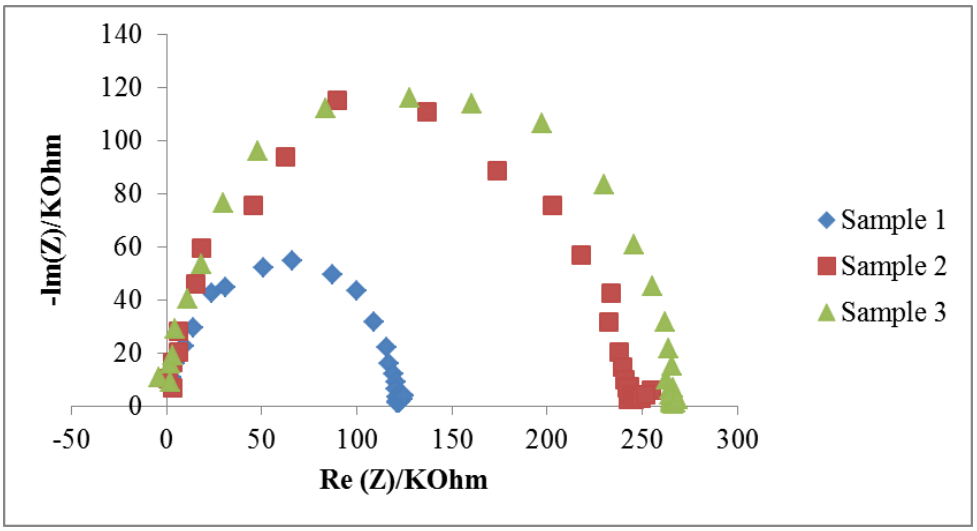

Figure A.23: Nyquist plots for three samples from first batch of 30% stainless steel

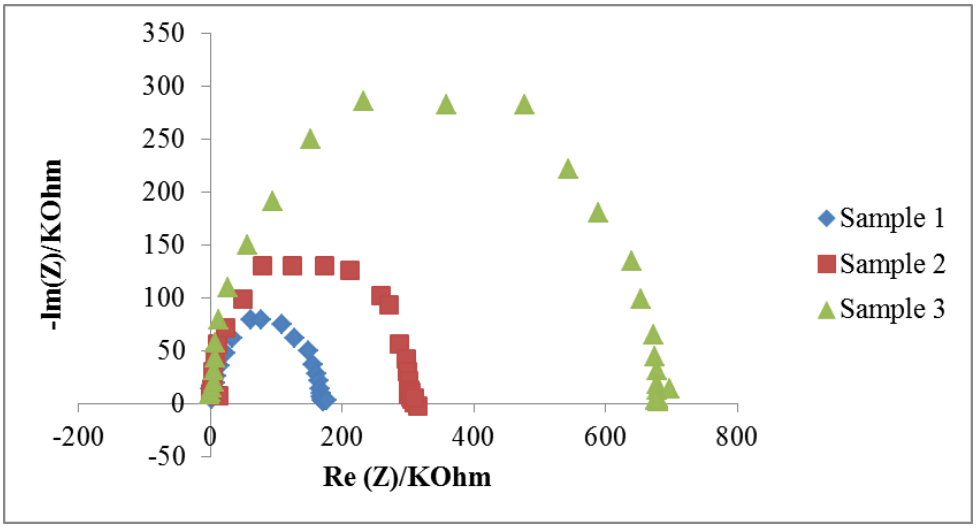

Figure A.24: Nyquist plots for three samples from second batch of 30% stainless steel

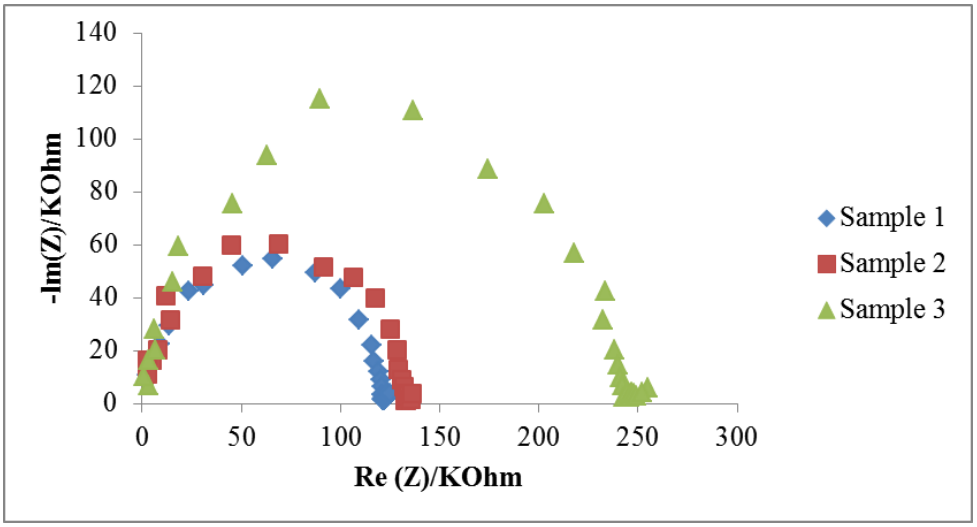

Figure A.25: Nyquist plots for three samples from third batch of 30% stainless steel

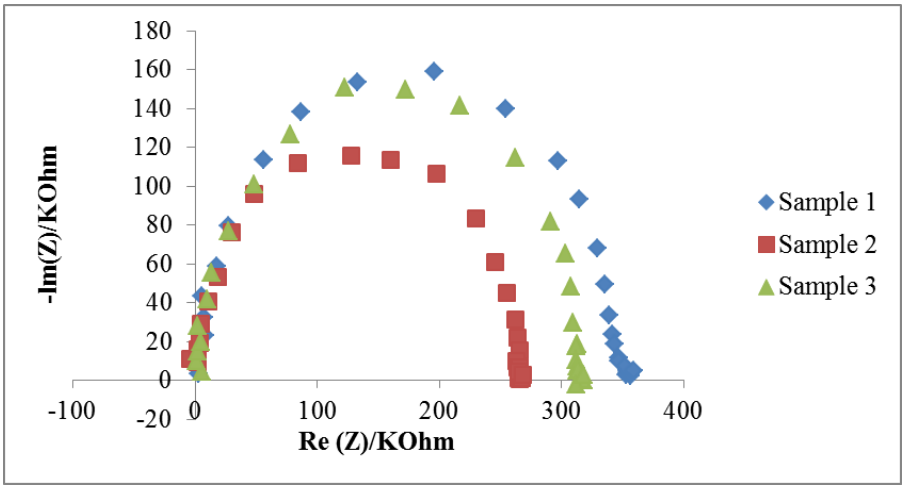

Figure A.26: Nyquist plots for three samples from fourth batch of 30% stainless steel

Table A.6: Bulk impedance results for four batches of 30% stainless steel-based samples

	Sample 1 Bulk Impedance (kΩ)	Sample 2 Bulk Impedance (kΩ)	Sample 3 Bulk Impedance (kΩ)
Batch 1	2.37	2.35	0.172
Batch 2	1.67	2.67	4.18
Batch 3	0.28	1.58	1.73
Batch 4	1.35	0.206	1.70

Table A.7: Impedance at 1 kHz results for four batches of 30% stainless steel-based samples

	Sample 1 Impedance at 1 kHz (kΩ)	Sample 2 Impedance at 1 kHz (kΩ)	Sample 3 Impedance at 1 kHz (kΩ)
Batch 1	679	2750	2730
Batch 2	171	307	443
Batch 3	1920	2070	2750
Batch 4	122	246	265

A.5. Stainless Steel-Based Samples Mechanical Testing Results

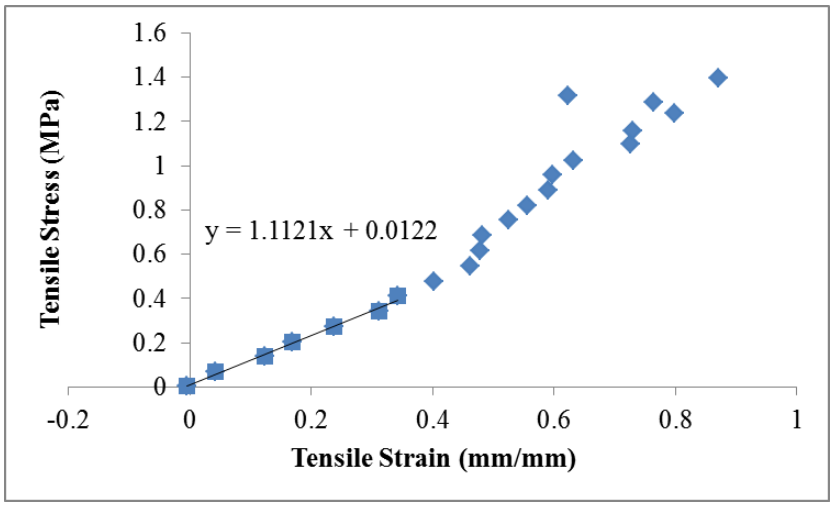

Figure A.27: Stress-strain curve for first 30% stainless steel sample

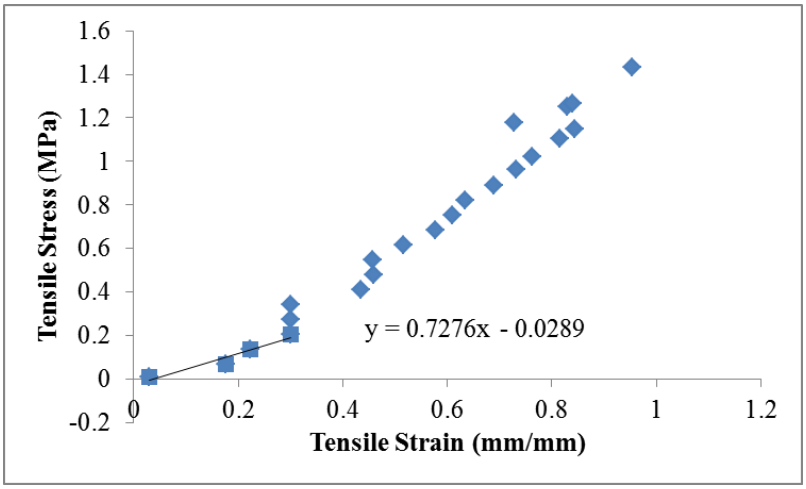

Figure A.28: Stress-strain curve for second 30% stainless steel sample

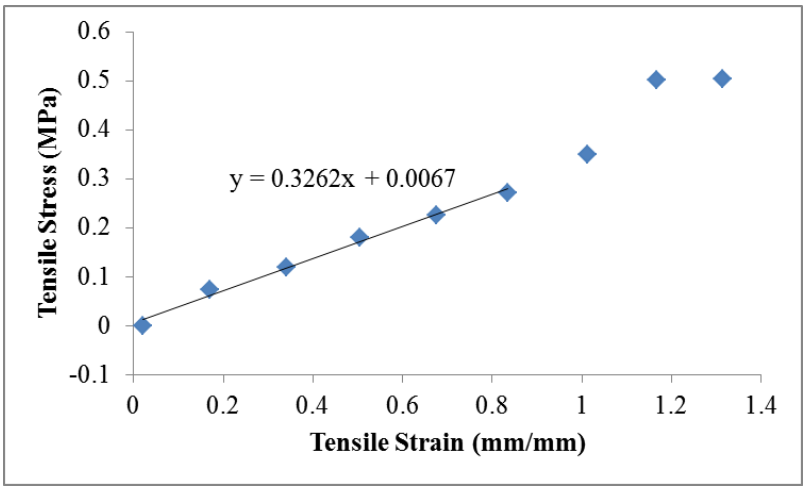

Figure A.29: Stress-strain curve for third 30% stainless steel sample

A.6. Stainless Steel-Based Samples Impedance with Time Test Results

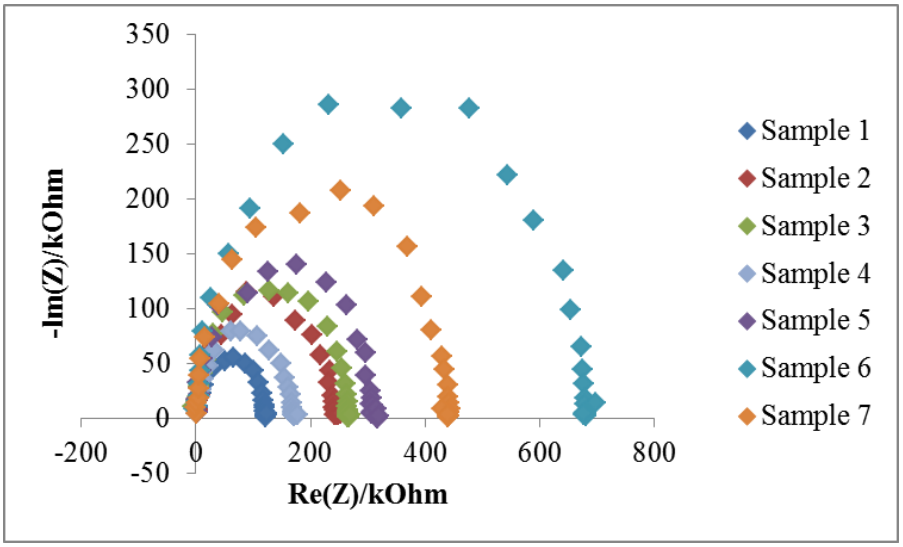

Figure A.30: Nyquist plots for three samples of 30% stainless steel pre-immersion

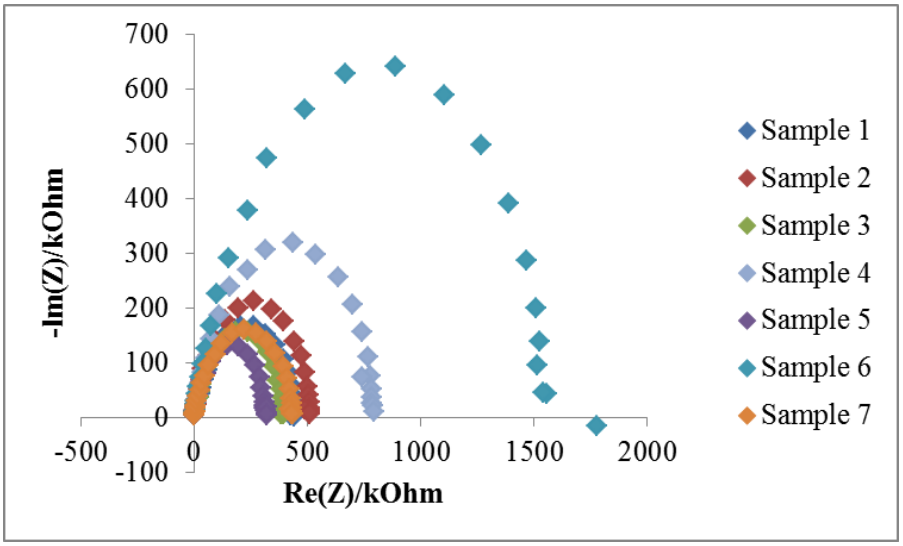

Figure A.31: Nyquist plots for three samples of 30% stainless steel one week post-immersion

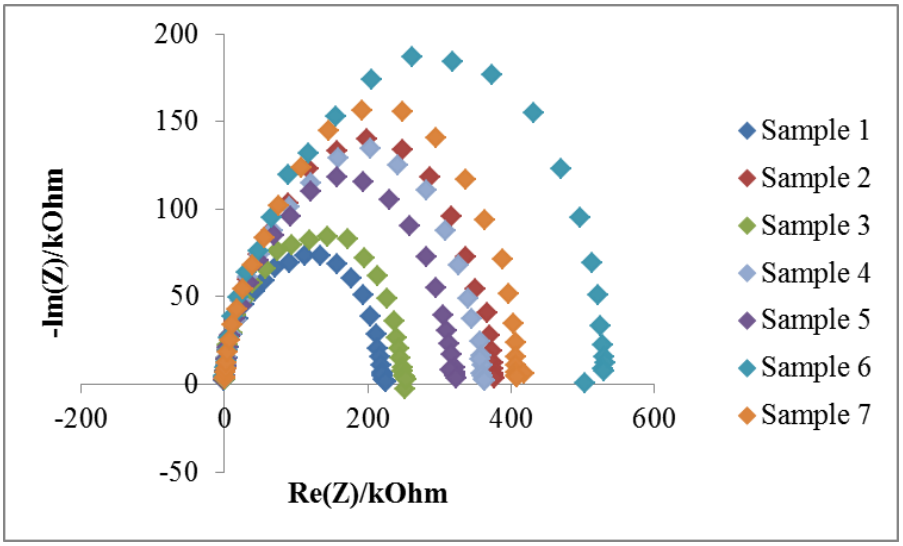

Figure A.32: Nyquist plots for three samples of 30% stainless steel two weeks post-immersion

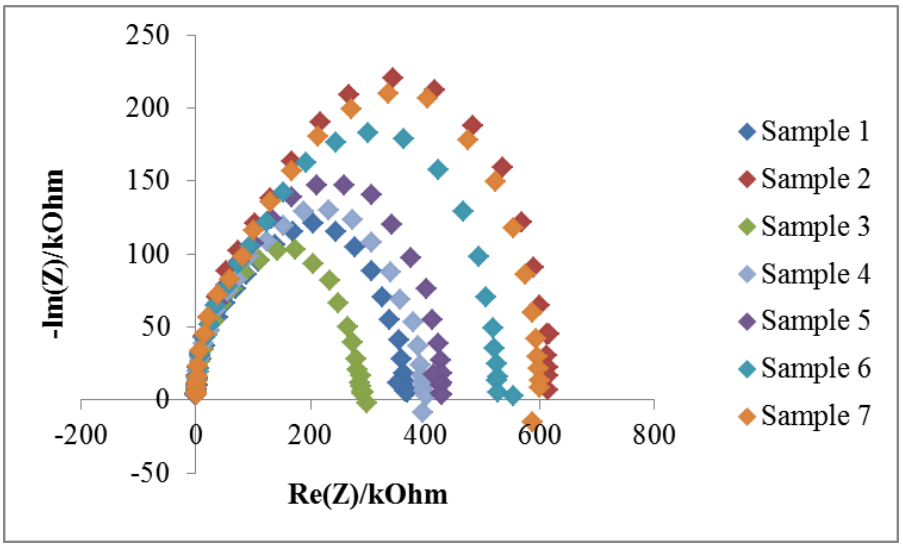

Figure A.33: Nyquist plots for three samples of 30% stainless steel three weeks post-immersion

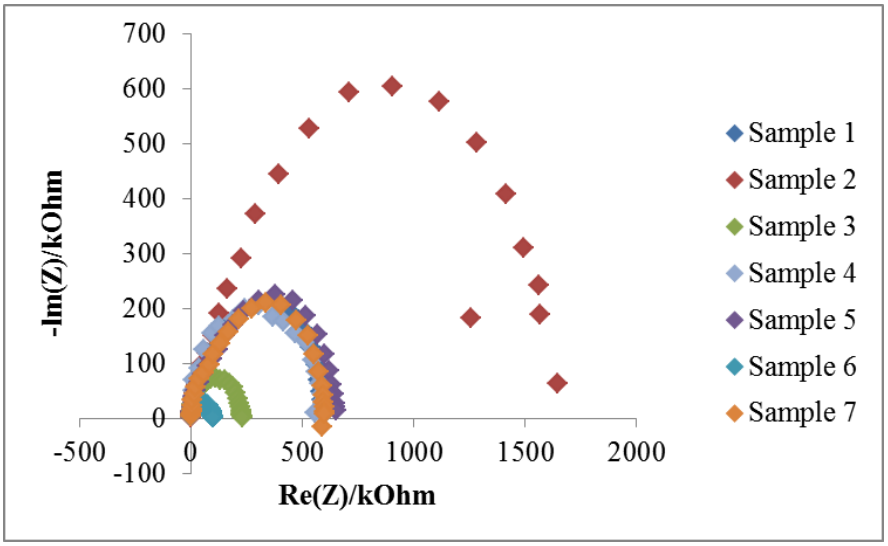

Figure A.34: Nyquist plots for three samples of 30% stainless steel four weeks post-immersion

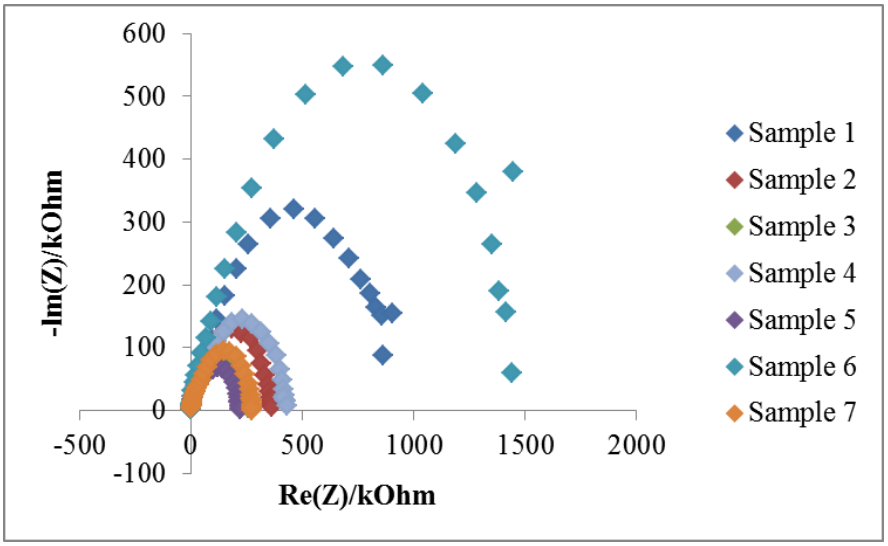

Figure A.35: Nyquist plots for three samples of 30% stainless steel five weeks post-immersion

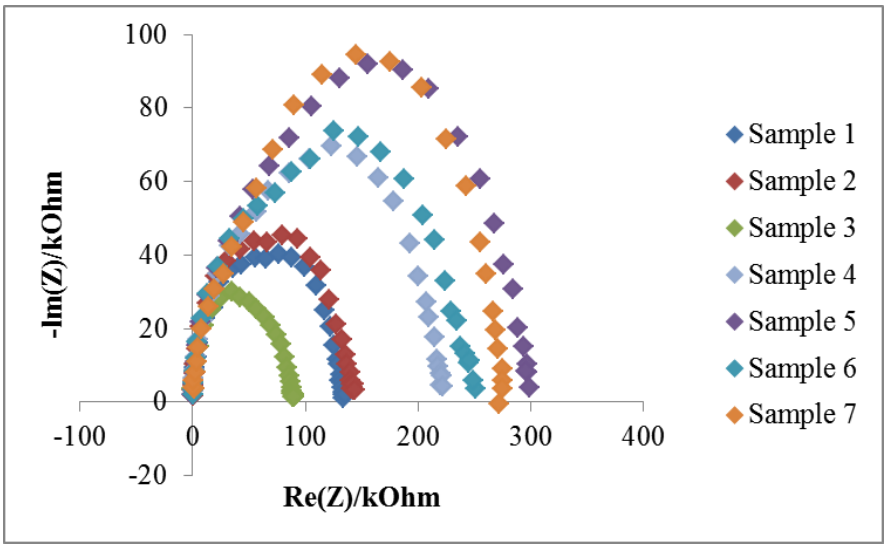

Figure A.36: Nyquist plots for three samples of 30% stainless steel six weeks post-immersion

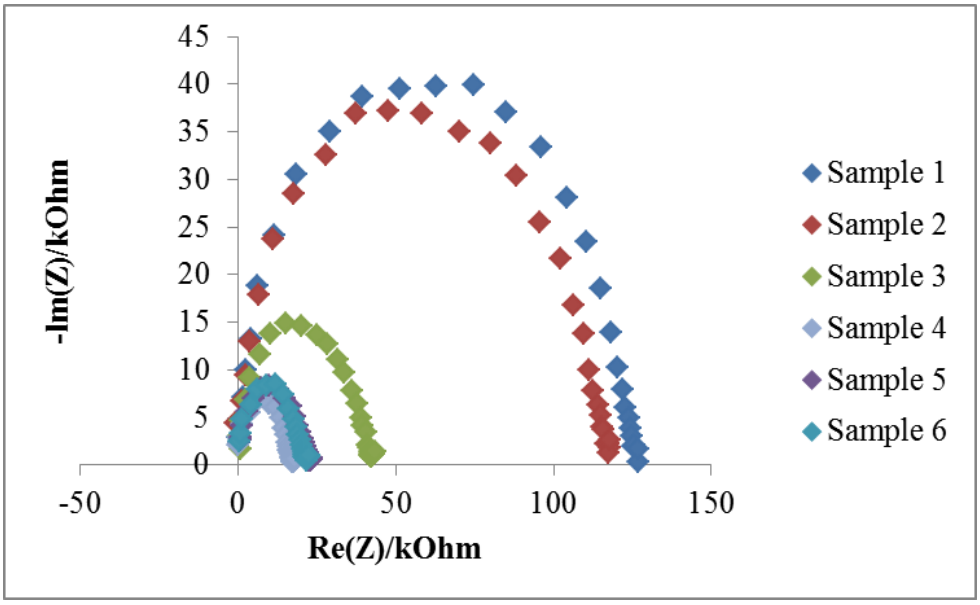

Figure A.37: Nyquist plots for three samples of 30% stainless steel seven weeks post-immersion

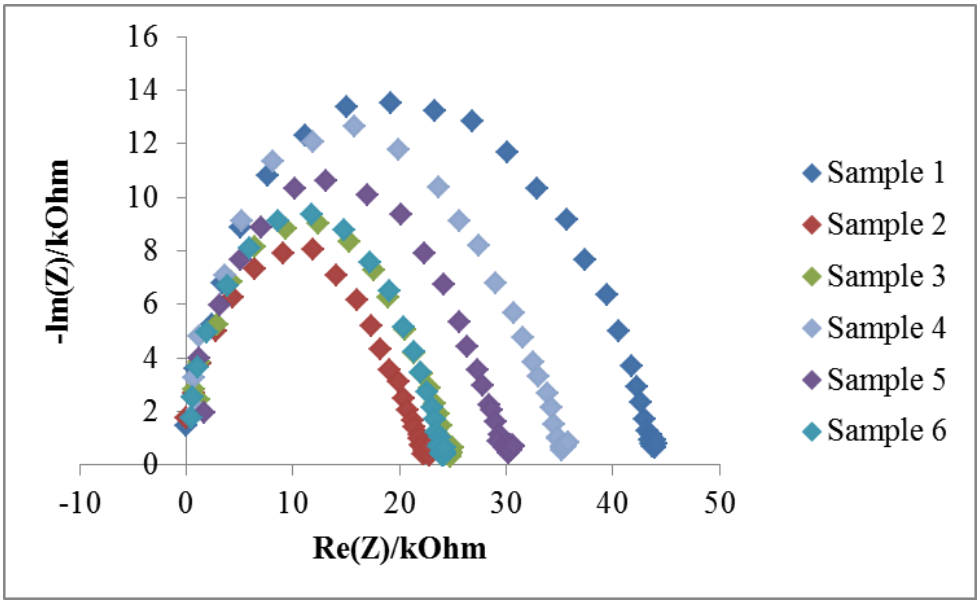

Figure A.38: Nyquist plots for three samples of 30% stainless steel eight weeks post-immersion

Table A.8: Change of bulk impedance in 30% stainless steel-based samples during immersion period

	S1 (Ω)	**S 2 (Ω)**	**S3 (Ω)**	**S4 (Ω)**	**S5 (Ω)**	**S6 (Ω)**	**S7 (Ω)**
Pre-Immersion	2370	3250	173	1670	2670	280	1580
One Week Post-Immersion	1910	1050	1320	1590	825	794	1330
Two Weeks Post-Immersion	-7.72	329	882	555	1050	707	860
Three Weeks Post-Immersion	210	417	550	1020	315	1250	1060
Four Weeks Post-Immersion	76.7	687	1060	4210	642	122	1320
Five Weeks Post-Immersion	157	707	939	582	325	401	1500
Six Weeks Post-Immersion	615	454	30.1	819	149	882	472
Seven Weeks Post-Immersion	459	394	733	170	577	453	
Eight Weeks Post-Immersion	314	212	833	874	1500	466	

Table A.9: Change of impedance at 1 kHz in 30% stainless steel-based samples during immersion period

	S1 (kΩ)	S 2 (kΩ)	S3 (kΩ)	S4 (kΩ)	S5 (kΩ)	S6 (kΩ)	S7 (kΩ)
Pre-Immersion	122	246	265	171	307	679	443
One Week Post-Immersion	439	509	394	781	330	1390	433
Two Weeks Post-Immersion	220	374	248	359	317	525	407
Three Weeks Post-Immersion	360	604	228	393	427	522	591
Four Weeks Post-Immersion	579	1380	225	596	626	97.3	584
Five Weeks Post-Immersion	752	353	251	413	216	1260	268
Six Weeks Post-Immersion	131	140	88.4	215	286	236	329
Seven Weeks Post-Immersion	124	116	423	17.6	22.7	21.8	
Eight Weeks Post-Immersion	43.6	22.2	24.5	35.2	30.1	23.9	

Table A.10: Change of charge storage capacity in 30% stainless steel-based samples during immersion period

	S1 (mC/ cm²)	S 2 (mC/ cm²)	S3 (mC/ cm²)	S4 (mC/ cm²)	S5 (mC/ cm²)	S6 (mC/ cm²)	S7 (mC/ cm²)
Pre-Immersion	56.5	29.8	35.8	28.4	23.5	23.8	24.5
One Week Post-Immersion	20.8	18.4	21.7	15	26.5	5.09	11.9
Two Weeks Post-Immersion	36.8	26.3	31.2	19.6	25.9	18.8	24.1
Three Weeks Post-Immersion	28.1	18.9	28	26.6	20.9	19.1	13.7
Four Weeks Post-Immersion	17.8	38.5	29.1	21.1	15.6	10.1	22
Five Weeks Post-Immersion	11.4	17.4	29.4	20.8	36.4	11.3	42.7
Six Weeks Post-Immersion	87.0	100	121	221	46.0	271	113
Seven Weeks Post-Immersion	177	162	28.3	81.6	67.3	177	63.0
Eight Weeks Post-Immersion	56.0	168	196	10.9	138	146	159

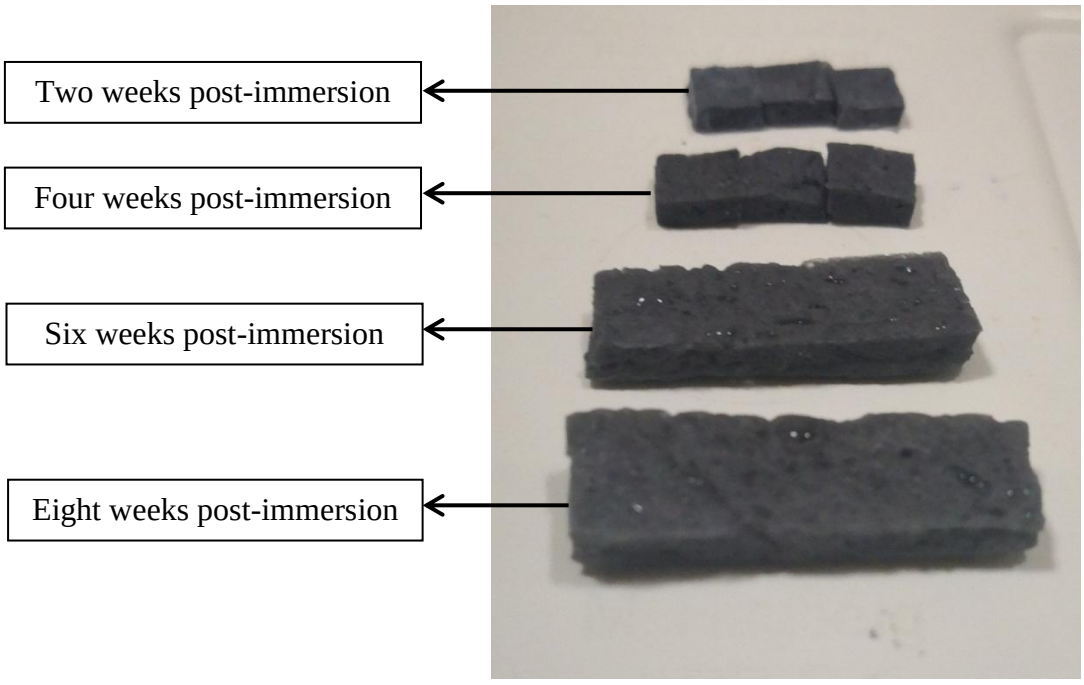

Figure A.39: Stainless steel samples post-immersion in PBS

A.7. Titanium Dioxide and Stainless Steel-Based Samples EIS Results

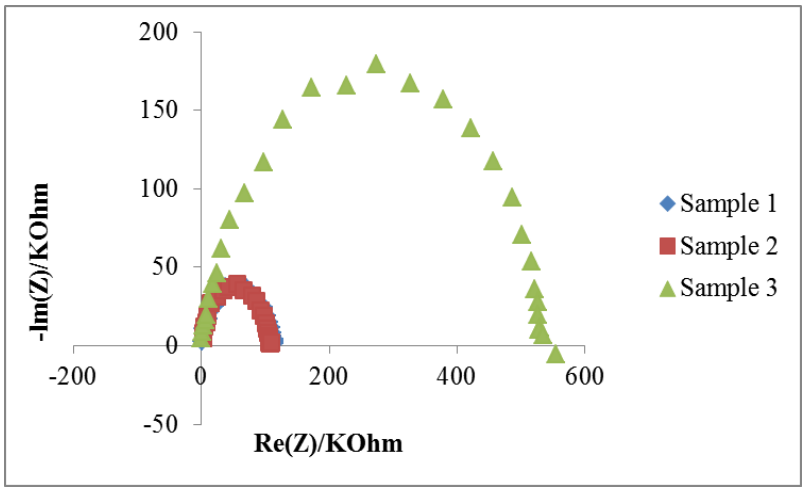

Figure A.40: Nyquist plots for three samples from first batch of 20% TiO_2 and 10% stainless steel

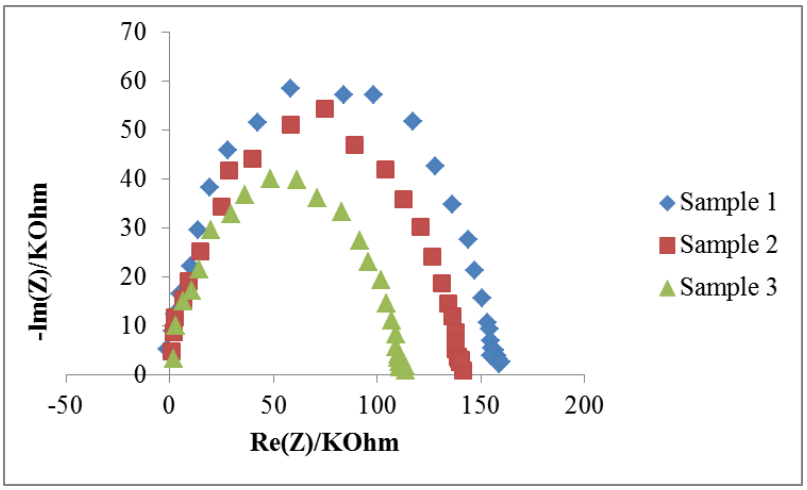

Figure A.41: Nyquist plots for three samples from second batch of 20% TiO_2 and 10% stainless steel

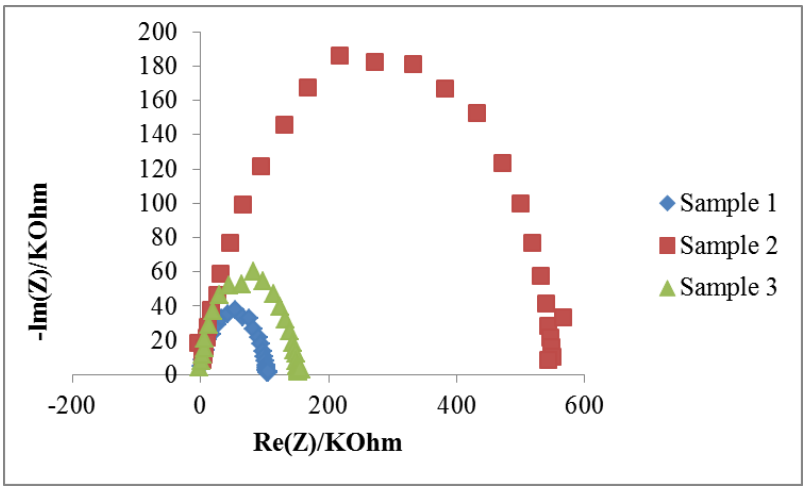

Figure A.42: Nyquist plots for three samples from third batch of 20% TiO_2 and 10% stainless steel

Table A.11: Bulk impedance results for three batches of mixture samples of 20% TiO_2 and 10% stainless steel

	Sample 1 Bulk Impedance (Ω)	Sample 2 Bulk Impedance (Ω)	Sample 3 Bulk Impedance (Ω)
Batch 1	2200	2400	770
Batch 2	185	1690	1890
Batch 3	871	1890	3460

Table A.12: Impedance at 1 kHz results for three batches of mixture samples of 20% TiO_2 and 10% stainless steel

	Sample 1 Impedance at 1 kHz (kΩ)	Sample 2 Impedance at 1 kHz (kΩ)	Sample 3 Impedance at 1 kHz (kΩ)
Batch 1	113	111	107
Batch 2	104	513	441
Batch 3	102	123	105

A.8. Titanium Dioxide and Stainless Steel-Based Samples Mechanical Testing Results

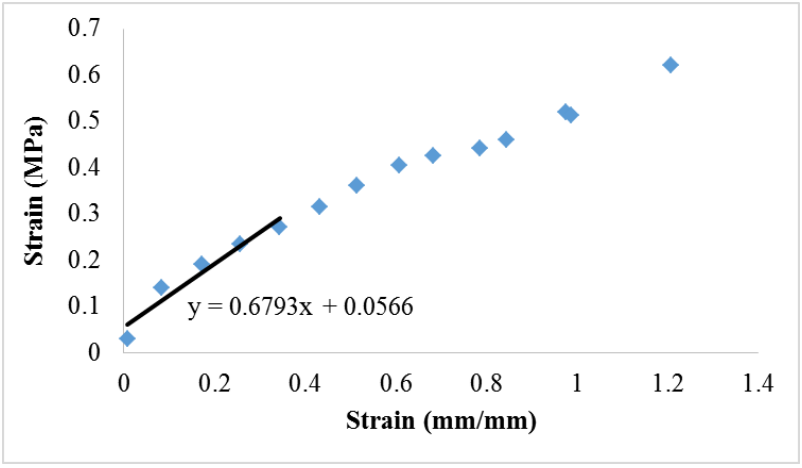

Figure A.43: Stress-strain curve for first 20% TiO_2 and 10% stainless steel sample

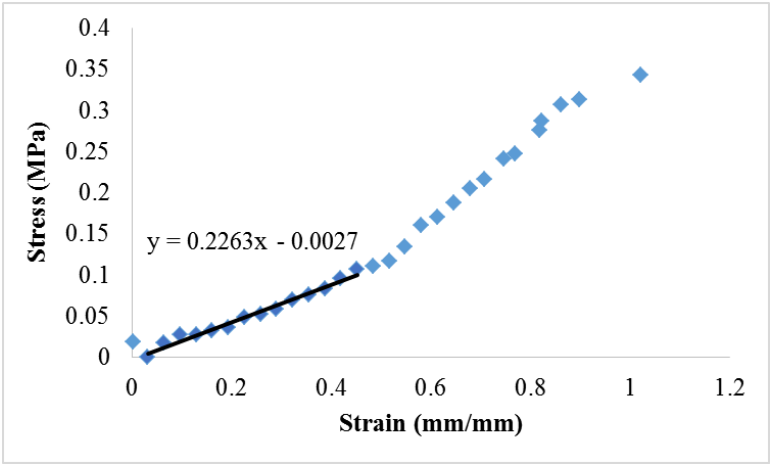

Figure A.44: Stress-strain curve for second 20% TiO_2 and 10% stainless steel sample

A.9. Code Used for Calculation of Charge Storage Capacity

```
j=1;
i=ImA; %Saving the current from the imported data
t=times1; %Saving the time from the imported data
for z=1:numel(i)
   i(z)=i(z)0.785; %To divide the current by the area to find current density
end
for z=1:numel(i)
   if i(z)<0 %To identify the negative (cathodal) current values
      x(j)=times1(z); %Save their corresponding time in a new matrix
      y(j)=i(z); %Save the values of current density in a new matrix
      j=j+1;
   end
end
c=abs(trapz (x, y)1); %Using the function to calculate the area under the curve
c=c/0.1; %Dividing by the square root of the scanning rate
```

Vita

Aseel Alatoom was born in 1994, in Abu Dhabi, United Arab Emirates. She received her primary and secondary education in Abu Dhabi, UAE. She received her B.Sc. degree in Biomedical Engineering from the Khalifa University for Science, Technology and Research in 2016.

In September 2017, she joined the Biomedical Engineering master's program in the American University of Sharjah as a graduate teaching assistant. During her master's study, she co-authored 3 paper which was presented in IEEE conferences. Her research interests are in biomaterials.